A Computational and Experimental Study of the Wave Load on a Horizontal Cylinder

Jørgen Fjøsne

A Master's Thesis in Ocean Technology

University of Bergen

Department of Physics and Technology

June 2022

This page is intentionally left blank

Abstract

This study aims to investigate how changing the wave and flow parameters influence the wave load on a partially submerged cylinder, placed horizontally and transversely against the waves in a fixed position. A 2D and 3D CFD model has been built using ANSYS Fluent, and the models are used to gather data for a parametric study. In order to validate the gathered data, experimental tests were executed at the hydrodynamical testing facility MarinLab, at Høgskulen på Vestlandet (HVL). Two different sized cylinder models were produced in polyethylene, and a custom-made load cell system was used to measure the drag force on the cylinders. A thorough analysis of the gathered data has been performed using MATLAB, taking a deeper look into how the wave amplitude, frequency/wavelength, flow speed, and submersion level influence the drag and lift force on the cylinder. The results show that an increase in wave amplitude leads to a proportional increase in drag and lift force, and an increase in the wave frequency leads to an increase in the drag force but a decrease in lift force. Furthermore, the drag force increases at an increasing rate when the cylinder is more submerged and decreases at an increasing rate as less of the cylinder is submerged, and the maximum lift force increases at a steady rate proportional to the submersion level.

This page is intentionally left blank

Sammendrag

Denne studien tar sikte på å undersøke hvordan endring av bølge- og strømningsparametre påvirker bølgebelastningen på en delvis nedsenket sylinder, plassert horisontalt og på tvers mot bølgene i en fast posisjon. En 2D- og 3D-CFD-modell er laget ved hjelp av ANSYS Fluent, og modellene brukes til å samle data til den parametriske studien. For å validere de innsamlede dataene ble det utført eksperimentelle tester ved det hydrodynamiske testanlegget MarinLab, ved Høgskulen på Vestlandet. To sylindermodeller i forskjellige størrelser ble produsert i polyetylen, og et skreddersydd lastcellesystem ble brukt for å måle dragkraften på sylindrene. En grundig analyse av de innsamlede dataene er utført ved hjelp av MATLAB, og for å undersøke hvordan bølgeamplituden, frekvensen/bølgelengden, strømningshastigheten og nedsenkningsnivået påvirker drag- og løftekraften på sylinderen. Resultatene viser at en økning i bølgeamplitude fører til en proporsjonal økning i drag- og løftekraft, og en økning i bølgefrekvens fører til en økning i dragkraften, men en reduksjon i løftekraften. Videre øker dragkraften med en økende rate når sylinderen er mer nedsenket og avtar med en økende rate når mindre av sylinderen er nedsenket, og den maksimale løftekraften øker med en jevn rate, proporsjonalt med nedsenkningsnivået.

This page is intentionally left blank

Acknowledgements

During the last year, I have been working on my master's thesis. This has been a process that has involved a lot of input and help from different people.

Firstly, I would like to thank my supervisors, Saeed Bikass, Mariusz Domagala, Hassan Momeni, and Harald Totland. You have inspired me with your enthusiasm, guided me with academic experience and shared your expertise with me in many different fields of knowledge. Without your help and guidance, I would have been lost many times.

I would like to thank my fellow students at Ocean Technology, as well as my fellow students from my time at HVL studying Marin Technology. Thank you to my family for supporting me in everything I do.

Finally, I would like to thank my partner, Laura. You inspire me and always believe in me, even when I don't. Thank you.

Contents

List of Figures

List of Tables

Nomenclature

Symbol	Explanation
ε	*Turbulent Dissipation Rate (Epsilon)*
ω	*Turbulent Dissipation Rate (Gamma)*
ρ	*Density*
λ	*Wavelength*
μ	*Viscosity*
ν	*Kinematic Viscosity*
τ_{ij}	*Scalar components of Reynolds stress tensor*
ψ	*Liquid volume fraction*
Ω	*Angular frequency*

Symbol	Explanation
a	*Wave Amplitude*
C_d	*Drag coefficient*
C_m	*Intertia coefficient*
d	*Water depth*
f	*Frequency*
F	*Force*
g	*Gravitational Acceleration*
h	*Water level*
K	*Wave number*
k	*Turbulent kinetic energy*
m	*Mass*
p	*Pressure*
T	*Wave period*
t	*Time*
u	*Velocity*
x,y,z	*Cartesian Coordinates*

1. Introduction

Technological development is constantly advancing science. The availability of computational power has had exponential growth over the last few decades, leading to the development of new and powerful tools for analysis and optimization. *Computational Fluid Dynamics* (CFD) is one of these tools. CFD is a method of simulating the motion and behaviour of fluids, and its application has been growing in a vast field of different engineering disciplines. It is a complex and powerful tool, and when used correctly, it can be of great value.

Understanding loads of waves and fluid flow is essential for marine engineering. Utilizing CFD analysis on this subject presents an exciting opportunity for both learning the methods of CFD and researching a topic that significantly impacts the choices made in designing a marine structure.

A cylinder is a shape that often appears in marine structures. For example, polyethene rings are used in fish farming cages in the aquaculture industry. In the offshore petroleum industry, the shape of cylindrical beams and piles is found in many structures, including oil rigs. An example from another industry is the offshore windmills, often mounted using a monopile or jacket on piles system, as shown in Figure 1.1.

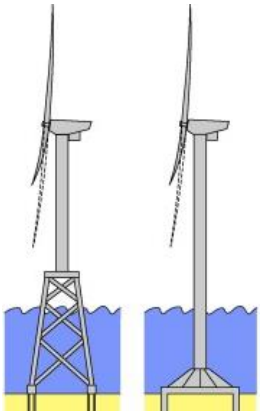

Figure 1.1 – Jacket on piles and monopile systems

Common for all of these structures is that they must be constructed to withstand the harsh marine environment and the forces applied by waves and fluid flow. Therefore, understanding the impact of changes in wave and fluid parameters on the force applied to the construction is of great value.

In recent years a race has started to be the first to succeed with offshore fish farming in the aquaculture industry. SalMar and their offshore fish farm *Ocean Farm 1*, as depicted in Figure 1.2, are among the innovators pushing the industry towards new horizons.

Figure 1.2 – SalMars Ocean Farm 1 (SalMar ASA, 2022)

If a fish farm breaks due to the mighty waves of a winter storm, it will result in catastrophic consequences if the 200 000 Salmon get loose. Moreover, if any working crew is present during a structure failure, the consequences could be even worse. Therefore, a deep understanding of the wave and the load they apply is imperative to continue the development of futuristic innovations like the *Ocean Farm 1*.

There are many ways to go forward when analysing the loads applied to a structure in a marine environment. For example, physical experiments in a controlled laboratory setting, utilizing loadcells or other ways of accurately measuring the force, different methods of CFD, or more traditional and simplified mathematical methods and models are all commonly used when investigating the phenomena of waves.

One of the primary purposes of this research is to study the wave and the resulting load when applied to a cylindrical shape. Investigating the influence of changes in wave and fluid parameters and seeing how it affects the forces applied to the cylinder might lead to valuable insight. The parametric study uses 2D and 3D CFD for data collection and validation through experimental tests in a hydrodynamical testing facility. The wave amplitude, wavelength, flow speed and submersion level are parameters that will be investigated.

1.1 Synopsis

A brief synopsis of the contents of the different chapters in this research:

- Chapter 2 covers the background theories of computational fluid dynamics, wave theory and models for wave load calculations.
- Chapter 3 consists of a literature review of recent research done on the subject of CFD, wave load calculations and experimental testing.
- Chapter 4 describes the design of experiments, and the setup of the wave load simulations, including software, 2D simulations and 3D simulations.
- Chapter 5 presents the validation experiments performed in the hydrodynamical testing facility at HVL. It includes a description of the facilities, the equipment, and the experimental method.
- Chapter 6 presents the results of the CFD, experimental tests and the process of data validation.
- Chapter 7 covers the discussion part of the research. In this chapter, the influence of parametrical changes is analysed and discussed.
- Chapter 8 consists of the conclusion and the suggested further works.

2. Theoretical Background

This chapter will cover the major theoretical background on which this thesis is built. The subchapters will cover the themes of fluid dynamics, CFD, VOF, scaling and wave theory.

2.1 Computational Fluid Dynamics

Computational Fluid Dynamics (CFD) is a method of computing and analysing different phenomena within the theory of fluid dynamics, such as fluid flows, heat transfer or any other behaviour of a fluid. This is done by utilizing computational power to numerically solve the governing equations, i.e., the *Navier Stokes Equations.*

2.1.1 The Navier Stokes Equations

The Navier-Stokes equations are a set of partial differential equations that, when solved, describe the motion of a fluid. The equations can for an incompressible fluid, in cartesian coordinates, be expressed as follows:

$$\rho g_x - \frac{\partial p}{\partial x} + \mu\left(\frac{\partial^2 u}{\partial x^2} + \frac{\partial^2 u}{\partial y^2} + \frac{\partial^2 u}{\partial z^2}\right) = \rho\left(\frac{\partial u}{\partial t} + u\frac{\partial u}{\partial x} + v\frac{\partial u}{\partial y} + w\frac{\partial u}{\partial z}\right) \qquad (2.1)$$

$$\rho g_y - \frac{\partial p}{\partial y} + \mu\left(\frac{\partial^2 v}{\partial x^2} + \frac{\partial^2 v}{\partial y^2} + \frac{\partial^2 v}{\partial z^2}\right) = \rho\left(\frac{\partial v}{\partial t} + u\frac{\partial v}{\partial x} + v\frac{\partial v}{\partial y} + w\frac{\partial v}{\partial z}\right) \qquad (2.2)$$

$$\rho g_z - \frac{\partial p}{\partial z} + \mu\left(\frac{\partial^2 w}{\partial x^2} + \frac{\partial^2 w}{\partial y^2} + \frac{\partial^2 w}{\partial z^2}\right) = \rho\left(\frac{\partial w}{\partial t} + u\frac{\partial w}{\partial x} + v\frac{\partial w}{\partial y} + w\frac{\partial w}{\partial z}\right) \qquad (2.3)$$

In these equations, u, v, and w are the velocity components in a three-dimensional cartesian coordinate system by the directions x, y, z. Furthermore, ρ is the density of the fluid, t is the time, g is the gravitational acceleration, μ is the viscosity, and p is the pressure (Steven H. Collicott, 2013, p. 134).

Essential for describing the behaviour of fluids is also the conservation of mass. For an incompressible flow, the equation of continuity can be expressed as follows:

$$\frac{\partial u}{\partial x} + \frac{\partial v}{\partial y} + \frac{\partial w}{\partial z} = 0 \qquad (2.4)$$

2.1.2 Reynolds Averaged Navier Stokes

It is possible to resolve every fluctuating motion in a flow, but this requires a very high grid resolution and small timesteps, and it extremely demanding regarding computational resources. This is called Direct Numerical Simulation (DNS) and is mainly performed with supercomputers for low Reynold-number flows. The CFD analysis is often performed using Reynolds Averaged Navier Stokes Equations (RANS) to reduce the required computational time and power. The RANS equation can be expressed as:

$$\frac{\partial \overline{u_i}}{\partial t} + \overline{u_j}\frac{\partial \overline{u_i}}{\partial x_j} = -\frac{1}{\rho}\frac{\partial \overline{p}}{\partial x_i} + \nu\frac{\partial^2 \overline{u_i}}{\partial x_j \partial x_j} - \frac{\partial \tau_{ij}}{\partial x_j} \tag{2.5}$$

The Reynolds stress tensor, τ_{ij}, for constant density is equal to $\overline{u'_i u'_j}$, t is time, u_i is the fluid velocity, x is position, ν is the kinematic viscosity, ρ is the density, and p is the pressure (Alfonsi, 2009).

2.1.3 Turbulence Models

The Reynolds-average Navier-Stokes equations contain some terms which need to be modelled. The primary purpose of a turbulence-mean-flow closure model is to relate the Reynolds stress correlations, $\overline{u_i u_j}$ to the mean velocity field U_i. The Reynolds stress tensor contains six unknowns, and the objective for the turbulence model is to express these unknowns and then close the RANS equations so that they may be solved to give high-quality approximations of the actual fluid behaviour.

Depending on the CFD software, the number of available turbulence models varies. In ANSYS Fluent, the software used in this research, there is support for a wide range of different turbulence models, including k-epsilon (k-ε), k-omega (k-ω), Scale-Adaptive Simulation (SAS), and Detached Eddy Simulation (DES). All turbulence models have different pros and cons, and their applicability must be evaluated depending on the specific case. Due to their robustness and range of suitability, the k-ε and *Shear Stress Transport* k-ω model (SST k-ω) are recommended for most engineering cases (ANSYS, 2014).

For the simulations in this research, the turbulence model SST k-ω is utilized. SST k-ω combines the advantages of k-ω for inner boundary layer calculations with the k-ε turbulence model for the outer layers, therefore effectively combining the qualities of the two. SST k-ω is also applicable for a wider range of different Reynolds number flows. The

robust turbulence model was developed by Menter (1994, p. 32) and is more trustworthy and precise for a wider class of different flows than the standard k-ω model and has become an industry standard (SIMSCALE, 2021).

2.1.2 Finite Volume Method

The Navier-Stokes equations describe the behaviours of fluids, and the *Finite Volume Method* (FVM) is a method of discretisation to solve these governing differential equations. The flow domain is divided into a finite number of cells. In each cell, the flux entering the control volume is equal to the flux leaving the volume (Rapp, 2017). That way, the governing equations can be solved for the centre of each cell to extract parameters like velocity or pressure and be interpolated between the cells.

2.1.3 Volume of Fluid Method

Within the FVM, there is a method for discretisation called the Volume of Fluid Method (VFM), which is used when dealing with multiphase flows and free surface fluids. The volume of fluid method is a numerical modelling technique for describing and discretising the behaviour of the interface between different fluids. VFM is an Eulerian method used to track and identify the interface between two fluids in a free flow state. This method was developed in 1981 by scientists B. D. Nichols and C. W. Hirt and then further modified by Berberović in 2009. The VOF method describes the amount of fluid in each cell by a phase fraction ψ and is defined by the following formula:

$$\frac{\partial \psi}{\partial t} + \boldsymbol{u} \cdot \nabla \psi = 0 \qquad (2.6)$$

where ψ is the liquid volume fraction, u is velocity, and t is time. To prevent instability, the VOF method calculates an approximation of the free surface instead of an exact water level. The VOF method is commonly used in various cases of two-phase flow analysis and is a suitable method for the simulations included in this research (Shuyu Sun, 2020).

2.1.4 Mesh/Grid

When setting up a CFD analysis, a computational domain is defined. A computational domain is a volume where the behaviour of the fluids is simulated. The domain is then divided by a grid that defines small control volumes, and these subdomains are often called elements or cells. When creating a mesh for CFD, the grid resolution must be

appropriately fine so that the velocity does not change much from one control volume to the next (P. K. Kundu, 2016, p. 229).

A high-quality mesh is vital to the accuracy of the solution, which is why the meshing process is such an important part of the CFD analysis. However, getting a high-quality mesh with a high enough resolution for an accurate result while keeping the need for computational resources low is challenging. For some cases, using wall functions instead of a high-resolution mesh near wall boundaries may give satisfactory results, but this depends on the individual case's specifics. It is also not only the mesh resolution that defines the quality of a mesh, but also the skewness, smoothness and aspect ratio are among other attributes associated with mesh quality (ANSYS, 2012).

Another critical factor for the quality of the mesh is the shape of the control volumes and the connectivity between the control volumes. There are different ways of classifying a mesh, but it is generally defined as structured, unstructured or hybrid mesh. A structured mesh can, for 2D simulations, be expressed as a two-dimensional array and for 3D simulations as a three-dimensional array. That means that a structured mesh is divided by quadrilateral shapes in 2D and hexahedral shapes in 3D. An unstructured mesh may also be dived by a triangular element, as shown in Figure 2.1.

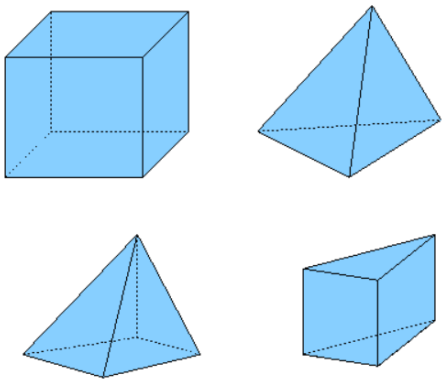

Figure 2.1 – Different 3D mesh elements (CFD Online, 2007)

The benefit of a structured mesh is far greater efficiency because it requires considerably less memory and easier data management due to the array storage and neighbour connectivity (Marshall Bern, 2000). However, it may be challenging to design a structured mesh for complex geometries. In these cases, a hybrid mesh is often applied. That means that the majority of the computational domain is divided by a structured mesh, and only the complex geometries are of an unstructured mesh.

In addition to the mesh structure, a few other attributes were mentioned that also decide the mesh quality. How these attributes influence the quality of a mesh depends on the solver used for the simulations. ANSYS Fluent is the chosen solver for this thesis. The recommended and maximum values for the attributes of skewness, smoothness, aspect ratio and y+ value are described in the ANSYS Theory guide:

Skewness

Skewness is the difference between the shape of a cell and an equilateral cell of the same volume. If a mesh consists of cells with a high level of skewness, this will negatively affect both the accuracy and the stability of a solution. According to the ANSYS Theory guide, the recommended maximum skewness should be below 0.95, and the average skewness should be kept within 0.33. The skewness of a grid may also be investigated by the orthogonal quality, which ranges from zero to one, where zero is worst and one is optimal.

Smoothness

The smoothness of a mesh is defined by the changes in cell volume by adjacent cells. If the difference in the volume of two neighbouring cells gets too substantial, it might lead to calculation errors. Therefore, adjacent cells should preferably not vary more than 20% in volume.

Aspect Ratio

Aspect Ratio is the ratio of the longest and the smallest distance from a cell centroid to a face centroid, and it is a way of quantifying the stretching of a cell. Ideally, the aspect ratio should be kept as low as possible, but according to ANSYS Theory Guide, the maximum aspect ratio should be kept below 35:1 (ANSYS, 2012).

Y+ Value

All of the mentioned attributes of the mesh may be checked within the ANSYS Meshing software. Another important concept for the meshing process is the dimensionless variable y+, which describes the distance from the wall to the first mesh node. Figure 2.2 illustrates the y+ value.

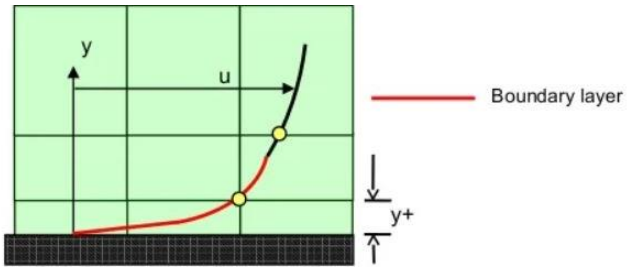

Figure 2.2 – y+ value (LEAP Australia, u.d.)

A y+ value ≈ 1 near the wall of the object exposed to the flow is recommended to achieve accurate results. However, this might require a very high resolution in the mesh, leading to more time-consuming computations. In these cases, wall functions can be utilized. According to LEAP CFD Engineering, the y+ value should ideally be more than 15 to avoid erroneous modelling in the buffer layer and the laminar sub-layer when using wall functions (LEAP Australia, 2020).

2.2 Wave Theory

To understand the effects of wave load, it is necessary to look at the wave theory describing the phenomena. This subchapter will present linear and nonlinear wave theory and the relationship between wavelength and wave frequency for intermediate waves.

2.2.1 Linear Wave Theory

For waves occurring in deep and intermediate waters, with a wave height much lower than the wavelength, the linear wave theory is applicable, assuming idealised properties and motions and gravitational force as the only external force. Linear wave theory is often called Airy wave theory after Sir George Biddell Airy, who first published the correct formulation in 1841 (Airy, 1841). For linear wave theory to be applicable, the following assumptions must be valid:

- The fluid must be considered inviscid
- The fluid must be homogenous and incompressible, which means that the fluid has a constant density (ρ)
- External effects like the Coriolis effect must be negligible
- The wavelength (λ) must be big enough so that surface tension is insignificant
- The pressure under the free surface area must be uniform and constant over time
- Water depth must be constant

Linear wave theory cannot be used for steep waves, short waves, or waves in very shallow waters. In these instances, other wave theories must be applied. Figure 2.3 illustrates when each of the different wave theories must be applied. T is the wave period, d is the water depth, λ is the wavelength, H is the wave height, and g is the gravitational acceleration.

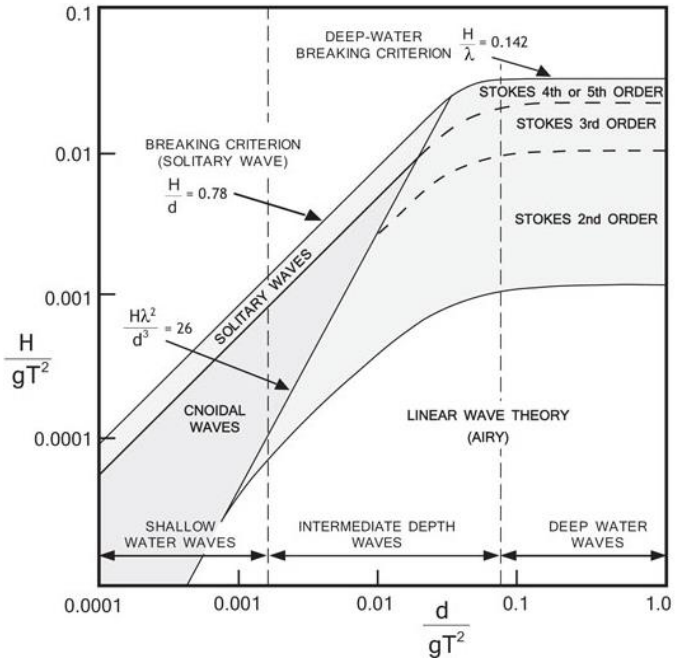

Figure 2.3 – Wave theories and when they are valid according to Le Méhauté (1976), (FLOW-3D, 2021)

Linear wave theory is based solely on a mass balance equation and a momentum balance equation. In Figure 2.4 below, a propagating harmonic wave is presented.

Figure 2.4 – Linear Wave

A propagating harmonic wave can be written as:

$$\eta(x, t) = \alpha \sin(\Omega t - Kx) \qquad (2.7)$$

Where t is time, α is the wave amplitude, K is the wavenumber defined by $K = 2\pi/\lambda$, and Ω is the angular frequency.

A wave with a harmonic surface profile only conforms to the basic linear equations and boundary conditions in linear wave theory. This means that the linear wave theory only approximates the nonlinear equations and boundary conditions. When the assumptions of linear wave theory are no longer valid, other more complex theories must be applied. For example, if the criteria for wave height compared to wavelength in linear wave theory get surpassed, Stokes (1847) and Dean (1965) theories should be used.

2.2.2 Nonlinear Wave Theory

When amplitudes get bigger compared to the wavelength, the linear wave theory gets less accurate. During the 19th century, Sir George Stokes developed the Stokes wave theory. The Stokes wave is nonlinear and may be modified by adding Stokes expansion up to the 5th order to account for the nonlinear effects. Figure 2.5 shows the 5th order Stokes wave compared to the linear Airy wave. Stokes wave theory is more accurate for a wider range of amplitudes and wavelengths. In addition, it gives a more realistic model for waves with a bigger amplitude propagating over an even seabed when compared to linear theory (Fenton, 1985).

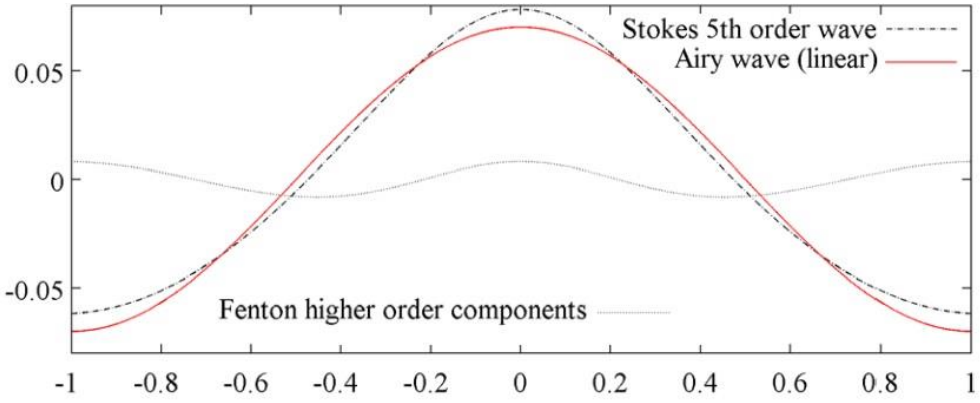

Figure 2.5 – 5th Order stokes wave compared to the airy wave

2.2.3 Wavelength and wave frequency

According to linear wave theory, there is a simple relation between wavelength and wave frequency, as described by formula 2.8.

$$\lambda = \frac{gT^2}{2\pi} \tanh\left(\frac{2\pi d}{\lambda}\right) \tag{2.8}$$

The formula may be solved for wavelength, λ , using iteration. T is the wave period, d is the water depth, and g = 9.81 m/s^2 is the gravitational acceleration. This relation is called the *dispersion* relation.

2.3 Models for wave load calculations

The calculation methods of the CFD software utilized in this project is based on three-dimensional fluid dynamics and the solving of Navier Stokes equations, specifically, Reynolds Averaged Navier Stokes equations, as described in chapter 2.1.1 and 2.1.2. However, there exist other methods and models for calculating the wave load. According to the DNV Class Guideline for Wave Loads (DNV, 2018), several other methods and approaches can be used to estimate wave-induced design loads.

The following methods are the most commonly used:

- Analytical calculations when the idealisation is considered valid
- Empirical relations when the basis is considered valid
- When viscous effects are negligible, 3-dimensional potential flow solvers

The Morrison equation (2.10) may be used to calculate the total force acting on a slender construction. The Morison equation is a summation of the inertia force F_i and the horizontal drag force F_d.

$$F = F_d + F_i \tag{2.9}$$

The force in the horizontal direction dF acting on an area with the length dz may be calculated by:

$$dF = \rho\, C_m\, \dot{u}\, dV + \frac{1}{2} C_d u|u| dA = dF_d + dF_i \tag{2.10}$$

Here C_m is the inertia force coefficient, C_d is the drag coefficient, ρ is the density of the fluid, u is the particle speed and $\dot{u}$ is the particle acceleration. However, when the construction size is large compared to the wavelength, it is no longer valid to rely on only the Morison equation to calculate the wave load. This is because the effects of diffraction and refraction have to be considered, as illustrated in Figure 2.6. When waves hit an obstacle, the waves will bend around the obstacle and refract in other directions.

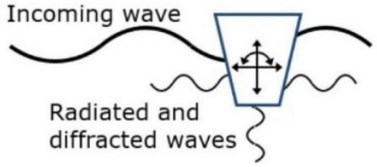

Figure 2.6 – Radiated and diffracted waves

The potential flow theory is used for calculating the wave loads for large volume structures. Potential flow is an idealized model that occurs when the fluid is inviscid, irrotational and incompressible. This model is used by different software for wave calculation, and in the case of SESAM, the solution is based on solving by applying Green's function formulation. Potential flow theory satisfies La Place's equation:

$$\nabla^2 \varphi(x, y, z, t) = 0 \tag{2.11}$$

SESAM is a software suite delivered by DNV. The software package consists of different tools made for analysing structures and hydrodynamics. The subprograms called WADAM and WASIM, provide hydrodynamical analysis based on the Morison Equation for slender structures and 3D potential theory for large volume structures.

It is also possible to combine the Morrison equation and potential theory when a structure is put together by parts consisting of large volumes and slender beams, which is often the case in modern engineering. For cylindrical structures, the forces induced by diffraction effects may be added and corrected by MacCamy-Fuchs diffraction:

$$C_M = \frac{4}{\pi (kR)^2 \sqrt{A_1}} \tag{2.12}$$

$$A_1 (kR) = J'^2_1 (kR) + Y'^2_1 (kR) \tag{2.13}$$

Here R is the radius of the cylinder, and J and Y are Bessel functions (Faltinsen, 1993).

3. Literature Review

As Chapter 2 gives an overview of the theory necessary to understand and research the topics of waves and wave loads, this chapter will go through some of the academic research done on the same subject, and perhaps provide valuable knowledge and inspiration regarding the design of experiments and experimental method for this research. The results of the literature review are presented in section 3.1.

3.1 Literature Review

In 2020 The International Journal of Naval Architecture and Ocean Engineering published a research paper called "Experimental and numerical study on the wave force calculation of a partially immersed horizontal cylindrical float". This research was done by Bijin Liu, Danjuan Fu, Youquan Zhang, and Xiaoyun Chen and takes a deeper look at wave loads specifically affecting the floating litter collectors consisting of polyethylene cylinders that are being used around the world. By modifying the Morison equation so that it is applicable for a semi-submerged cylinder, they calculate the wave loads for different wave periods, amplitudes and submerge levels. The results are then validated through scaled experiments in a running water tank with a wave generator.

The validation process provides encouraging results, and so the analysis proceeds. The influence of wave height change on the wave force shows that larger wave heights give a greater output in wave load, and the positive distribution of the wave force is larger than the negative. Furthermore, Bijin Liu et al. research shows that as the wave period increases, the drag force of the wave decreases. After evaluating the results and comparing them with experiments, it is concluded that a modified Morison equation can accurately predict the wave force on a semi-submerged, horizontally placed cylinder (Bijin Liu, 2020).

In 2017 the Coastal Engineering journal published the research "Solitary wave-induced forces on horizontal circular cylinders: Laboratory experiments and SPH simulations" by authors Francesco Aristodemo, Domenico Davide Meringolo, Giuseppe Tripepi and Paolo Veltri. This paper looks at the hydrodynamic forces on submerged horizontal circular cylinders induced by solitary waves. The experimental tests of the research were performed in the hydrodynamical laboratory of the University of Calabria. A cylinder is

placed horizontally and transversely against the flow direction, 9 meters from the wavemaker. Inside the cylinder, pressure transducers are mounted and measuring pressure changes at 12 evenly placed points around the cylinder.

Aristodemo et al. also performed a numerical study, opting for the computational method of *Smoothed Particle Hydrodynamics* (SPH). SPH is a Lagrangian simulation method that requires no mesh and is suitable for multiphase flows (Steven J. Lind, 2020). After executing both the simulations and the laboratory tests, the agreements between numerical analysis and experiments are deemed "quite satisfactory" in terms of force magnitude and phase. After analysing the numerical and experimental data results, it is concluded that the drag force initially (when $0.05 < A/d < 0.25$) increases as the amplitude increases. A/d is the dimensionless wave amplitude, where A is amplitude and d is the water depth of the tank. However, as the amplitude increases further, this effect is reversed after $A/d > 0.25$ (Aristodemo, 2017).

Another interesting research paper on the subject was published by *The Indian Journal of Engineering and Materials Sciences* in 2001. Dr Gazi Khalil is the author who presented the study "Experimental investigation of wave forces on submerged horizontal cylinders". Dr Khalil performed his experiments in the towing tank of the University of Tokyo, investigating wave forces on a cylinder placed horizontally and transversely against the wave. Two different cylinders were tested, one circular and rectangular. In addition, the different cylinders were tested at different submersion levels, and a multi-component loadcell measured the forces.

The research concludes that the breaking of waves behind a semi-submerged cylinder is the reason for non-linear wave forces and that the negative drifting force on the cylinder is a direct consequence of this. This effect is more significant for the rectangular cylinder than the circular cylinder. However, when the cylinder is deeply submerged ($D/B > 2$, where D is the depth of the cylinder centre, and B is the cylinder radius), the effect of the negative drift force disappears (Khalil, 2001).

There are different methods of performing experimental, numerical or theoretical studies of the wave load. For example, some studies design the hydrodynamical experiments in a two-dimensional setup, like the research of Bijin Liu et al. Other researches include three-

dimensional effects, like the case of Aristodemo et al. This depends on the available facilities and the objectives of the investigation.

In terms of numerical and theoretical analysis of the wave load on a cylinder, both CFD methods and the more traditional Morison and potential theories may be relied upon.

4. Wave Load Simulations

Chapter 4.1 will cover the design of experiments, including the investigated variables, the number of samples, and the limitations of experiments, and chapter 4.2 will cover the software programs used for CFD simulations, 3D modelling and data analysis. Then chapters 4.3 and 4.4 will present the procedure of setting up and executing the CFD analysis of the wave loads, for 2D and 3D respectively.

4.1 Design of Experiments

The objectives of this thesis are to investigate the wave load. As described in chapter 1, a cylinder is a commonly used geometrical shape for structures in marine engineering. By exposing a cylindrical shape to waves and fluid flow and then measuring or calculating the resulting drag or lift force, valuable data and insight may be gathered.

The influence on the wave load of the following parameters is to be studied:

- Wave Amplitude
- Wave frequency/length
- Flow speed
- Submersion/water level

CFD analysis is a commonly used method to gather data and will be used for this research. However, as a comprehensive CFD study is a very time-consuming process that requires a lot of computational power, there are some definite limitations when investigating a number of different parameters.

To be able to thoroughly validate the data gathered from CFD, the experiments should ideally be tested physically. This is also a time-consuming process, where the experimental setups must be altered depending on the specifics of the case. For example, if a parameter like flow speed is substantially altered, the loadcell must be replaced, and the entire setup must be disassembled and recalibrated. Many different students and researchers also need access to the MarinLab at HVL, so it is only available for a limited time for each student.

Due to these limitations, the parameters of amplitude and wave frequency/length are only tested for three different values. Amplitudes of 0.04 m, 0.06 m, and 0.08 m are tested,

along with frequencies 0.3 Hz, 0.4 Hz and 0.5 Hz. The flow speed is tested at 0.0 m/s, 0.5 m/s, 0.75 m/s and 1.0 m/s.

Because of the aforementioned limitations, as well as technical limitations of the available equipment of the testing facilities, the MarinLab experiments were executed for two cylinders of different diameters, measuring drag force only. The experimental setup is illustrated in Figure 4.1.

Submersion levels +2 cm, +1 cm, 0 cm, -1 cm and -2 cm are investigated using CFD analysis, where 0 cm is when exactly half the cylinder is submerged. When analysing changes in submersion level, this is done after processing and analysing all other experiments and simulations. That way, the cases that showed the highest level of validity may be chosen. In these cases, there are no experimental data to compare with. However, the CFD data for submersion level 0 cm is deemed to be of high quality, and it is assumed that the small changes in water level do not significantly affect the validity of the data.

The validation process of the thesis is described in depth in Chapter 6.3, and complete testing and simulation plans for both CFD and experiments are presented in Appendix A-10.1.

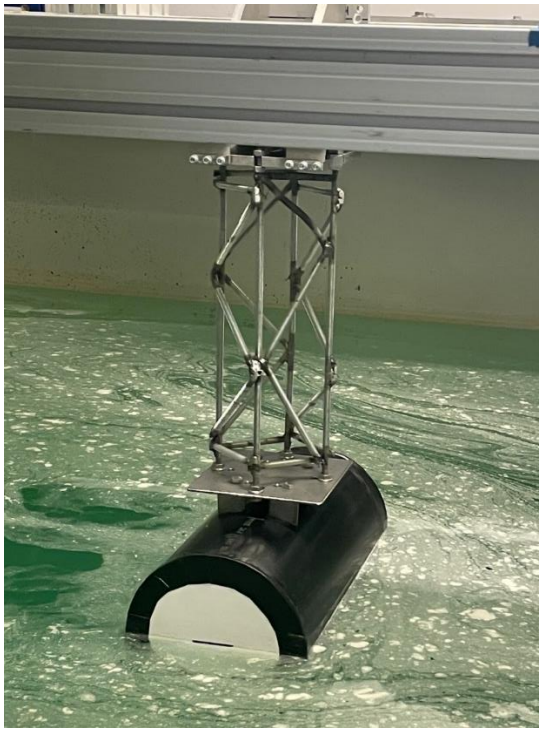

Figure 4.1 – Experimental setup of the Cylinder

4.2 Software

This chapter will present all the software used for simulations, 3D modelling, CFD, data analysis, and data presentation. A big part of this research is simulating wave forces using CFD and analysing all the gathered data. A few different software is utilized to complete this phase of the project:

4.2.1 ANSYS

This thesis uses the commercial simulation software ANSYS for the CFD simulations. The ANSYS software is based around the program hub called Workbench, which relates different subprograms suited for the different parts of the process. The ANSYS program modules called CFX and Fluent can be utilized for CFD analysis. In work surrounding this thesis, ANSYS Fluent is most suited for wave generating and open channel flow and is therefore chosen for these simulations. CAD software is used to adjust or create geometry and fluid domains. The implemented program modules *DesignModeler* and *SpaceClaim* may be used for this purpose. ANSYS workbench also has a program module for mesh, allowing for efficient and easy generation and adjusting of the model's mesh or grid. Before running a simulation, the parameters must be set. The parameters are set in the ANSYS Fluent solver. Boundary conditions, turbulence model and materials are adjusted in *SETUP* and monitors, and initialization and calculation details are set in *SOLUTION.* Ansys Fluent also have a built-in post-processor, but the simplicity of CFX-post is preferred when extracting and analysing simulation results.

4.2.2 PTC Creo Parametric

The ANSYS software has two different software built-in for 3D modelling features in their portfolio, but PTC Creo Parametric is used for more advanced requirements. Creo is a powerful 3D CAD software developed by the American computer software and service company PTC Inc, formerly known as Parametric Technology Corporation. Creo Parametric is the main program hub and is used for solving a wide range of different 3D modelling and design needs. It is a widely used tool and will be used for geometry modifications and 3D modelling of the experimental design.

4.2.3 MATLAB

Most of the plots presented in this thesis are made using MATLAB. The data from both experiments and simulations are stored in .txt files, which are then read through MATLAB code and presented and plotted in various ways. MATLAB is a commercial programming

and numeric computing platform developed by MathWorks. The software is widely used by engineers, scientists, and students to plot and present data, analyse, develop algorithms, and create models (MathWorks, 2022).

4.3 ANSYS FLUENT: 2D Simulations

This chapter will cover the procedure when setting up and executing CFD analysis for wave load on a cylinder in a 2-dimensional state, using ANSYS Fluent as a solver.

4.3.1 Fluid domain

The flow domain is created in DesignModeler, with the cylinder placed in an open channel flow. The computational domain is modelled after the MarinLab at HVL, presented in chapter 5.1.1. The fluid domain is presented in Figure 4.2, and it has a length of 15 m and a total height of 4.5 m. The water level is set at 2.5 m, and the cylinder centre is placed at [10 m, 2.5 m]. The area around the cylinder is sliced into different parts, as shown in Figure 4.2, to prepare for producing a uniform mesh.

Figure 4.2 – Fluid Domain

The dimensions are set as Input Parameters, as shown in Figure 4.3, so they may easily be modified during testing. Initially, the cylinder was intended to be of a diameter of 1500 mm. However, due to restrictions for validation tests in MarinLab, the cylinder model is changed to 200 mm diameter. This change in dimensions requires a different mesh than the initial geometry, and the model is built so that the mesh can easily be modified.

Table 4.1 – Dimensions set as Input Parameters

Outline of All Parameters

	A	B	C	D
1	ID	Parameter Name	Value	Unit
2	Input Parameters			
3	Fluid Flow (Fluent) (A1)			
4	P1	tank_length	15000	mm
5	P2	tank_heigth	4500	mm
6	P3	cylinder_pos_Y	2500	mm
7	P4	cylinder_pos_X	10000	mm
8	P5	cylinder_dia	1500	mm

4.3.2 Mesh

As the fluid domain is sliced in parts and prepared for mesh, the function edge sizing is applied so that the mesh can gradually decrease in size when nearing the cylinder. The edge sizing around the cylinder is shown in Figure 4.3 (a, b).

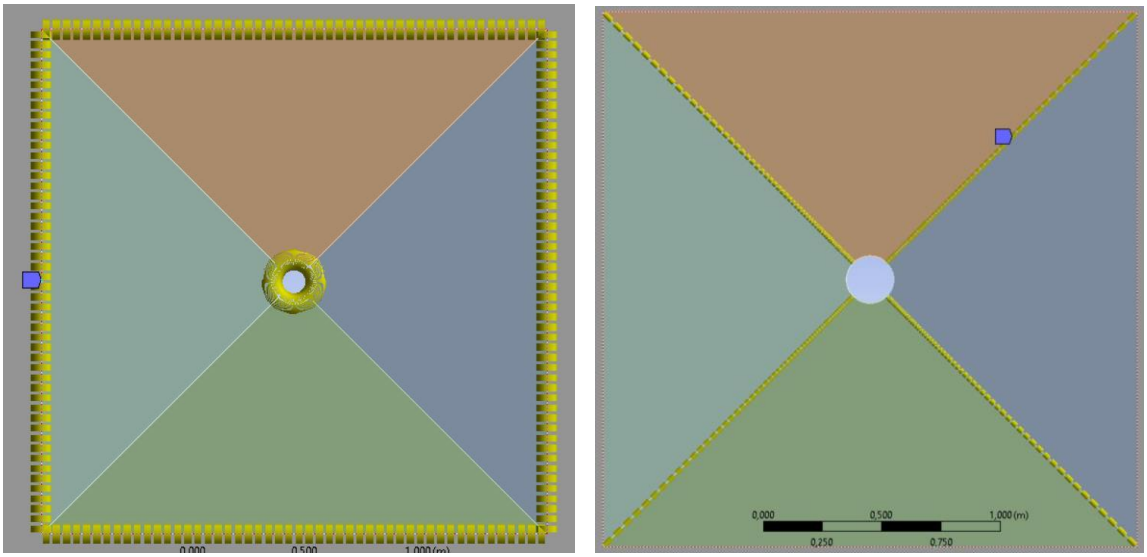

Figure 4.3 (a, b) – Edge sizing around the cylinder

These functions allow for easy mesh manipulation after running initial tests to investigate the y+ value near the cylinder. After running tests and checking y+ values and simulation times, the final mesh is presented in Figure 4.4 (a, b).

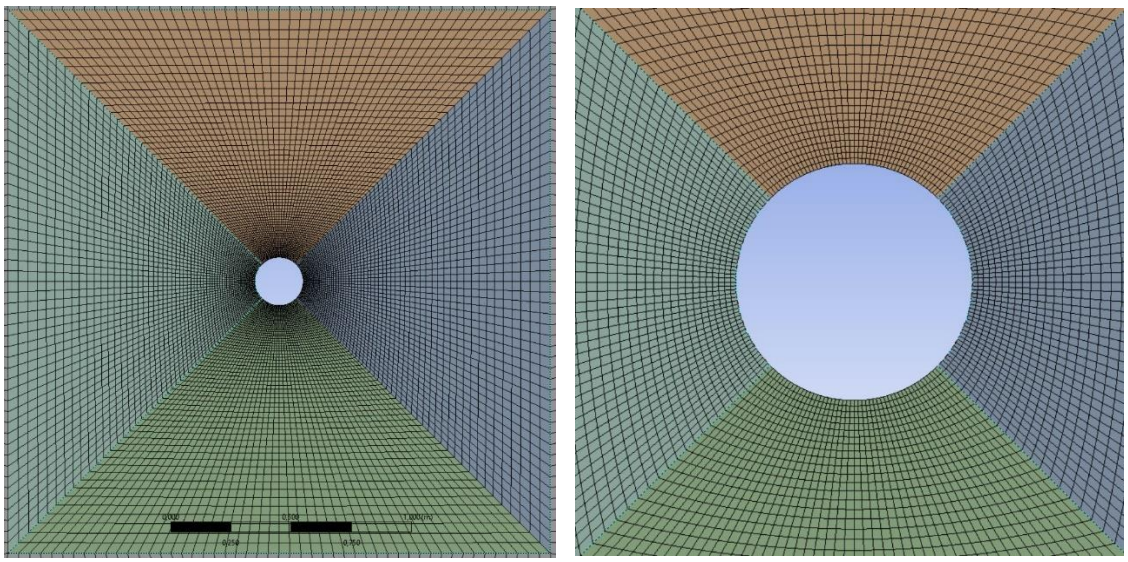

Figure 4.4 (a, b) – Close up: fine mesh near cylinder wall

As described in chapter 2.1.4 about mesh, the desired y+ value near the cylinder wall is ≈ 1 to capture the laminar sub-layer. In this research, a total of 72 different simulations are

going to be executed. Depending on the specific case, they may take up to 72 hours to run. Instead of running every simulation several times and adapting the mesh for each case, the same mesh is used for all simulations. In order to achieve an appropriate mesh for all cases, a few of the most turbulent cases are checked. The most turbulent scenarios are assumed to be the cases where the flow speed, amplitude and frequency are highest. The Y+ value is then checked at a timestep when the wave is fully developed and hitting the cylinder. The contour of the y+ value is found through the Fluent post-processing, and an example of a case is shown in Figure 4.5, where the y+ value is 1.34 near the cylinder.

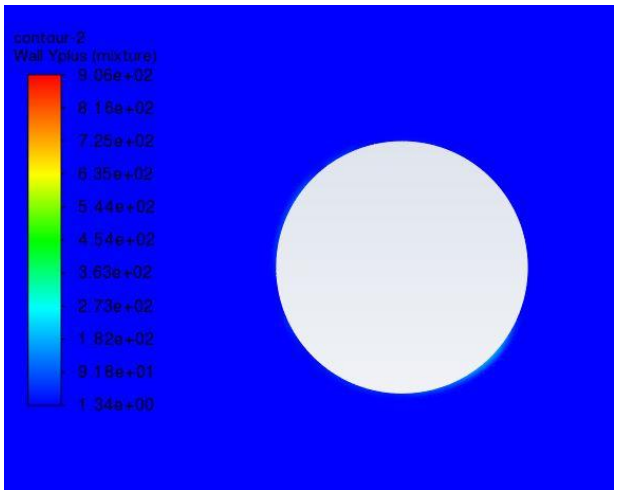

Figure 4.5 – Contour of y+ value

The final mesh of the entire domain is shown in Figure 4.6, and it consists of a total of 23933 nodes and 23579 elements.

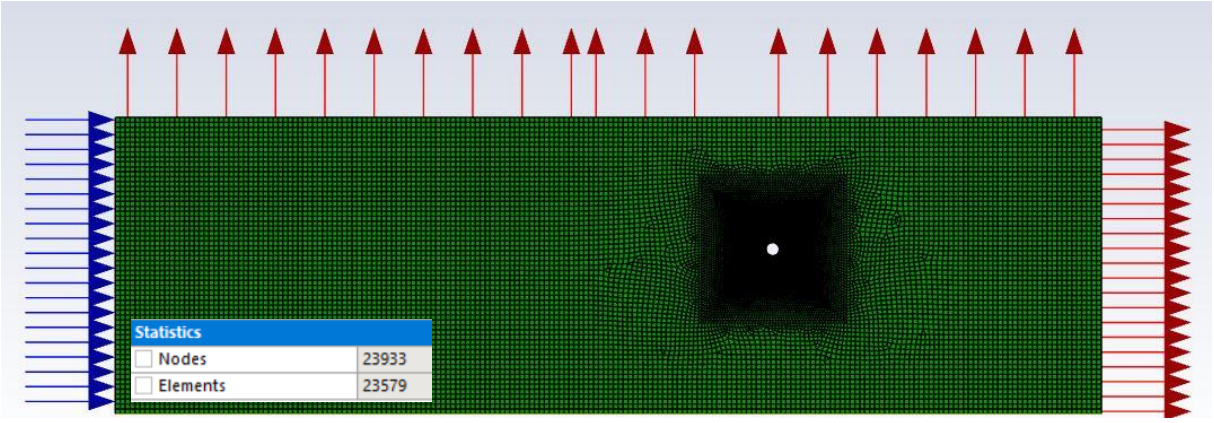

Figure 4.6 – Mesh of entire domain, with very high mesh resolution near cylinder wall

The quality of the final 3D mesh is then further investigated by looking at the aspect ratio, skewness, and smoothness of the mesh. This investigation is based on the Mesh theory described in Chapter 2.1.4.

Tables 4.2-4 are extracted from ANSYS Mesh. Table 4.1 shows that the maximum aspect ratio is 2.78, which is well within the recommended maximum value of 35. The average aspect ratio is 1.22, quite close to the ideal and lowest possible value of 1.

Table 4.2 – Aspect Ratio 2D Mesh

Mesh Metric	Aspect Ratio
Min	1
Max	2.7758
Average	1.2189
Standard Deviation	0.28666

From Table 4.3, the orthogonal quality is reported to have an average of 0.96, quite close to the ideal. The minimum value is 0.71.

Table 4.3 – Orthogonal Quality 2D mesh

Mesh Metric	Orthogonal Quality
Min	0.71217
Max	1
Average	0.95839
Standard Deviation	0.0661

The average skewness of the cells in the mesh is 0.13, well within the recommended 0.33. The maximum skewness of the 2D mesh is 0.52, and it is also well within the recommended 0.95.

Table 4.4 – Skewness of 2D mesh

Mesh Metric	Skewness
Min	$1.3057 \cdot 10^{-10}$
Max	0.5246
Average	0.12601
Standard Deviation	0.14455

4.3.3 Solver Settings

This subchapter will go through the solver settings used for the 2D simulations. That includes general, multiphase, viscous, and material settings and boundary conditions.

The solver is set to pressure-based. According to ANSYS User Guide, this setting is more suitable for incompressible and mildly compressible flows. The simulation settings are set to transient and multiphase, applying a volume of the fluid model, with the Ansys Fluent sub-models Open Channel Flow and Open Channel Wave BC activated. The two-phased flow consists of the two fluids: air with a constant density of 1.225 kg/m^3 and a constant viscosity of $1.7894*10^{-5}$, and freshwater with an assumed constant density of 998.2 kg/m^3. SST k-omega is chosen as the turbulence model, and the gravitational acceleration is set to 9.81 m/s^2.

As shown in Figure 4.6, there is an inlet marked with blue arrows, which is defined as a velocity inlet. A pressure outlet is applied on the top of the domain and the opposite end from the velocity inlet. The free surface flow is set in both outlet and inlet, and the specific wave and flow parameters are set in the velocity inlet.

4.3.4 Setup

This chapter will present the solver setup, including report definitions, initialization settings and calculation settings. This section will also cover wave theory checks, checking if the model is correct (calculating buoyancy force).

Under report definitions, the solver is set to save a force report for drag and lift at every timestep of the simulation. The initialization is set to hybrid and is computed from the channel's inlet. The hybrid initialization method consists of different methods for boundary interpolation, and it solves the Laplace equation to produce a pressure and velocity field that suit the specific computational domain. The standard initialization method requires these initial values to be defined manually.

After the initialization, the simulations are set to run for 14000 timesteps. The timestep size is 0.005 seconds, with a maximum of 20 iterations per timestep. This results in a 70-second simulation, which takes the computers at the HVL computer lab about 12 hours to calculate. Finally, the calculated drag and lift forces are stored in text files, ready for analysis.

To check if the intended wave theory is valid, the Ansys Fluent has an implemented wave theory check. This theory check evaluates whether current wave parameters and wave theory are applicable. Validation of wave theories is described in Figure 2.3 in chapter 2.2.1 – Linear wave theory.

After running the wave checks for the different waves in the simulation plan in Table 10.4 (Appendix A), it is concluded that the Airy Wave theory is valid for every wave except those of amplitude 0.08 m and frequency 0.5 Hz. In those cases where the Airy Wave theory is not applicable, the fifth-order Stokes theory is applied.

As the 2D simulations were initially finished before the validation experiments in MarinLab, a simple analysis of the calculated lift force is performed on the original cylinder of 1500 mm diameter. This test is done by calculating the buoyancy force of the cylinder and comparing it with the lift force from the first simulation.

Buoyancy force, F_B, is found by the formula (4.1):

$$F_{Buoyancy} = V \cdot \rho_{Fluid} \cdot g \qquad (4.1)$$

In this case, the water height is 2.2 m, and the cylinder centre is placed at 2.5 m. V is the volume of liquid displaced, commonly referred to as the *Displacement Volume,* and in this case, V = 1m x 0,4459 m^2. The letter g is the gravitational acceleration, and ρ_{Fluid} is the density of the fluid. For this spesific case, ρ_{Fluid} = 1025 kg/m^3 and g = 9.81 m/s^2. This results in F_B = 4483 N. The submerged volume of the cylinder is displayed in Figure 4.7, where the isosurface is shown. The red colour indicates the water, and the blue indicates the air.

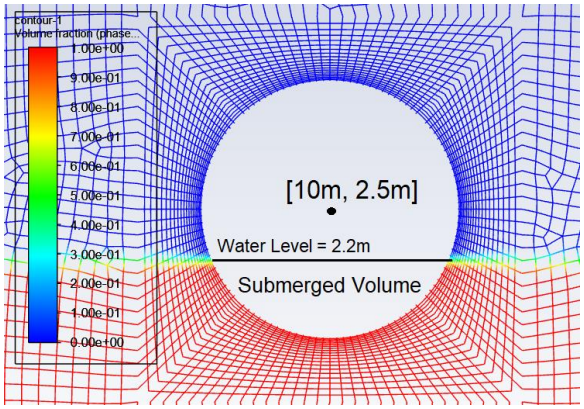

Figure 4.7 – Isosurface of the CFD model, red is water and blue is air

The buoyancy force was compared to the calculated force on the cylinder from the simulation test, as shown in Figure 4.8. The blue line indicates the buoyancy force, and the red line indicates the lift force plotted against time.

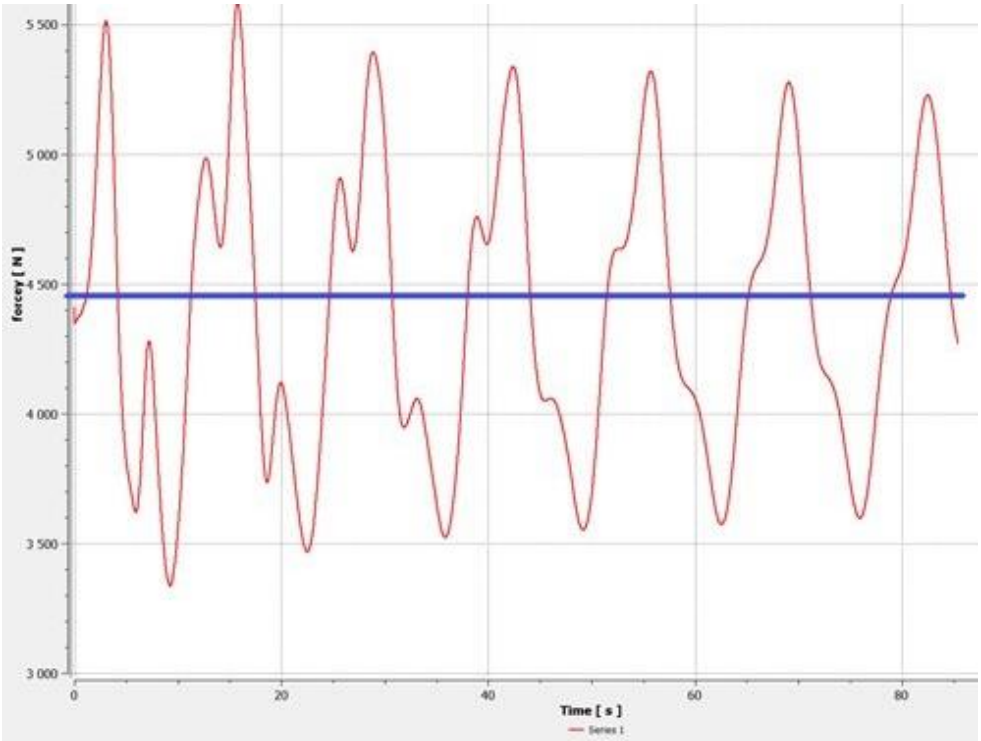

Figure 4.8 – Blue line indicates buoyancy force 4483 N, and red is the lift force

When comparing the lift force with the buoyancy force, it is observable that the lift force fluctuates around 4500 N, depending on the placement of the wave relative to the cylinder. This is as expected when the buoyancy force was calculated to be 4483 N.

A similar test is performed for the final simulation model, but in this case, the simulation is changed from transient to steady. In the report definitions, the lift force is set to be calculated. Then the simulation is run, resulting in a calculated 153.5 N force acting on the cylinder.

Comparing this to the calculated buoyancy force for the smaller cylinder, which is half-submerged and with a diameter of 200 mm. The cylinder then has a displacement Volume V = 1m x 0.0157 m^2, while the density of the fluid in this case equal 998.2 kg/m^3 and gravitation = 9.81 m/s^2, and when put into formula (4.1) finally results in F_B = 153.8 N.

These simple tests indicate that the 2D model may be accurate, and all 36 simulations are ready to be executed and will be further validated in chapter 6.3.

4.4 ANSYS FLUENT: 3D Simulations

This chapter will cover the procedure when setting up and executing CFD analysis for wave load on a cylinder in a three-dimensional state, using ANSYS Fluent as a solver. First, in chapter 4.4.1, the fluid domain is presented. Then in chapter 4.4.2, the mesh is presented, and in chapter 4.4.3, the solver settings are presented. Finally, in chapter 4.4.4, the setup and execution of the simulations are presented.

To be able to confirm the validity of the results, the simulations must be set up in a way that makes them able to be replicated for experiments in MarinLab. That means that the limitations of the MarinLab facilities also must be considered for the simulations. According to Jan Bartl, associate professor at HVL and responsible for the MarinLab department and lab engineer Harald Moen, there are some geometrical limitations. To have negligible effects from sidewall reflections, the model must not exceed a width of 400 mm. Of course, this depends on several parameters, such as the model shape or the tow speed. Furthermore, wall effects from experiments in waves are more complicated than in calm water, as shown by the research of Zhi-Ming Yuan et al. (Yuan, 2018). Still, after conferring with the MarinLab specialists, it is assumed that a cylinder of 400 mm width should have negligible side wall effects.

There is also a limited amount of loadcells for measuring force loads, and the most suitable for these tests is a 100 N loadcell. This means that the drag force values for the CFD simulations should not exceed the value of 100 N, and the flow speed and wave parameters must be set accordingly.

4.4.1 Fluid Domain

The fluid domain is modelled according to the International Towing Tank Conference (ITTC) guidelines and dimensions after the MarinLab facilities. A cylinder with a diameter of 200 mm and a length of 400 mm is set up horizontally with the long side towards the fluid flow, as illustrated in Figure 4.9.

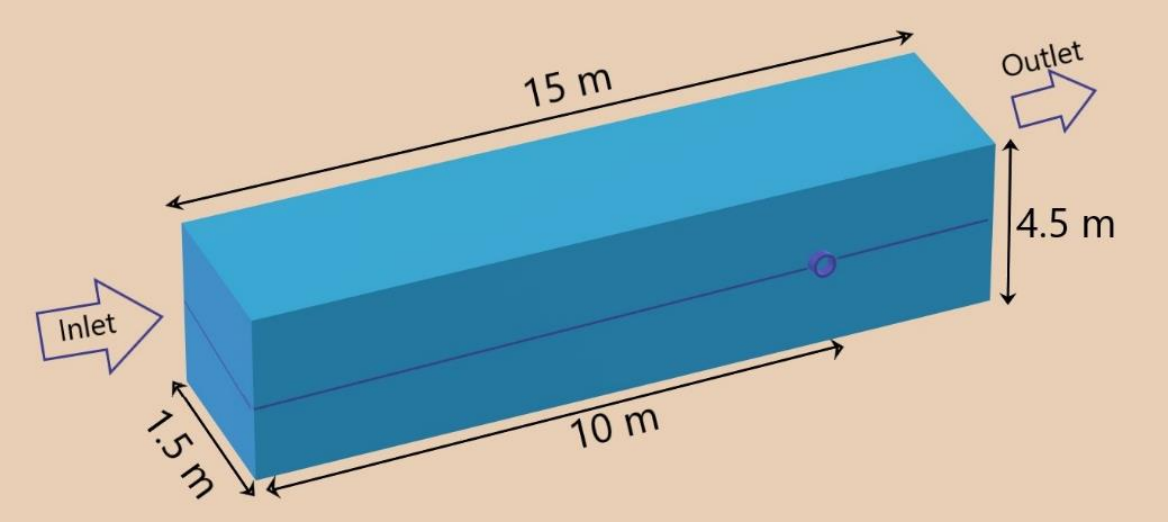

Figure 4.9 – Fluid Domain Illustration

The computational domain should be sufficiently large, which is especially important for blunt bodies (ITTC, 2017).herefore, the total length of the domain is set to 15 m, and the height to 4.5 m. The setup is symmetrical in the XY-plane, so the fluid domain may be modelled in half to speed up computational time. This means that the width of the domain is set to 1.5 m.

The centre of the cylinder is placed at 10 m from the inlet to allow the flow to stabilize. The fluid domain is also modelled as similar as possible to the MarinLab in HVL to be able to validate the results through hydrodynamical experiments. From the centre of the cylinder and to the outlet measures 5 m. When comparing the dimensions of the fluid domain to the cylinder dimensions, and the placement of the cylinder, this should be well within the guidelines of the ITTC.

The fluid domain is 3D modelled using the *DesignModeler* software module. The dimensions are as described in the last paragraph. In addition, the fluid domain is split into different parts to allow for different edge sizing of the mesh, which is essential to achieving a high-quality mesh. The entire fluid domain, including the split up parts, is presented in Figure 4.10.

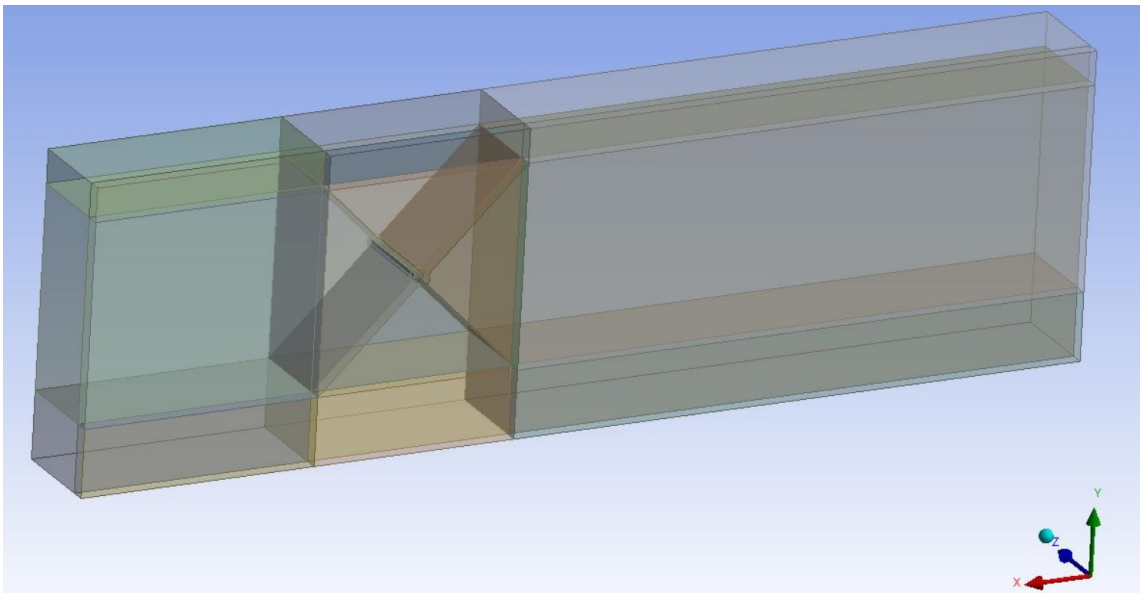

Figure 4.10 – Actual 3D Fluid Domain from ANSYS Mesh

4.4.2 Mesh

The geometry constructed in *DesignModeler* is imported into the ANSYS Mesh software. The resolution of the mesh is adjusted so that the cell size gets smaller closer to the boundary of the cylinder and around the surrounding area. This adjustment is made in all three directions (x, y, z), using the functions of edge sizing and face mesh. Figure 4.11 shows the finished mesh of the entire computational domain.

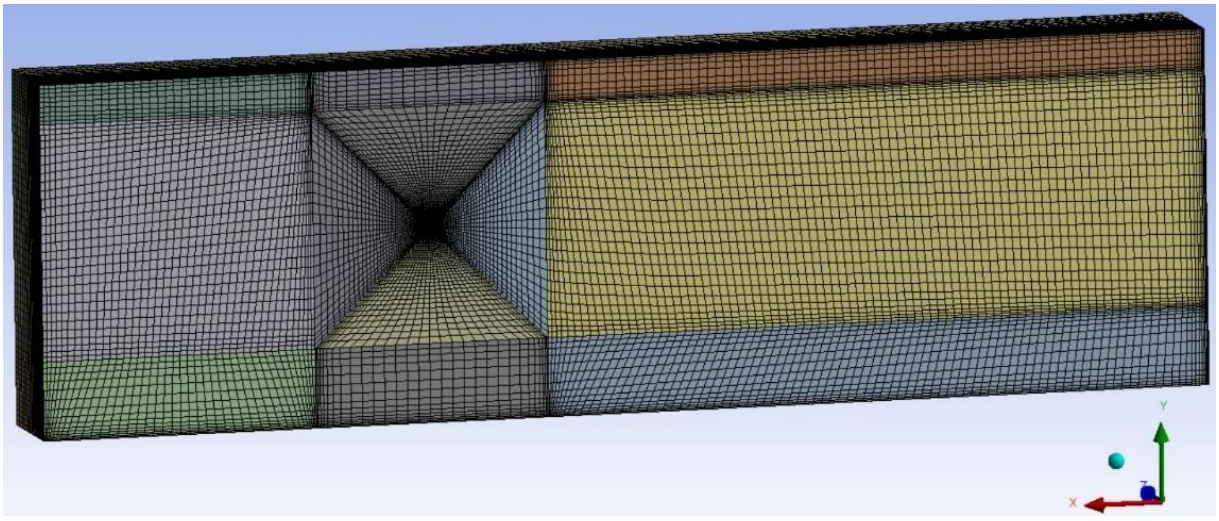

Figure 4.11 – Mesh of entire computational domain

Closer to the boundary of the cylinder, the mesh is significantly increasing in resolution, as illustrated by the close-up screenshot in Figure 4.12.

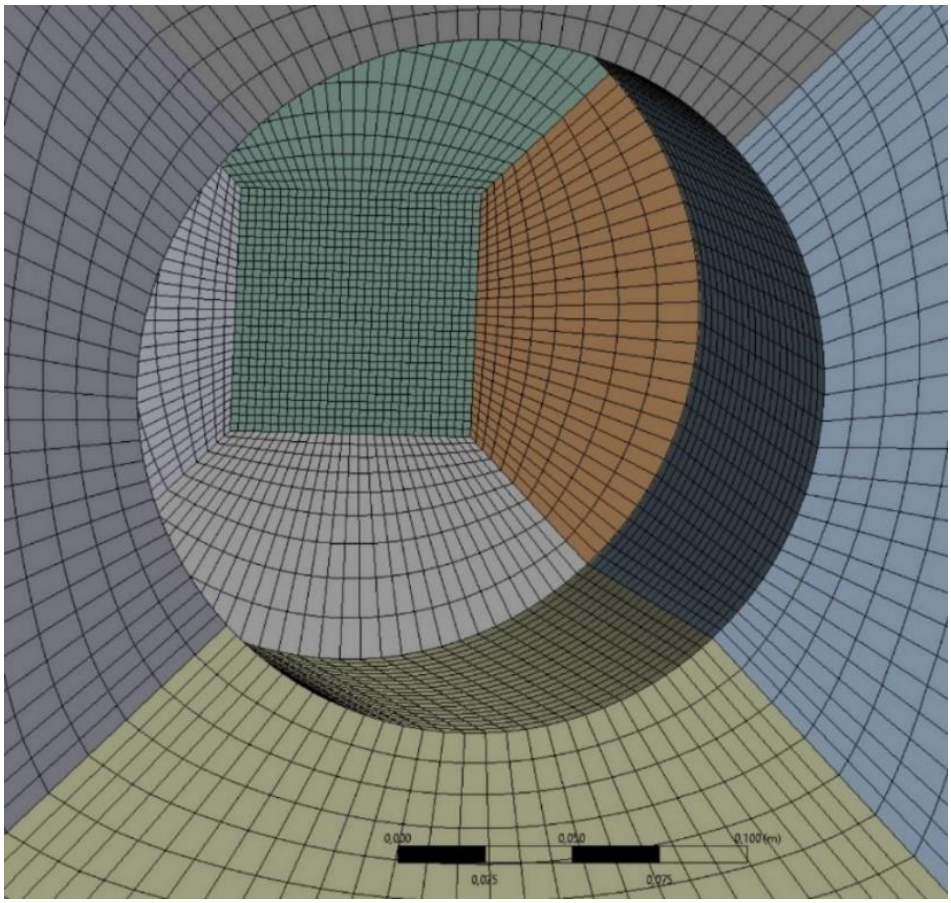

Figure 4.12 – Finer mesh resolution close to a cylinder boundary

The total number of cells of 554 640 and 579 655 nodes is high enough to ensure the accuracy of computations but within the realm of acceptable computational time.

Due to limitations in computational power, it is not possible to refine the mesh with a low enough resolution near the cylinder wall so that the y+ value is 1. So instead, the calculation will rely upon the automatic wall functions of the SST k-omega model, which are implemented in the Ansys Fluent solver.

With the importance of the y+ value described in chapter 2.1.4 in mind, the y+ value for the 3D model is inspected at several different flow speeds and wave parameters and checked that the dimensionless value is indeed above 15. The y+ value is checked when the wave is fully developed, and screenshots of the y+ contour at the cylinder are shown in Figures 4.13 and 4.14 for wave 23 and wave 8, respectively.

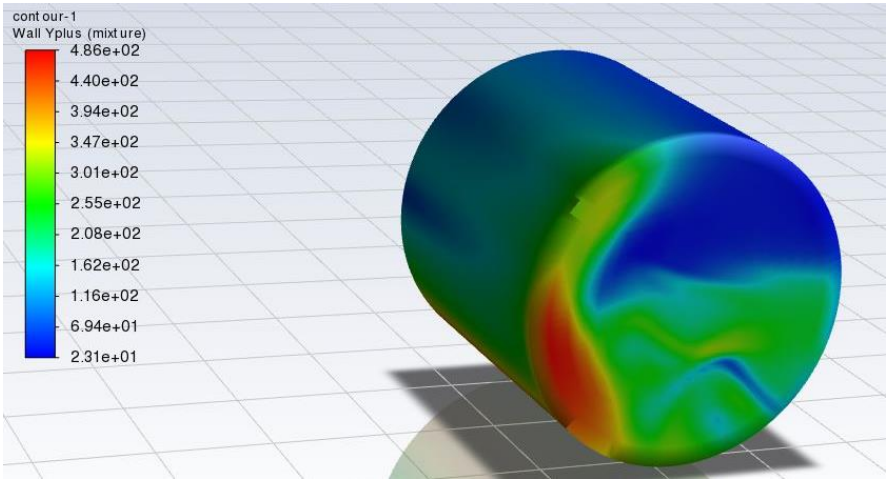

Figure 4.13 – Y+ contour at wave 23

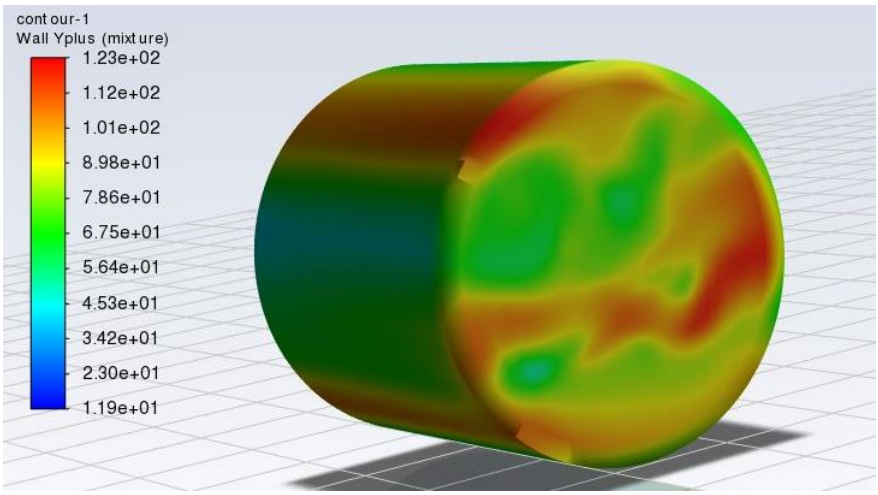

Figure 4.14 – Y+ contour at wave 8

The quality of the final 3D mesh is then further investigated by looking at the aspect ratio, skewness, and smoothness of the mesh. The data presented in Tables 4.5-7 is extracted from ANSYS Mesh. Table 4.5 shows the aspect ratio for the 3D mesh.

Table 4.5 – Aspect ratio 3D mesh

Mesh Metric	Aspect Ratio
Min	1.0025
Max	73.179
Average	7.4746
Standard Deviation	7.8615

The maximum aspect ratio is 73.18, which is over the recommended maximum value of 35. However, the high aspect ratio cells are situated near the wall opposite the cylinder, as shown in Figure 4.15.

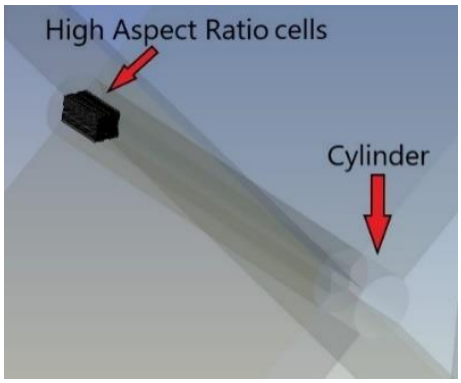

Figure 4.15 – High Aspect Ratio cells position

Though the high aspect ratio cells near the wall may lead to inaccurate modelling of the flow in that surrounding area, it is assumed that it will have little influence on the calculated force on the cylinder. The average aspect ratio is 7.4746, well within the recommended max value of 35.

From Table 4.6, the orthogonal quality is reported to have an average of 0.92839, with a minimum value of 0.36775.

Table 4.6 – Orthogonal Quality 3D mesh

Mesh Metric	Orthogonal Quality
Min	0.36775
Max	1
Average	0.92839
Standard Deviation	0.095394

The positions of the cells of lower orthogonal quality are shown in Figure 4.16 and are not near the area of interest marked with red. It is therefore assumed to have little impact on the calculated wave load.

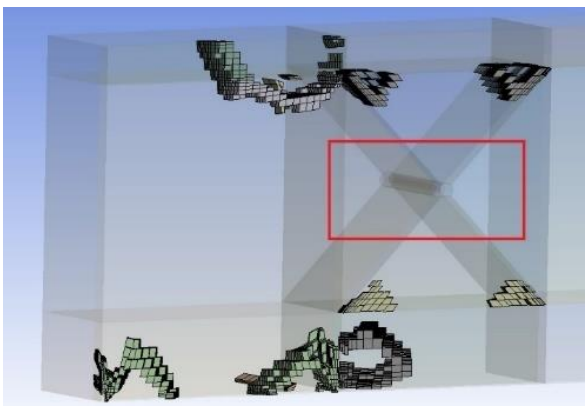

Figure 4.16 – Position of cells of lower orthogonal quality

For the 3D CFD model, there are more limitations in terms of computational resources, so a few suboptimal aspects like those mentioned above can be tolerated.

Table 4.7 – Skewness 3D mesh

Mesh Metric	Skewness
Min	$1.3057 \cdot 10^{-10}$
Max	0.76141
Average	0.18947
Standard Deviation	0.15175

The average skewness of the cells in the mesh is 0.18947, well within the recommended 0.33. The maximum skewness of the 2D mesh is 0.76141, and it is also well within the recommended 0.95.

4.4.3 Solver Settings

This subchapter will go through the solver settings used for the simulation. That includes general, multiphase, viscous, material settings, and boundary conditions.

A multiphase flow is applied, consisting of freshwater with $\rho_{freshwater}$ = 998.2 kg/m^3 and air with ρ_{air} = 1.2 kg/m^3. The fluent solver is set to use a volume of the fluid model, with the sub-models Open Channel Flow and Open Channel Wave BC settings activated. Gravitational acceleration is set to 9.81 m/s^{2,} and the simulation is set to transient. The k-ω SST turbulence model is applied with a turbulence intensity of 0.05, and the turbulence length scale is set to 0.01. The Open Channel Wave BC is activated in the velocity inlet and the pressure outlet for the settings concerning inlet-outlet boundary conditions. The water level is set to be at 2.5 m, precisely at the centre of the cylinder. Symmetry is applied.

4.4.4 Setup

In this subchapter, the calculation setup of the simulations is presented. This includes report definitions, initialization settings and calculation settings.

The lift and drag forces are stored in a .txt file at every timestep. The simulation is set to run in timesteps every 0.01 seconds, with a maximum of 20 iterations per timestep. A maximum number of timesteps is set to 6000, meaning that the simulation length is one minute. The files then reach around 900 GB, just within the available 1 TB hard drives of the computers in HVLs computer lab.

Hybrid initialization is activated, assuming a calm water surface before the simulation starts. Similar to the case of 2D, The Fluent solver has a built-in wave theory check, which validates the current wave parameters and wave theory. Validation of wave theories is described in Figure 2.3 in chapter 2.2.1 – Linear wave theory.

After investigating which wave theory fits each wave in the simulation plan, the Airy wave theory is assumed for waves with an amplitude of 0.04 m and 0.06 m for all frequencies and waves with an amplitude of 0.08 m at frequencies 0.3 and 0.4 Hz. Next, waves of the amplitude of 0.08 m and a frequency of 0.5 Hz are set to Stokes fifth-order wave theory. In Ansys Fluent, the waves are defined by wavelength and wave height. However, in the wavemaker software for MarinLab, the waves are defined by amplitude and frequency. The dispersion relation is used to calculate the wavelength from the frequency. This relation is described in chapter 2.2.3.

Each case's wave and flow parameters are set in the velocity inlet boundary condition. All wave and flow parameters are described in the simulation plan in Appendix A – 10.4.

5. Validation of Wave Models in Wave Tank

The objective of these experiments is to apply wave loads on a cylindrical object and acquire as much data as possible. Next is to analyse the acquired data and investigate the wave load regarding changes in wave parameters, flow speed, and cylinder dimensions. Finally, the physical experiments also need to be performed to validate the CFD simulations and analysis of the wave loads done in ANSYS.

5.1 Testing facilities and equipment

This chapter covers the experimental method, the testing facilities where said experiments are performed, the equipment used to gather data, the software used to process the data and finally, the method used when executing the experiments.

5.1.1 MarinLab

The experimental testing presented in this chapter is performed at the MarinLab facilities at HVL Kronstad. The MarinLab is a hydrodynamic research lab consisting of a 2.2x3 meter section tank of 50-metre length, with a layout as shown in Figure 5.1. Edinburgh Designs have delivered the six force-feedback wave generator system installed in the tank. The wave generator consists of six hinged wave paddles, and it has the ability to produce wave heights up to 0.5m, with a wave period of up to 2 seconds. It can generate sinusoidal waves, irregular waves, and wave spectra like the Pierson-Moskowitz and JONSWAP spectre. A passive beach is installed at the opposite end of the wave generator. The beach is a porous construction with an exponential profile that asymptotes to 8 degrees. The angled porous beach allows for efficient absorption of waves with minimal reflections.

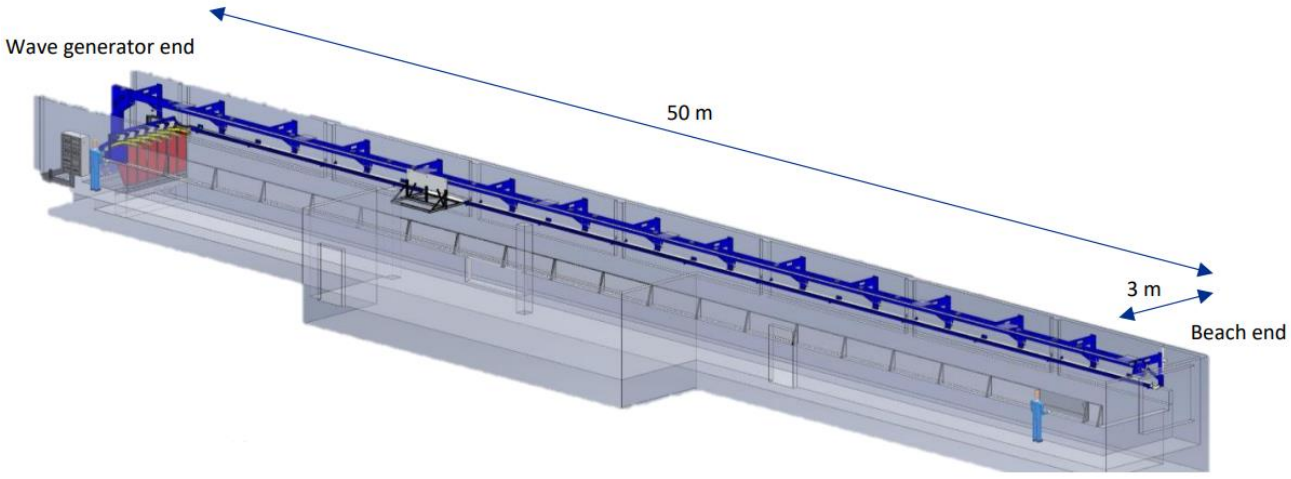

Figure 5.1 – The MarinLab at HVL Kronstad

5.1.2 Equipment

The MarinLab is fitted with various equipment for executing hydrodynamical tests.

Wave Gauges

Wave gauges for measuring wave height can be mounted at different locations in the wave tank to calibrate the wavemaker or validate the exact wave height at a location of interest.

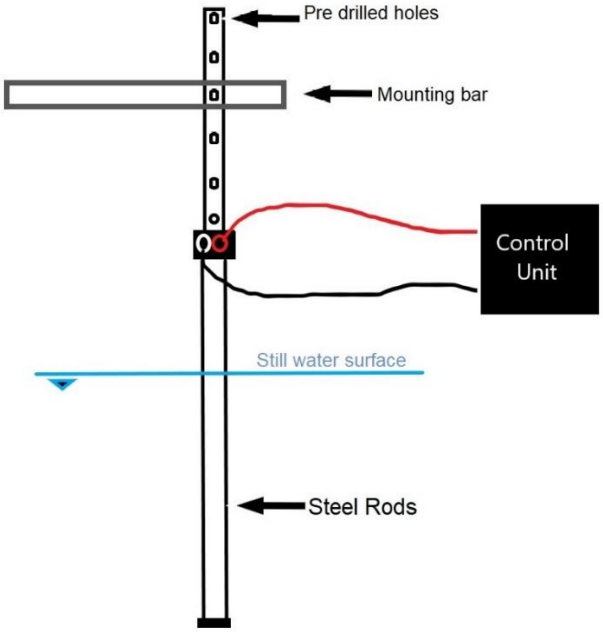

Figure 5.2 – Wave Gauges for mounting in MarinLab

National Instruments DAQ system

To be able to receive and gather data, the MarinLab is fitted with an extensive Data Acquisition system, with hardware for a wide range of measuring, acquiring and data processing, as shown in Figure 5.3.

Figure 5.3 - MarinLab uses National Instruments for DAQ systems

Towing Carriage

The MarinLab is fitted with a towing carriage, as shown in Figure 5.4. It can tow an object at speeds up to 5 m/s, with a maximum acceleration of 1.2 m/s^2. In addition, the towing carriage can move the entire length of the towing tank in both directions.

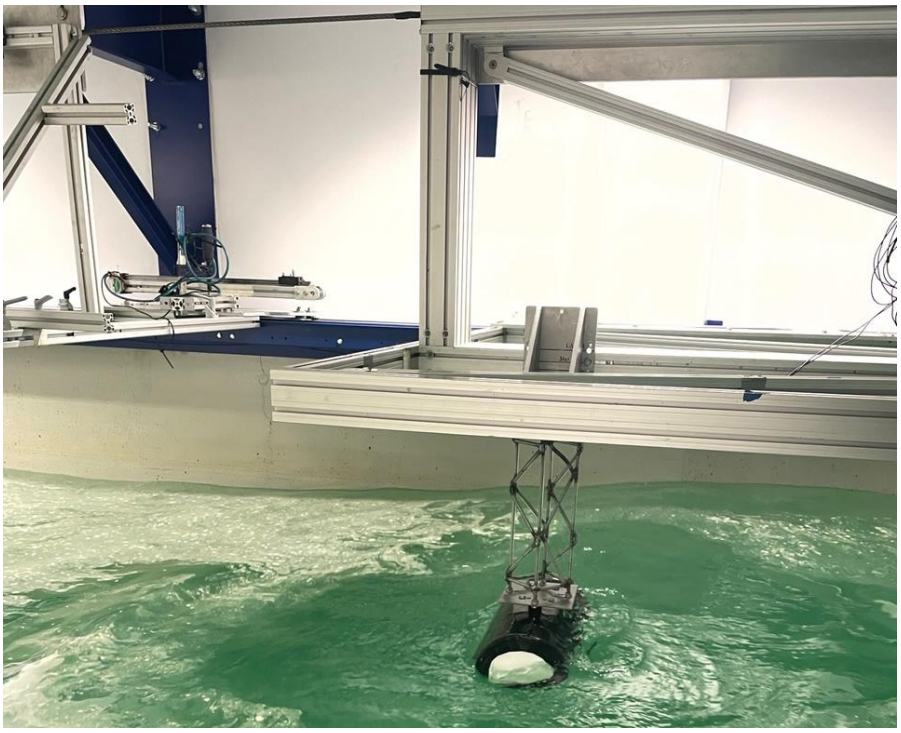

Figure 5.4 – Towing carriage with cylinder mounted

Loadcell

For measuring the wave loads, a 100N loadcell is utilized. The measuring device is put together by three metal plates, with two loadcells mounted in between to allow for measuring in both x and y directions. Changing the loadcell requires too much time due to changes in setup and calibration, so only one loadcell is utilized. The loadcell used for these tests has an accuracy of 99%, measuring up to 100 N.

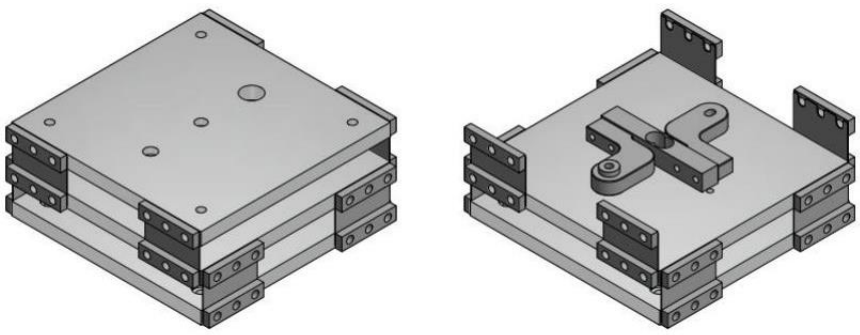

Figure 5.5 – 100 N Loadcell

5.2 Software for testing

This subchapter will present the different software used for capturing and processing data and running the wave generator during testing.

5.2.1 Njord Wave Synthesis

Njord Wave Synthesis software is used to generate waves for experimenting in the MarinLab, the hydrodynamic testing facility at HVL. Edinburg Designs deliver this software, and it is used for designing waves, running the wave generator in the wave tank, and analysing the waves.

5.2.2 LabView

The loadcell is connected to the DAQ system, linking the live data feed to the LabVIEW software. LabVIEW is a graphical programming software that gives a visual representation of the hardware and is used to process the raw data from the loadcell and store it in .txt files.

5.3 Experimental method

This chapter will cover the procedure for the lab experiments performed at MarinLab. It will include a detailed description of the testing setup, production of models and mountings, and calibration of loadcells and wave gauges. As earlier mentioned, the objective of the experimental tests is to gather as much data as possible. However, some compromises have to be made due to the limitations of available time in testing facilities.

5.3.1 Models

The MarinLab is, as mentioned, a 3 m wide and 2.2 m deep tank, and these measurements are the main limitations when dimensioning the models. According to associate professor Jan Bartl at HVL and MarinLab engineers Harald Moen, a model may have a total width of a maximum of 400 mm to have neglectable sidewall effects.

Two different dimensioned models are produced for the experiments, one cylinder with a diameter of 200 mm and one with a diameter of 400 mm. Both cylinders are 400 mm long. The cylinders are produced in Polyethylene. PE has a density of about 952-965 kg/m^3, quite close to the density of freshwater, which is convenient when mounting the models at an even buoyancy level [Dielectricmfg.com].

The cylinders are stuffed with foam so that if filled with water for adjusting buoyancy level, sloshing and other free surface effects on the insides are avoided. Figure 5.6 shows PE pipes before cutting, and Figure 5.7 shows the foam inside and the silicone gasket seal.

Figure 5.6 – PE pipes before cutting, and foam for fitting inside

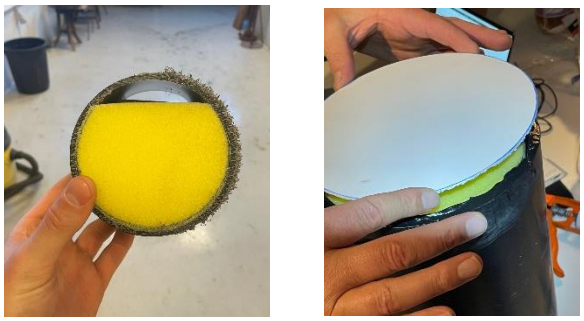

Figure 5.7 – Foam in place inside, and both ends are sealed with a silicone gasket

5.3.2 Custom Fitting Brackets

To be able to measure the drag force on the cylinder, the cylinder must be mounted onto the measuring device with the 100 N loadcell. The arm keeping the cylinder at its required depth, connecting it to the towing carriage, must be designed to be rigid and able to withstand the applied forces without moving or flexing. A suggested design is 3D modelled in PTC Creo Parametric, as shown in Figure 5.8 (a, b) below.

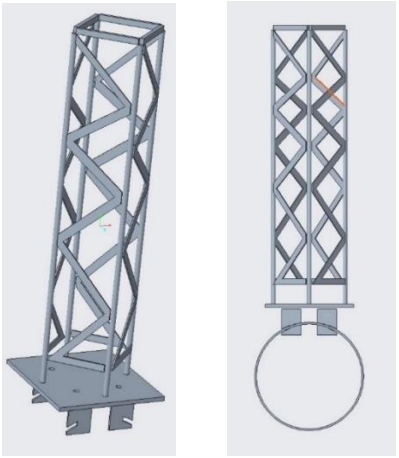

Figure 5.8 (a, b) - Rigid arm made up of steel threaded rods, welded in a truss system

The cylinder is connected to the arm with a custom bracket, as shown in Figure 5.9. This bracket is in contact with water in the tank and must be produced in stainless steel to prevent rust and sediments from releasing into the tank. Two custom brackets are made to fit the two different sized cylinders. The mounting plate connecting the arm to the two bracket arms is also stainless steel.

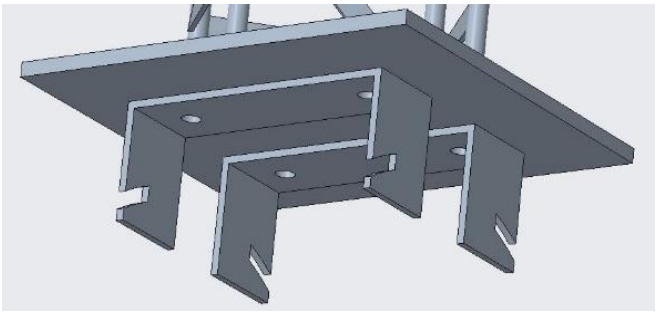

Figure 5.9 - Custom bracket made by bent stainless steel

The model is produced after the design, as shown in Figures 5.8-5.9. After producing the parts, they are put together using nuts and bolts. The final result is presented in Figure 5.10 below.

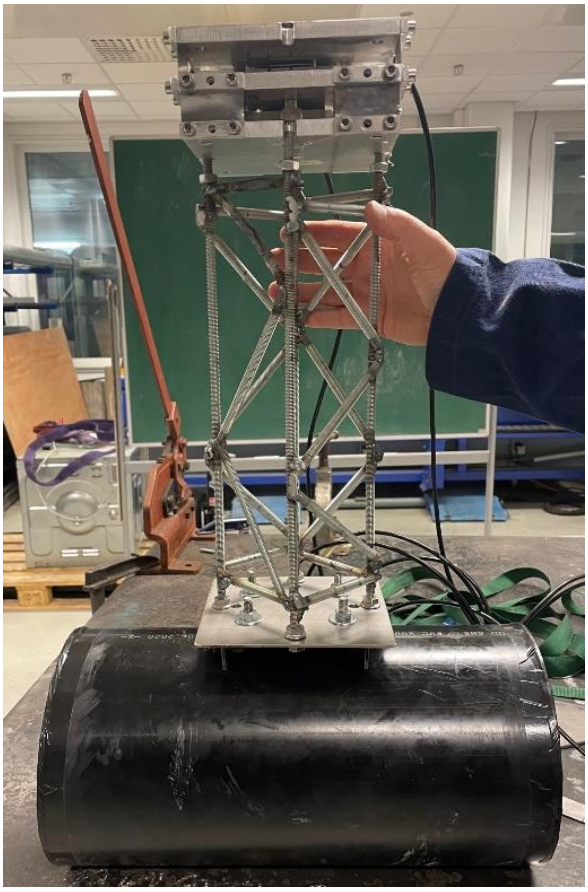

Figure 5.10 - Cylinder mounted to measuring device

5.3.3 Calibration of Loadcell

The next step is to calibrate the loadcell used for measuring the drag force applied to the cylinder. The loadcell is now attached to the arm and cylinder and is calibrated in this position. Figure 5.11 (a) shows a simple schematic drawing of the intended setup.

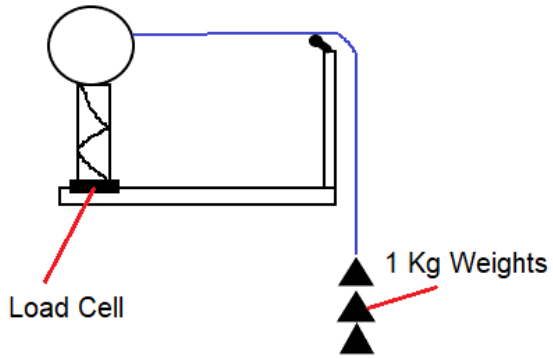

Figure 5.11 (a) – Initial Calibration Setup

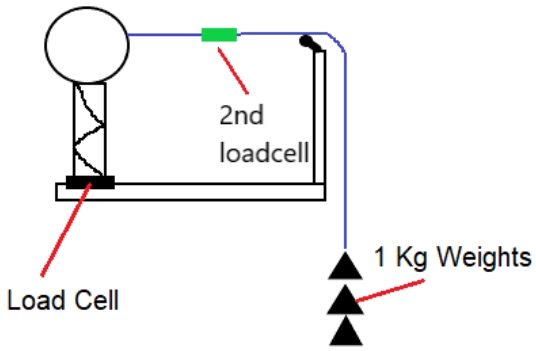

Figure 5.11 (b) - A second loadcell added

The loadcell measures a voltage, and a calibration process will give a linear approximation function to convert the said voltage reading to a force value [N].

The cylinder with the measurement unit is mounted on a rigid system, as shown in Figure 5.12. First, the angles are measured using a laser to calibrate the loadcell for a force load strictly horizontally on the cylinder. Then the 1 kg weights are added one by one, and the measured value from presented in LabView is plotted into the excel document.

Before each new weight is added, the readings must stabilize. However, after finishing the first iteration of the calibration, as presented in Appendix A – 10.3.1, the results showed a deviation of 5.6%. The hysteresis was also too significant, as shown in Appendix A – 10.3.1. The considerable hysteresis is presumably due to friction or elasticity in the bearings, a common problem known by the lab engineers at MarinLab.

This problem is solved by adding a second support loadcell on the wire. The final calibration setup is shown in Figure 5.11 (b).

The support loadcell is calibrated with a deviation of 0.1%, with detailed results presented in Appendix A – 10.3.2. The outcome from the final calibration of the main loadcell is presented in Appendix A – 10.3.3. The results show a deviation of 0.6 % after

calibrating using a second loadcell on the rope to adjust for friction and elasticity in the bearings on the calibration system. This is deemed acceptable, and the cylinder measurement setup is ready for mounting.

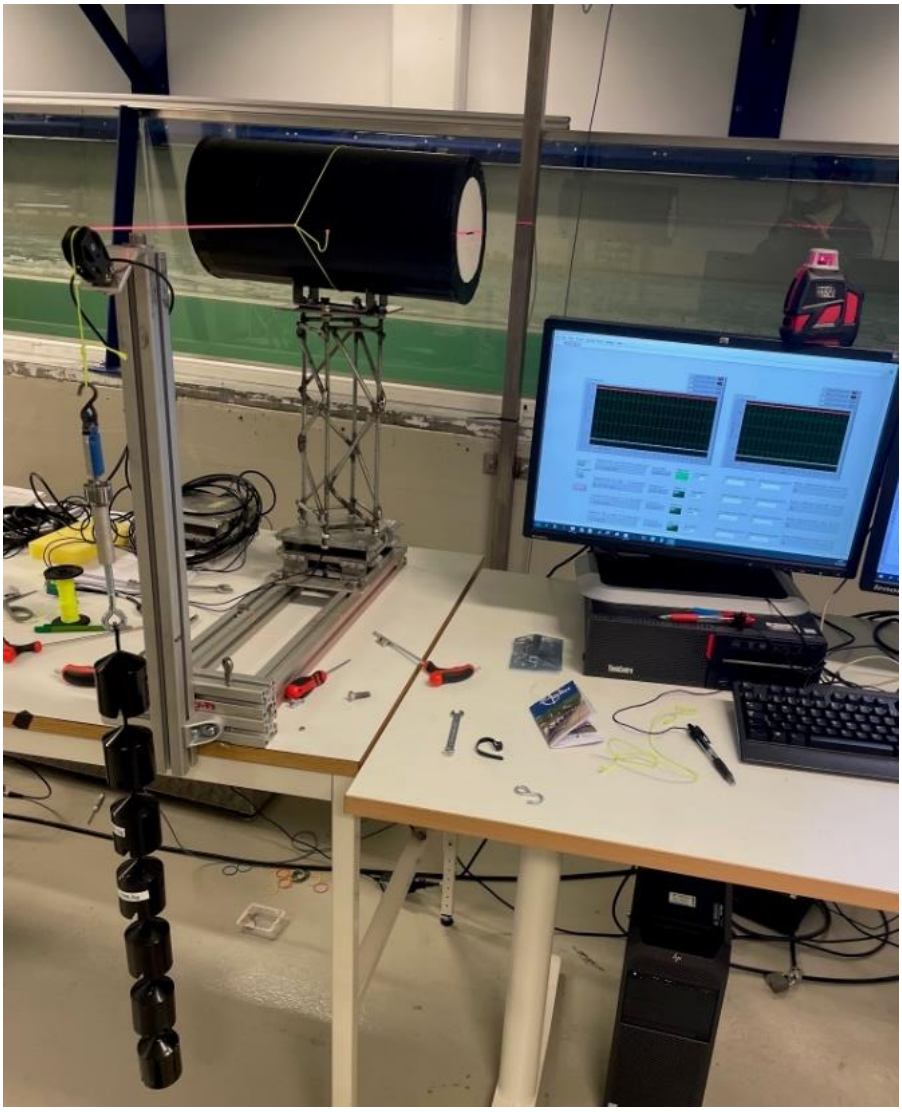

Figure 5.12 – One of the initial calibration setups, with laser measuring angle of the load

5.3.4 Mounting of Models

Before the calibration process is started, the mounting bracket for the towing carriage is installed on the towing carriage. After finding the ideal position for the bracket, a marker is used to indicate and save the optimal mounting locations for all the nuts and bolts, as shown in Figure 5.13.

Figure 5.13 - Mounting bracket for Towing carriage

After calibrating the loadcell while mounted to the cylinder, the loadcell is disconnected from the calibration system. Then the entire construction is carefully turned around and moved to the mounting bridge at the side of the tank. The mounting bracket is attached cautiously and locked in place at the marked spots. Then the cylinder is placed in the water and tightly bolted to the towing carriage at the intended position, as shown in Figure 5.14 (a, b). After mounting is finished, the position of the cylinder is checked with the marks as shown in Figure 5.14 (b). The position of the cylinder is adjusted so that the marker tags indicating the centre of the cylinder touch the water surface. Finally, the angle of the cylinder towards the flow direction is verified with a laser.

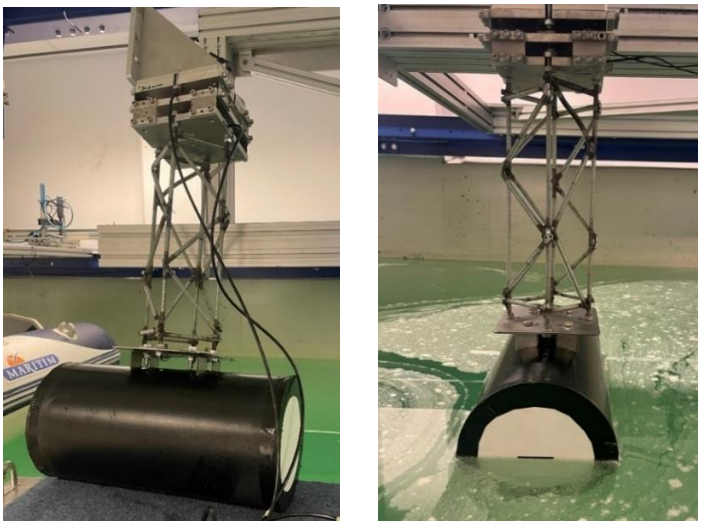

Figure 5.14 (a, b) - Mounting the entire setup to towing carriage

5.3.5 Calibration of Wave Gauges

The Njord Runtime Client/Engine software has a built-in module to calibrate the wave gauges. The wave gauges are mounted as described in chapter 5.1.3 and shown in Figure 5.15. The pre-drilled holes on the metal rod have a distance of 5 cm between them. In the Njord software, the measuring area must be set for the wave height intended for calibration, depending on the wave height of the experiments. The highest wave in these experiments is 0.16 m, and the wave gauge is calibrated for waves with amplitudes up to 0.20 m.

The calibration process is then initiated. The calibration software notifies the user that the rod should be adjusted in position. The position is changed in 3 intervals, using the pre-drilled holes, which are exactly 5 cm apart, first 10 cm up, then 20 cm down, and then back to the start position. The position is then zeroed, and the process is repeated for each of the three wave gauges. The wave gauges are placed at 10 m, 18.5 m, and 20 m from the wave generator.

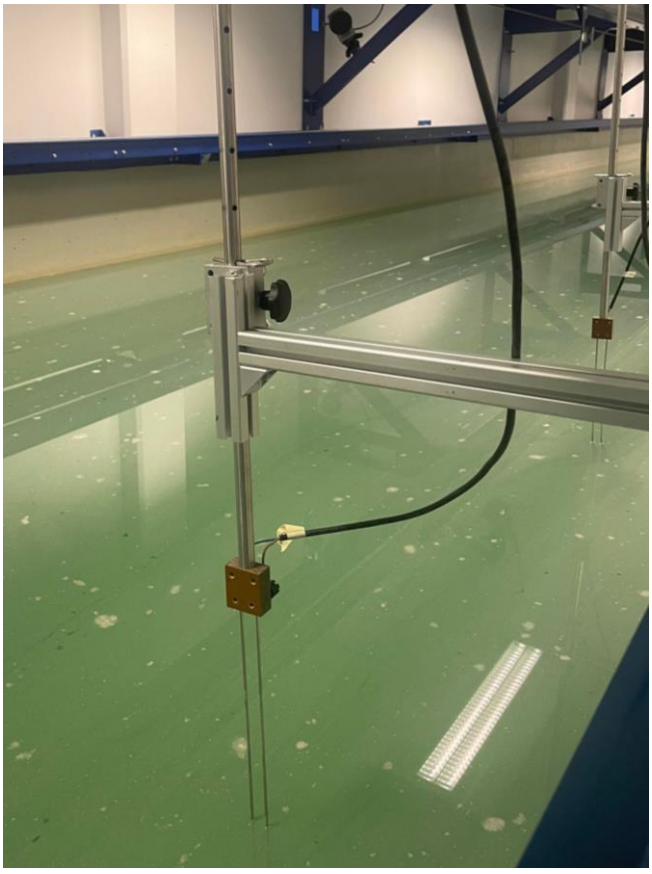

Figure 5.15 - Wave Gauge Mount

5.3.6 Executing Experiments

The experiments performed in the MarinLab are executed as planned in the test plan, see appendix A – 10.2. Before starting each test, the carriage is moved to the towing start point at 26 m, except for the tests at zero tow speed. Though the tank is 50 meters long, only the first 26 meters are utilised during testing to minimise the effects of reflection from the other end of the tank. For experiments with no flow speed, the carriage is placed beside the second wave gauge so that the effects of reflections from the other end of the tank take longer to reach the cylinder.

The LabView software for recording the measured data is then started, and the wavemaker starts producing waves. It takes a few waves to build up to the proper size, and when the first wave hits the cylinder, the towing carriage is started. That way, it achieves a constant speed around the area of the third wave gauge, and at the same time, it starts going through the fully developed waves. That gives a few seconds of high-quality measuring before it starts decelerating at 12 m and finally stops at 10 m. A schematic drawing of the tank setup is presented in Figure 5.16, showing a 3D model of the MarinLab and the position of the wave gauges.

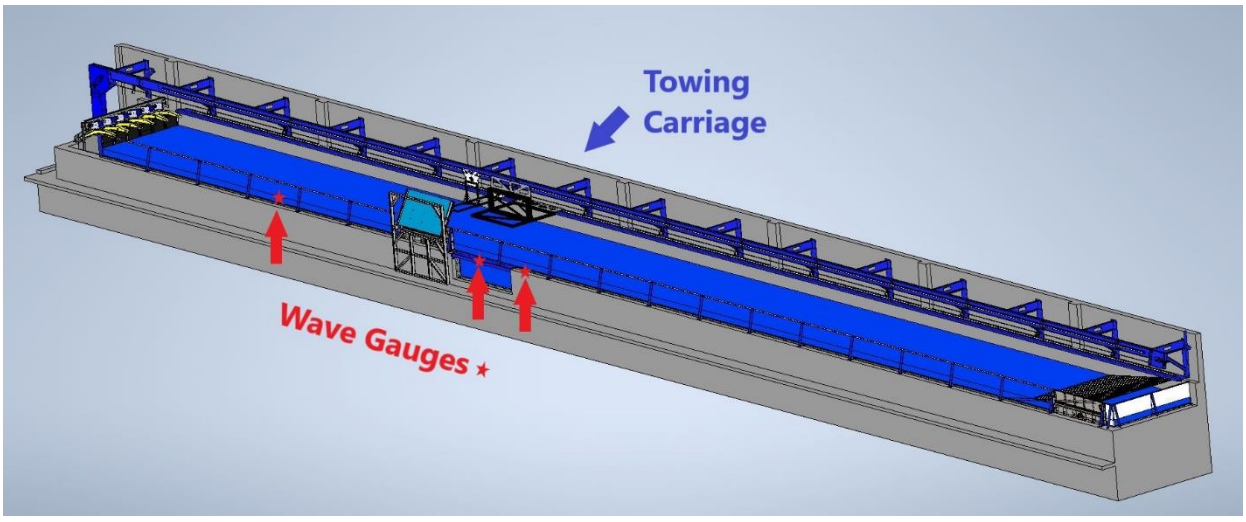

Figure 5.16 - Bird view of the schematic drawing of tank setup

5.4 Investigating loadcell measurements

After comparing CFD results with MarinLab experiments, as shown in Chapter 6.3, it was discovered that MarinLab experiments showed a greater output in terms of negative force values than was apparent in the CFD results. This subchapter covers the additional tests performed in MarinLab to investigate this phenomenon further.

5.4.1 Discrepancy in negative force values compared to CFD

The calibration process of the loadcell is described in detail in chapter 5.3.3. A force is applied to the loadcell by adding 1 kg weights, one by one, until 92.65 N is reached. The weights are then removed, one by one, back down to 0 N. This method only calibrates the force measured in one direction. However, when waves hit the cylinder, it is affected by forces in both directions. The magnitude of the negative force depends on the specific parameters of the waves and flow speed. The force in the negative direction is only apparent in low flow speeds and is in general of a much lower order than the positive direction.

Further experiments are then performed to assess whether the loadcell is measuring correctly in both directions and whether the greater negative force values are due to some elasticity in the loadcell or in the setup in general, or that the measured force in the negative direction is wrong due to the calibration of the loadcell is executed in only one direction.

5.4.2 Experimental investigation of loadcell measurements

This chapter covers the experiments performed during the investigation of loadcell measurement accuracy depending on direction. The procedures during these experiments are very similar to the experiments described in Chapter 5.3. However, due to technical problems with the DAQ ethernet connections in the MarinLab, the loadcell must be calibrated from the wave tank platform. The calibration process is then executed as described in chapter 5.3.3, resulting in a deviation of 0.4 %, as shown in the calibration table in Appendix A – 10.3.4. Firstly, the cylinder is mounted onto the towing carriage. Then, the measured load is zeroed after the water surface has calmed. Finally, the towing carriage is moved to the position 10 meters from the wave generator end, and the tests are ready to start.

Due to the technical issues with the DAQ system in MarinLab, a new LabView program is created for these tests. The LabView system is programmed so that the signal coming from the loadcell may be gain corrected and offset with the values from the calibration process, and the measured data is stored in .txt files for post-processing and analysis. The towing carriage pulls the cylinder from its starting position at 10 meters to an end position at 40 meters from the wave generator. Then, the cylinder is pulled back at the same towing speed, and this procedure is repeated at 0.5 m/s, 0.75 m/s and 1.0 m/s.

6. Results

Chapter 6.1 presents the results from experiments in MarinLab and the investigation of loadcell measurement. Next, Chapter 6.2 presents the results from CFD simulations in 2D and 3D, including some examples of the gathered data. However, a more in-depth discussion is presented in chapter 7. Then the validation process of the CFD simulations is presented in chapter 6.3, and finally, a comparison of the results from 2D and 3D simulations is presented in chapter 6.4.

6.1 Results from MarinLab Experiments

This chapter will cover the results from the experiments in the MarinLab at HVL Kronstad. A total of 72 tests were completed, as described in Table 10.4 and 10.5 in Appendix A. During the experiments with the smaller cylinder (diameter 110 mm), it became apparent that the custom holding bracket was hit by waves of amplitude higher than 0.06m, and for speeds more than 0.5 m/s. This means that the measured force values were too big, as more than the cylinder surface came in contact with the wave load. Consequently, only the data for towing speeds 0.5 m/s and below and wave amplitude 0.06 or smaller were studied. These values proved to be too low for the loadcell to measure accurately. For that reason, the analysis is concentrated on the results from tests on the 200 mm diameter cylinder.

6.1.1 Results from wave experiments

The sampling frequency of the loadcell for force measurements is 2000 Hz, and the experimental setup is as described in chapter 5. The raw data from the .txt file for wave 26 is read through a Matlab script and presented in Figure 6.1. The red rectangle shows the cropped data for when the towing speed is constant.

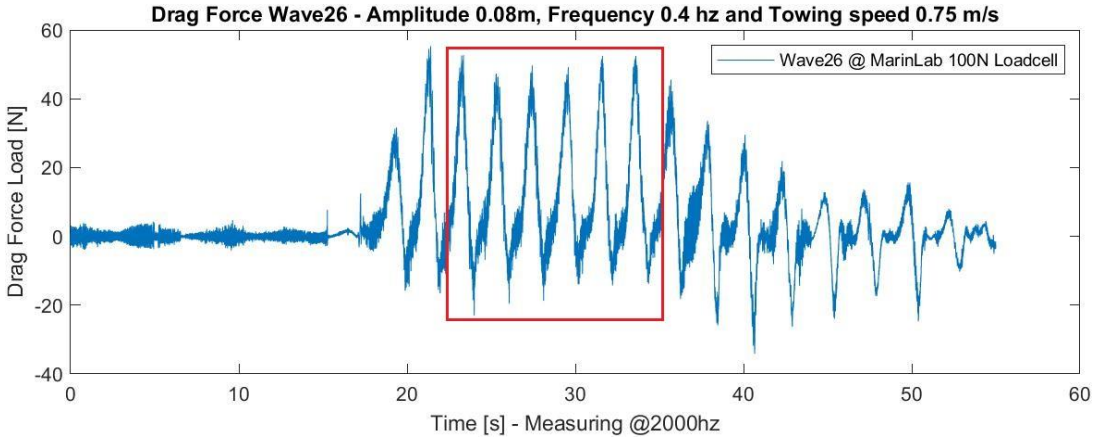

Figure 6.1 – Wave 26 raw data

Wave 26 has an amplitude of 0.08 m and a frequency of 0.4 Hz, and the towing speed is 0.75 m/s. The experimental process is initiated as described in chapter 5.3.6. During the beginning of the test, the towing carriage accelerates for about 3 seconds, as shown in Figure 6.2. In the case of wave 26, the process is initiated by first starting the wave generator. Next, the towing carriage is started after the first wave hits the cylinder, at around 3 seconds. Then after 3 seconds, the towing carriage reaches a constant speed of 0.75 m/s, and the data is presumed to be valid from around 6 seconds. Then the carriage holds a constant speed for about 18 seconds before it deaccelerates and stops at 10 m away from the wave generator. This results in about 13.5 seconds of measuring assumed valid, as indicated by the red rectangle in Figure 6.1.

Figure 6.2 – Carriage motion with time

This process is repeated for every wave, and the data that is assumed valid is then ready for further analysis and comparing with CFD results. Figure 6.3 shows the cropped data from wave 26.

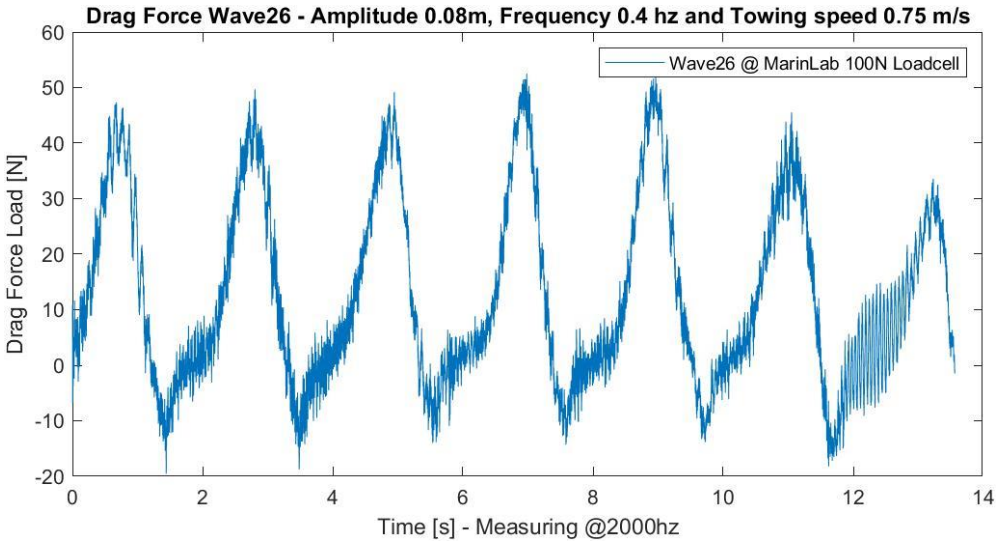

Figure 6.3 - Cropped data from wave 26

6.1.2 Results from investigating loadcell measurements

This section presents the results from the investigations of the loadcell measurements. A total of 6 different experiments were executed as described in chapter 5.4.2. These experiments are executed using the same method as the wave load experiments, using the same loadcell and saving the data via a LabView script in .txt files. The raw data from towing tests at 1.0 m/s in the positive direction is presented in Figure 6.4. The capturing of data is initiated before starting the towing carriage, and the towing carriage requires a few seconds to reach the intended speed. After running at a constant speed for a while, the carriage deaccelerates towards the end. The data is appropriately cropped so that only the part at constant speed is investigated. The red rectangle in Figure 6.4 shows the cropped data.

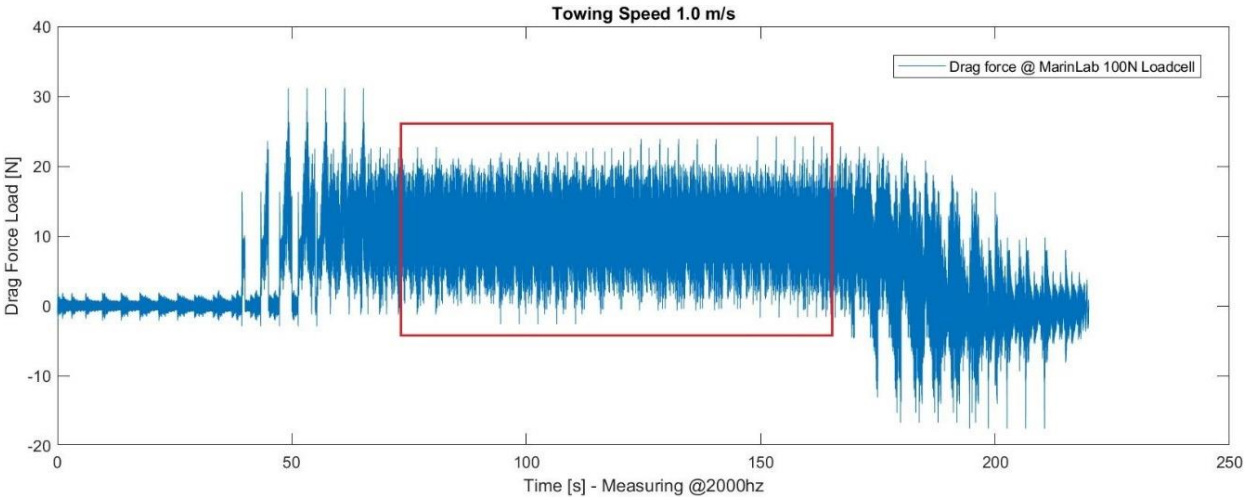

Figure 6.4 – Raw data from investigating loadcell measurements

Ideally, the plot in Figure 6.4 should have been one straight line. However, the measured force value seems to fluctuate between 0 and 20 N. As stated in Chapter 5.4; there were extensive technical issues with the measuring system at the MarinLab at the time of the experiments. Other students who performed tests the days after reported the same fluctuations or oscillations in the signal. This issue may be due to some electrical interference in the signal or some error in the LabView software storing the data. As these tests were mainly performed to look at the differences in the measured load in the positive and negative direction, the signal interference can be overlooked, and the average force measurements studied.

The data cropping is done using MATLAB. Using the mean function in MATLAB, the average drag force for each speed in each direction is then calculated and presented in

Figure 6.5. Both numbers are set to positive for illustrational reasons. Though the results appear to be quite similar, the negative force measurements seem to increase more than in the positive direction.

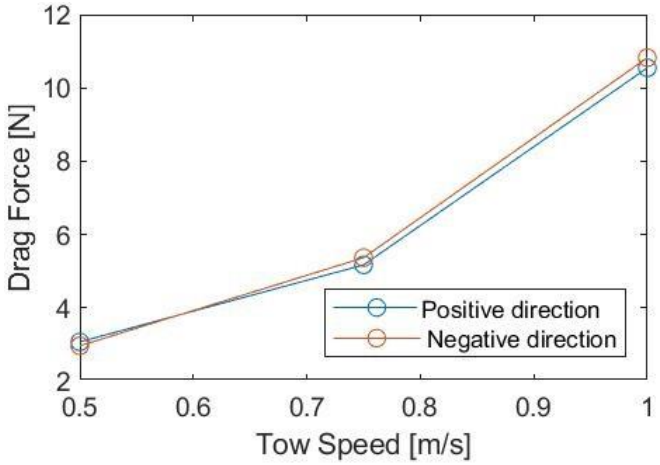

Figure 6.5 - Drag force in both directions plotted against time

6.2 Results from ANSYS CFD Analysis

This chapter presents the results from the Ansys Fluent CFD simulations. Chapter 6.2.1 covers the results gathered from the 2D model simulations, and chapter 6.2.2 cover the results from the 3D model simulations.

The procedures are the same for 2D and 3D simulations when processing results. All the simulations are set to store .txt files for drag and lift force acting on the cylinder. These files are read through a MATLAB script, but the data need to be processed correctly before being analysed.

Depending on the specific case, the simulation may require some time to stabilize and give accurate results. That means that each case must be individually assessed, but after 20-40 seconds, most cases appear to stabilize. After that, it appears to be consistent in most cases. In general, the final 20-30 seconds of the simulation are assumed to be valid and will be compared to the results from MarinLab.

6.2.1 Ansys Fluent 2D results

The raw data from 2D results are plotted using MATLAB. Each case is then considered, and the data is cropped when it stabilises. This process is shown in Figure 6.6, where the red rectangle contains the data, which will be further analysed. The example shown in Figure 6.6 is the case of wave 24, which consists of a flow speed of 0.75 m/s, an amplitude of 0.06 m and a frequency of 0.5 Hz. The data seem to stabilize after about 35 seconds in this specific case.

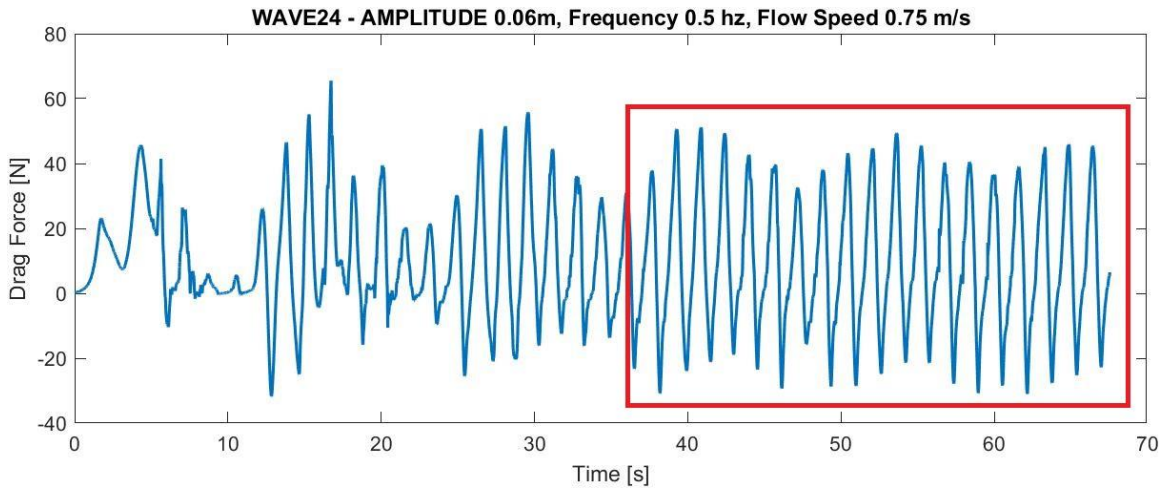

Figure 6.6 – 2D CFD: Cropping of stable data: Drag force on the cylinder, plotted against time

A more extensive analysis of the 2D results compared to the 3D simulation results is presented in Chapter 6.4.

6.2.2 Ansys Fluent 3D results

The 3D simulations are simplified due to symmetry. Due to symmetry, the calculated force values must be doubled when comparing the calculated forces to the measured forces from tests in MarinLab. The 3D simulations also have bigger timesteps, so this must also be considered when analysing the data. Both the timestep and the doubling of force values are implemented in the MATLAB code.

As mentioned in chapter 6.2, each case must be individually assessed when cropping the data. An example of the cropping process for 3D simulations is presented in Figures 6.7 and 6.8.

Figure 6.7 shows the case of wave 29, which has 0 flow speed, a small amplitude of 0.04 m and a wave frequency of 0.4 Hz, which is more or less stable from the initialization. In this case, the data is cropped from 20 seconds to 60 seconds.

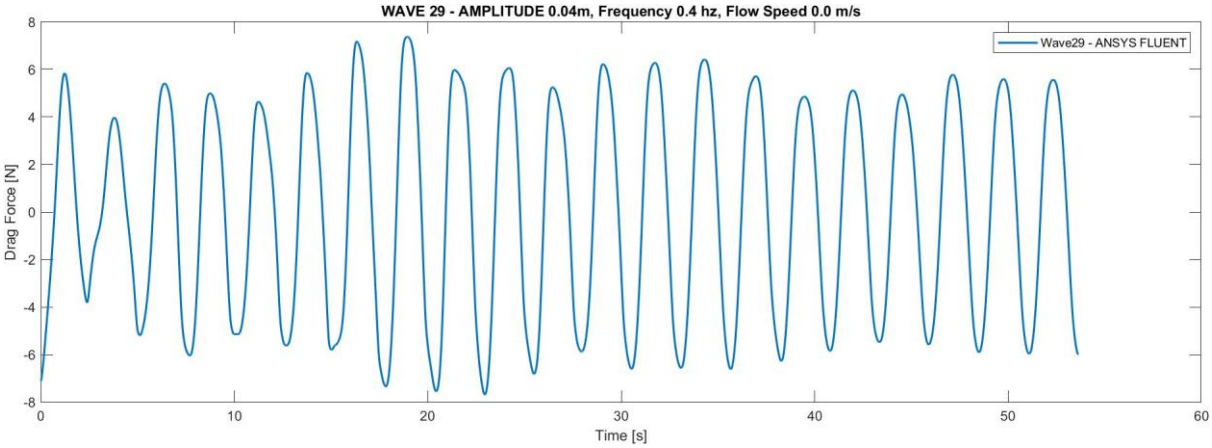

Figure 6.7 – 3D CFD: The drag force on the cylinder, plotted against time

Another example of the data cropping process is shown in Figure 6.8. This example is of wave 21, which consists of a wave with an amplitude of 0.04 m, a frequency of 0.5 Hz and a flow speed of 0.75 m/s, and it requires a bit more time for stabilization than wave 29. For wave 21, the calculated drag force varies a great deal until it more or less evens out the last 20 seconds.

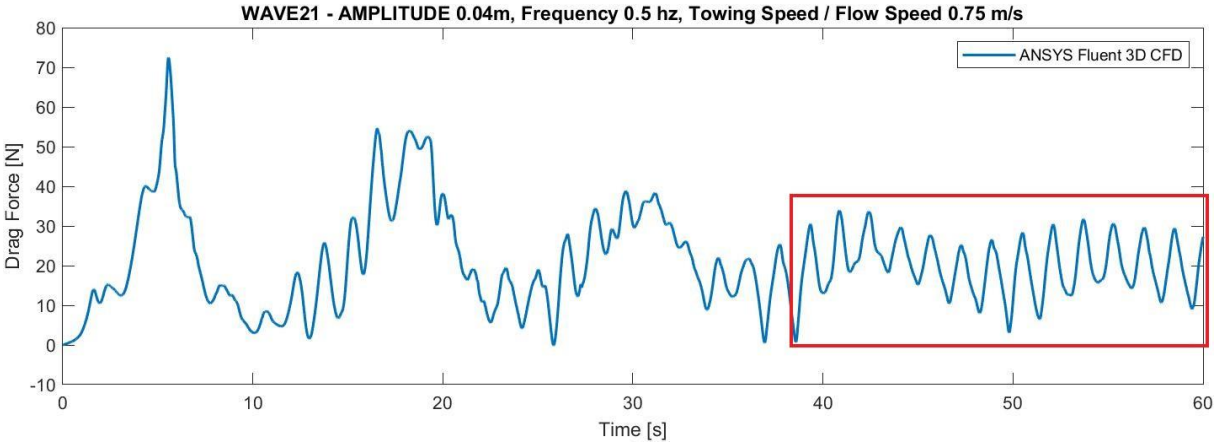

Figure 6.8 – 3D CFD: Cropping of stable data - drag force on the cylinder, plotted against time

The evaluation of data is performed using MATLAB for each individual simulation case. First, the CFD data is cropped depending on the time it stabilises, then plotted against the data recorded from the wave tests in the MarinLab for validation purposes in Chapter 6.3, before the effects of parameter changes are further studied in Chapter 7.

6.3 Validating CFD Results with MarinLab Experiments

This chapter presents the process of validating the data gathered from CFD simulations. One of the objectives of this research is to gather data regarding how changing the parameters of a wave influences the wave load on a cylinder. Analysing the wave data can lead to a deeper understanding of how to design a durable structure that can withstand a marine environment. A structure mostly tends to break due to the magnitude of the maximum force values. Therefore, one of the priorities when evaluating the validity of the data will be to investigate the accuracy of the maximum force values.

The maximum force values from CFD and experiments will be evaluated and divided into four classifications. The classifications are *good* (90-100% accuracy), *decent* (80-90% accuracy), *ok* (60-80 % accuracy) and *poor* (40-60% accuracy). The overall curve fit will also be examined when dividing the validation results into these four classifications. This approach is less quantifiable, but several examples will be shown for each classification. Table 6.1 shows an overview of the classification and the accuracy of the average of the maximum drag force.

Table 6.1 – Table of classification categories

Classification	**Accuracy**
Good	90-100 %
Decent	80-90 %
Ok	60-80 %
Poor	40-60 %

The validation process begins with plotting the results from CFD are plotted against the results from MarinLab. Then the phases of the curves are adjusted and fit against each other. Each simulation or experiment includes several waves crashing into the cylinder, and the average of the highest values recorded for each wave is calculated in MATLAB. This will be referred to as the average of the maximum force. Finally, the results are evaluated, and the validity of the specific case is classified within the four categories.

An example of the comparison of the drag force from CFD and experiments is shown in Figure 6.9. Here the drag force curves from wave 29 are plotted, with CFD and MarinLab results fitted together for comparison. For this case, the average of the maximum drag force from CFD is within 98 % accuracy compared to the results from experiments.

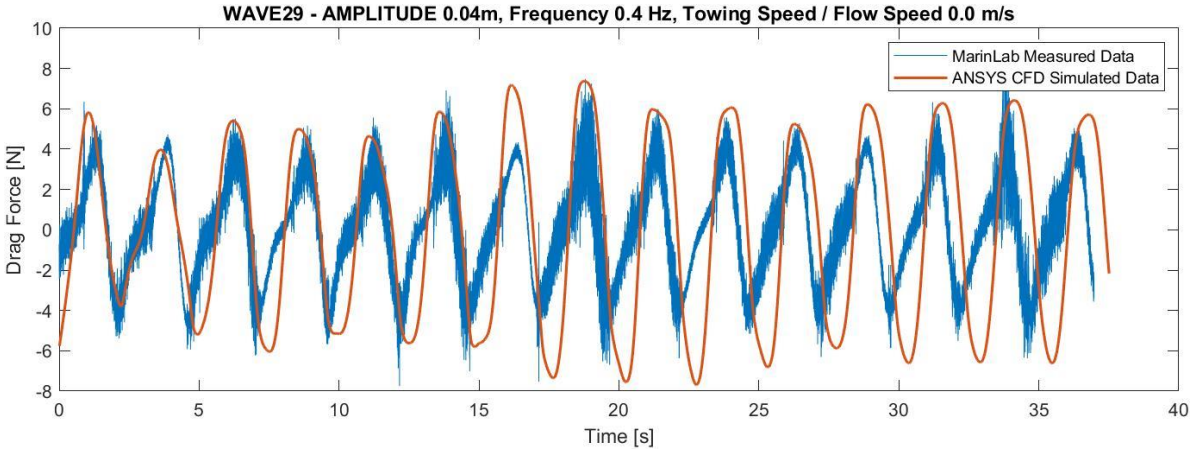

Figure 6.9 – Wave 29 shows a good fit between data from CFD and MarinLab experiments

The process of comparing CFD results to experiments is repeated for every wave in the simulation plan, as presented in Appendix A-2. After finishing this process, the results of the validity classification for each case are summarised and presented in Tables 6.2-5. Chapters 6.3.1-6.3.4 will go through all the validation results in detail.

6.3.1 Validation of results at 0.0 m/s flow speed

Table 6.2 show the validation classification results at flow speed 0.0 m/s. For frequency 0.3 Hz, the waves of amplitude 0.06 m and 0.08 m are deemed *poor* (below 60 % accuracy). However, 0.0 m/s flow speed and 0.3 Hz is the lowest speed and the lowest frequency tested. In this range, the measured drag force varies between -8 N and 8 N, which is not ideal in terms of accuracy for the 100N loadcell used in the experiments.

Table 6.2 – Classification of waves at 0.0 m/s flow speed

Flow Speed 0.0 m/s		Frequency [Hz]		
		0.3	0.4	0.5
Amplitude [m]	0.04	Decent	Good	Good
	0.06	Poor	Good	Ok
	0.08	Poor	Good	Ok

Wave 29, as shown in Figure 6.9, shows a good fit between the drag force curve from CFD and MarinLab. Wave 32 is presented in Figure 6.10 and is another example of a good fit.

In this case, the average of the maximum drag force from CFD is 7.4 N, and from experiments, it is 7.3 N. That results in an accuracy of 98 %, and it is classified as *good.*

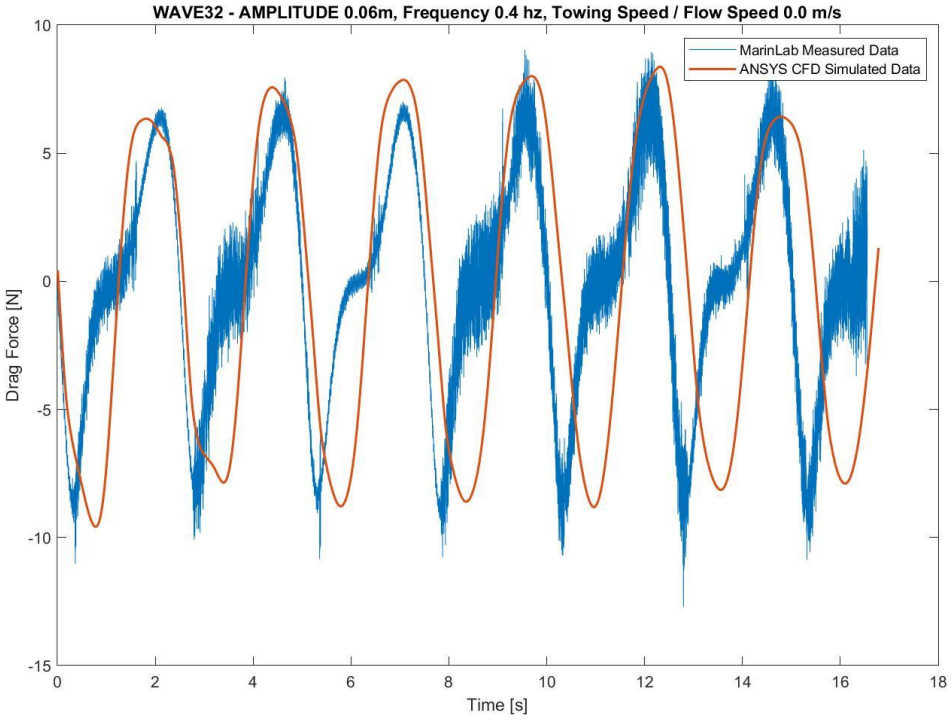

Figure 6.10 – Wave 32 shows a good curve fit between CFD and MarinLab tests

An example of a poor fit is presented in Figure 6.11, which shows wave 34. This case consists of waves at an amplitude of 0.08 and with a frequency of 0.3 Hz. There are some noticeable differences between the results from CFD and MarinLab. The average of the maximum drag force accuracy of the CFD is only 45 % compared to the experiment results, and the two curves bearly seem to overlap, as opposed to the examples shown in Figures 6.9 and 6.10.

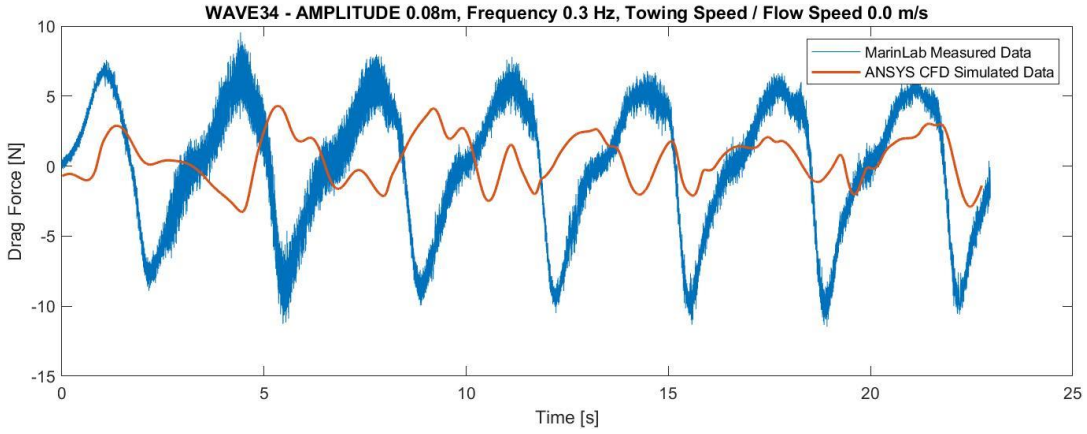

Figure 6.11 – Wave 34 show a poor fit between data from CFD and MarinLab experiments

6.3.2 Validation of results at 0.5 m/s flow speed

Table 6.3 shows the validation classification results at a flow speed of 0.5 m/s. All cases show *good* or *decent* classification (80-100 % accuracy). Six out of nine cases are within 90 – 100 % accuracy in terms of the average of the maximum drag force. For the test cases at 0.0 m/s flow speed, only five out of the nine cases showed an accuracy above 80 %. When the speed is increased to 0.5 m/s, the overall accuracy is improved. The improved accuracy might be due to the loadcell used for the experiments, as the measured force values range between -30 N and 40 N at a flow speed of 0.5 m/s. That is more within the intended measuring range of the 100N loadcell.

Table 6.3 – Classification of waves at 0.5 m/s flow speed

Flow Speed 0.5 m/s		Frequency [Hz]		
		0.3	0.4	0.5
Amplitude [m]	0.04	Decent	Decent	Good
	0.06	Good	Good	Good
	0.08	Good	Good	Decent

Figure 6.12 presents another example of a comparison between CFD results and experiments. The specific case is wave 6, a wave with an amplitude of 0.06 m and a frequency of 0.5 Hz. Even though the negative force value measured in MarinLab shows a higher output, this is still classified as a *good* fit. That is because the maximum average drag force is within 98 % of each other and quite a good curve fit when disregarding values below 0 N.

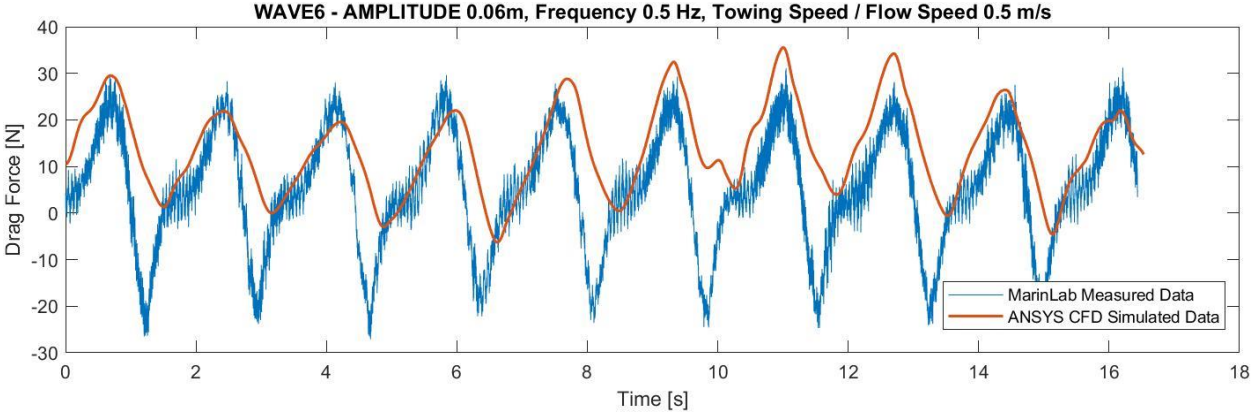

Figure 6.12 – Wave 6 shows a good fit between data from CFD and MarinLab experiments

These presumed exaggerated negative force readings are, as discussed in Chapter 5.4.2, the reason why the loadcell measurements were further investigated during a subsequent test in MarinLab. Though the results were somewhat inconclusive due to interference in the measuring signal, the measured negative force showed a steeper increase than the positive measured force. Along with effects due to elasticity, this might substantiate the claim that the bigger negative force readings in MarinLab do not affect the validity of the CFD data, especially when the focus is on the maximum values.

In three cases at 0.5 m/s flow speed, the classification was assessed as *decent* (80-90 % Accuracy). Figure 6.13 displays the drag force curves for wave 2 from both MarinLab experiments and CFD. This wave has an amplitude of 0.04 m and a frequency of 0.4 Hz.

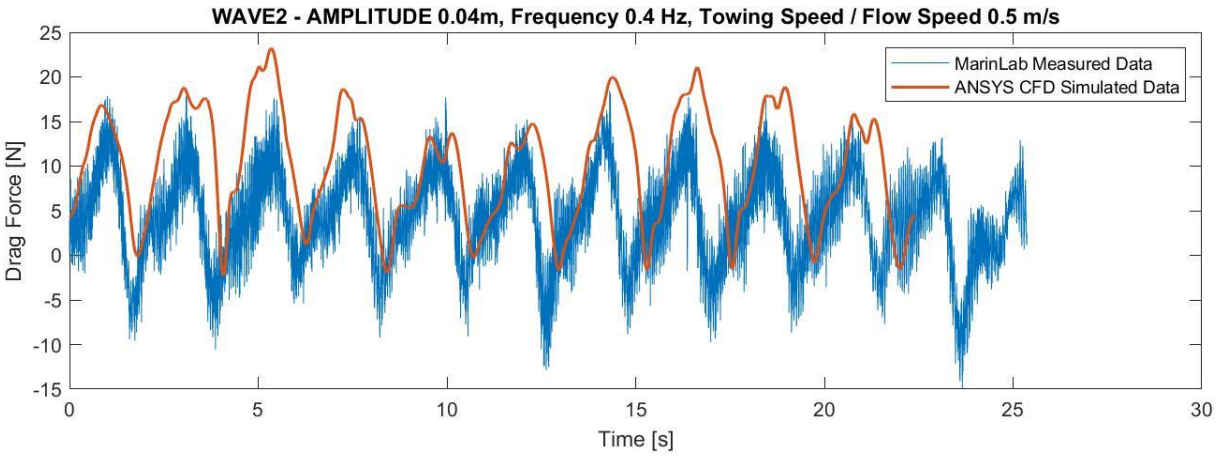

Figure 6.13 – Wave 6 shows a decent fit between data from CFD and MarinLab experiments

6.3.3 Validation of results at 0.75 m/s flow speed

Table 6.4 show the validation classification results at a flow speed of 0.75 m/s. All cases show *good* classification except the waves of frequency 0.3 Hz and amplitude 0.04 and 0.06, as well as frequency 0.5 Hz and amplitude 0.08 m, which are classified as *decent* and *ok*.

Table 6.4 – Classification of waves at 0.75 m/s flow speed

Flow Speed 0.75 m/s		Frequency [Hz]		
		0.3	0.4	0.5
Amplitude [m]	0.04	Decent	Good	Good
	0.06	Decent	Good	Good
	0.08	Good	Good	Ok

An example of a result classified as good is the case of wave 26, as shown in Figure 6.14. This case consists of waves at 0.4 Hz frequency with an amplitude of 0.08 m. The average of the maximum drag force from CFD is 40.9 N, and from MarinLab experiments, it is measured to be 44.7 N. That results in an accuracy of 91 %.

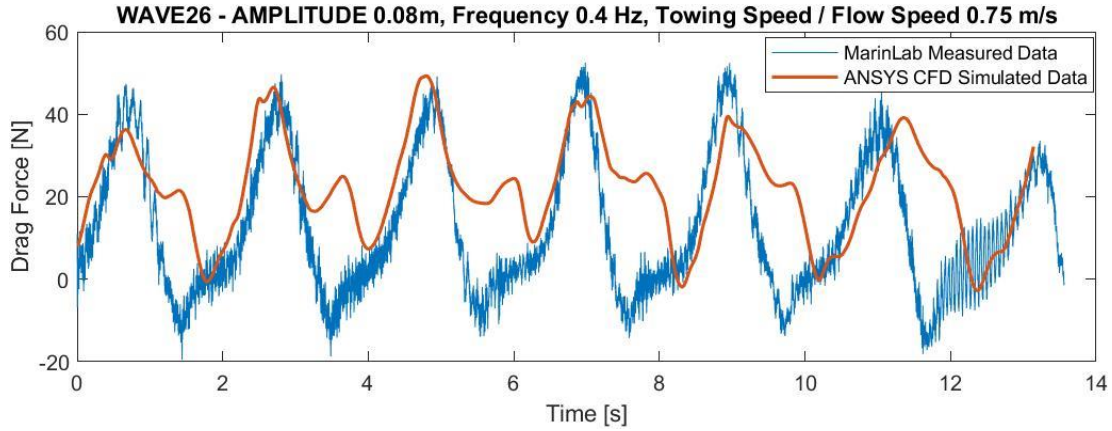

Figure 6.14 – Wave 26 shows a decent fit between data from CFD and MarinLab experiments

Figure 6.14 shows the same tendencies regarding a higher negative force reading from MarinLab experiments, as discussed in the case of 0.5 m/s. However, this trend is occurring more as the frequency increases, as shown in Figure 6.15. This Figure presents the case of wave 21. Even though the results from MarinLab show a more considerable output in the negative direction, the average of the maximum drag force from CFD is still 95 % accurate compared to experimental data. This results in a *good* classification.

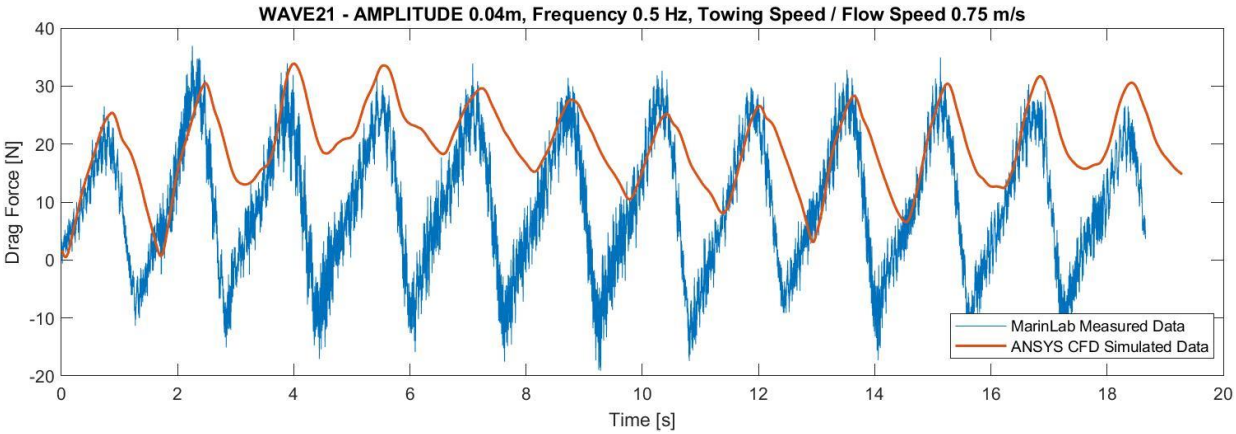

Figure 6.15 – Wave 21 shows a good fit between data from CFD and MarinLab experiments

Eight out of nine cases tested at 0.75 m/s flow speed showed to be within an accuracy of 80-100 %. However, in one of the cases, a result is classified as *ok*. This case is presented in Figure 6.16.

This is the case of wave 27, consisting of an amplitude of 0.08 m and a frequency of 0.5 Hz. The peak values from CFD regarding drag force appear to be lower than the results from MarinLab experiments. In this case, the average of the maximum value from CFD is 25% lower than the measured value from MarinLab.

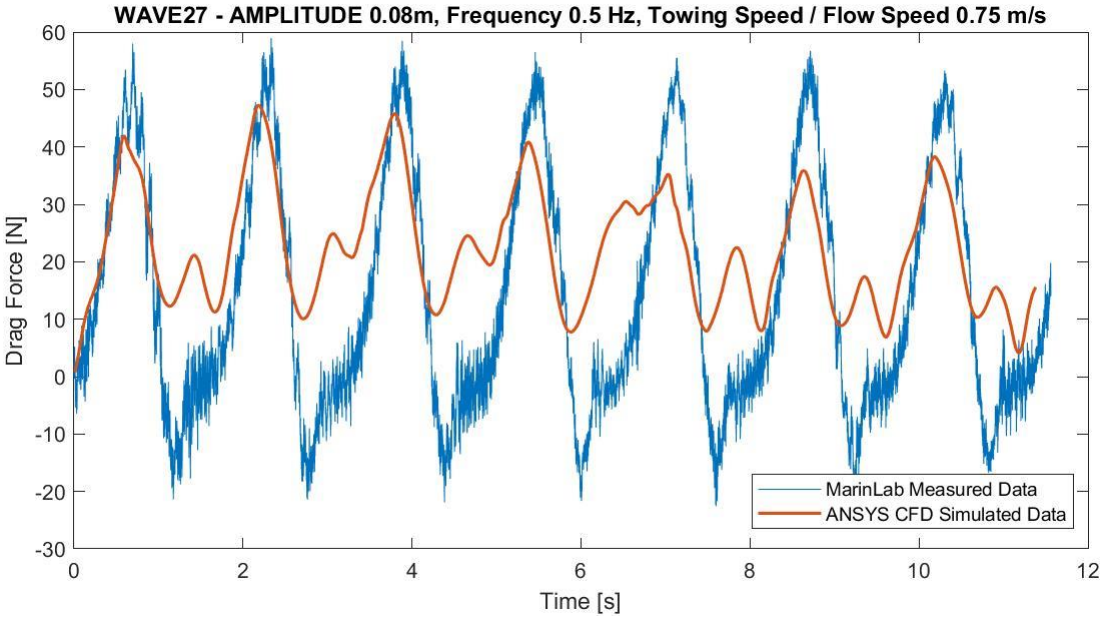

Figure 6.16 – Wave 6 shows an ok fit between data from CFD and MarinLab experiments

6.3.4 Validation of results at 1.0 m/s flow speed

Table 6.5 show the validation classification results at a flow speed of 1.0 m/s. At this speed, the quality of the results starts to deteriorate. Most of the cases show either an ok or a poor fit, except for a few low frequency and low amplitude cases.

Table 6.5 – Classification of waves at 1.0 m/s flow speed

Flow Speed 1.0 m/s		Frequency [Hz]		
		0.3	0.4	0.5
Amplitude [m]	0.04	Decent	Good	Ok
	0.06	Ok	Decent	Ok
	0.08	Poor	Ok	Ok

The trend of a higher negative force reading from MarinLab experiments compared with CFD data seems to further increase as the flow speed increases. This only appears for higher frequency cases at lower flow speeds, but at 1.0 m/s, this is happening for all frequencies. An example of this is presented in Figure 6.17.

Figure 6.17 presents the case of wave 17, a wave of amplitude 0.08 m, frequency 0.4 Hz at a constant flow speed of 1.0 m/s. The accuracy of the average of the maximum drag force of the CFD is 68 % when compared with experiments. Therefore, Wave 17 is classified as *Ok* (60-80 % accuracy).

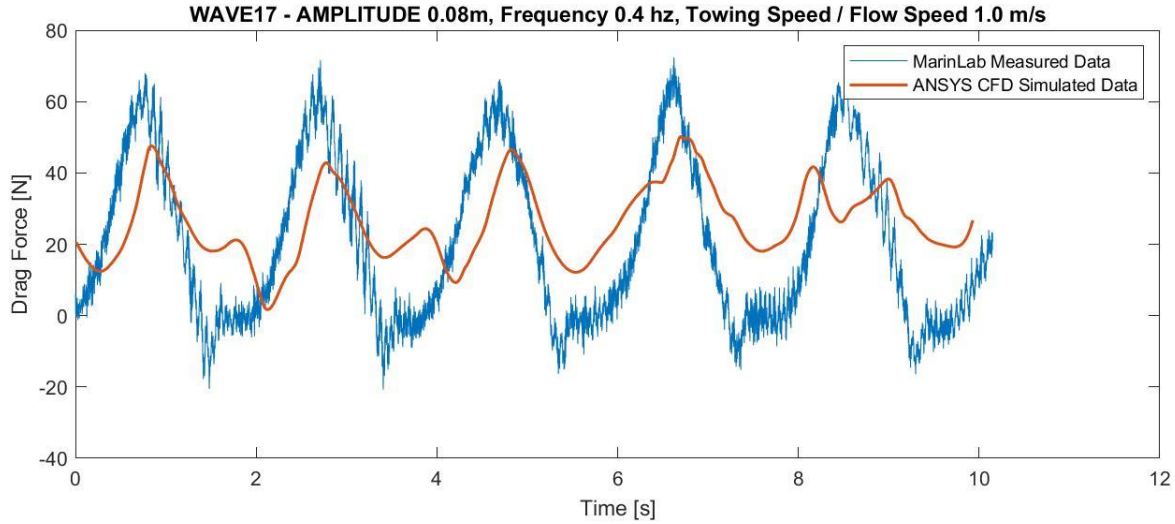

Figure 6.17 – Wave 17, 3D CFD results compared with MarinLab experimental data

When validating data with MarinLab, the more waves to compare with, the better. In the case of 1.0 m/s tow speed, it is only possible to measure a few waves before the cylinder has been moved to the other end of the tank. This is another reason why most of the validity of the data at flow speed 1.0 m/s is graded so low compared to the cases of 0.5 m/s and 0.75 m/s. An example of this is presented in Figure 6.18, the case of wave 13. The low frequency of 0.3 Hz meant that only three wave peaks were measured during experiments. This case is classified as *Ok,* due to an accuracy of 72 %.

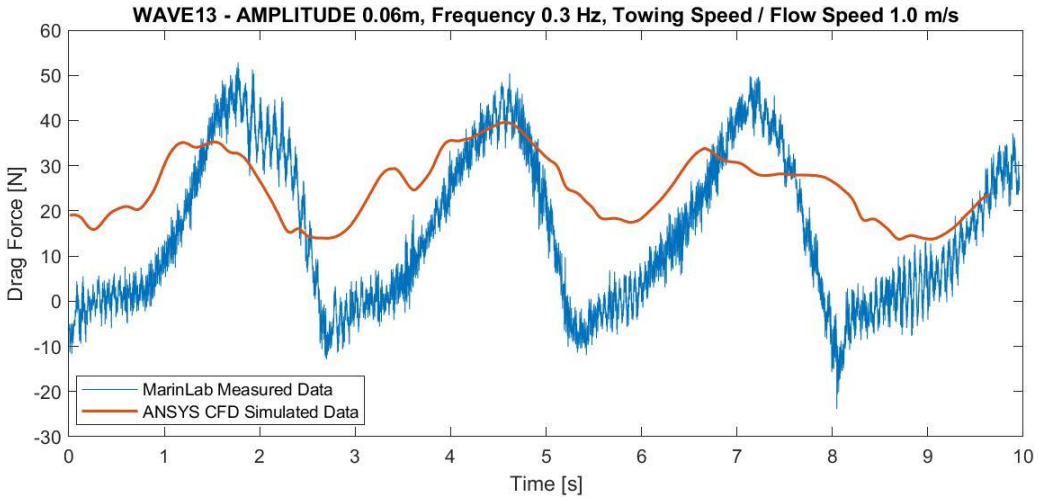

Figure 6.18 – Wave 13, 3D CFD results compared with MarinLab experimental data

6.4 Comparing 2D and 3D simulations

This chapter will compare the results from the two methods and hopefully substantiate some of the results from the validation process described in chapter 6.3.

The quality of the parametric analysis highly depends on the validity of the gathered data. The 2D simulation is a simplification of the 3D CFD, and the results from 3D CFD will be prioritised in this research. However, the results from 2D may still be valuable in terms of validating the results from 3D. Furthermore, the 2D model is not reliant on wall functions for near-wall modelling due to a higher mesh resolution. This might give the 2D simulations an advantage in some cases.

An example of a comparison of 2D and 3D simulations is presented in Figure 6.19. This Figure presents the drag force curves from MarinLab experiments compared with 3D and 2D CFD simulations for the case of Wave 6. The fit between the curves of the 2D simulation and the experimental test is remarkably good, even though the maximum values are higher for the 2D simulations. The higher negative values from MarinLab, which were not evident in the 3D results, are present in the case of 2D.

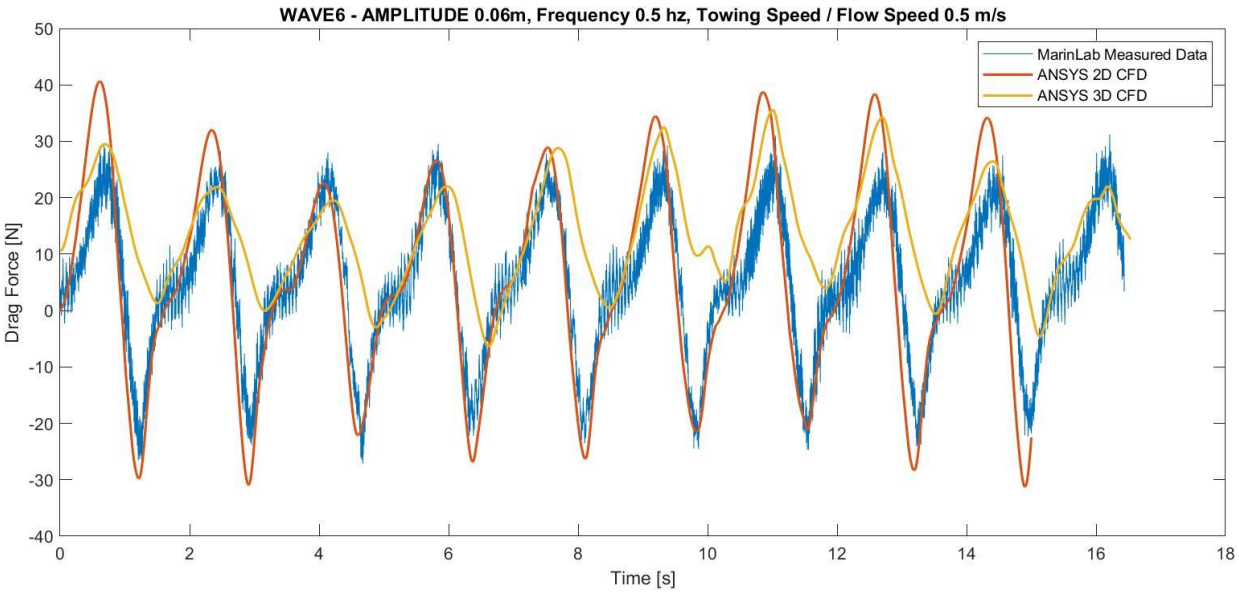

Figure 6. 19 – Wave 6, MarinLab vs 2D vs 3D

Looking further into the average of the maximum drag force, the results for wave 6 were: 26.2 N (MarinLab), 27.1 N (3D CFD), and 32.9 N (2D CFD). Even though the curve fit of 2D compared to MarinLab is arguably better, the accuracy of the average of the maximum drag force is higher for the 3D simulations.

In most cases, the results from 3D and 2D are similar. An example of this is Wave 7, plotted in Figure 6.20. This wave has an amplitude of 0.08 m, a frequency of 0.3 Hz, and a flow speed of 0.5 m/s. The average of the maximum drag force values for 2D versus 3D show quite a consistent result and are within 92% of each other. Both 2D and 3D results are classified as *good* (90-100 % accuracy) when validated with results from experiments in MarinLab.

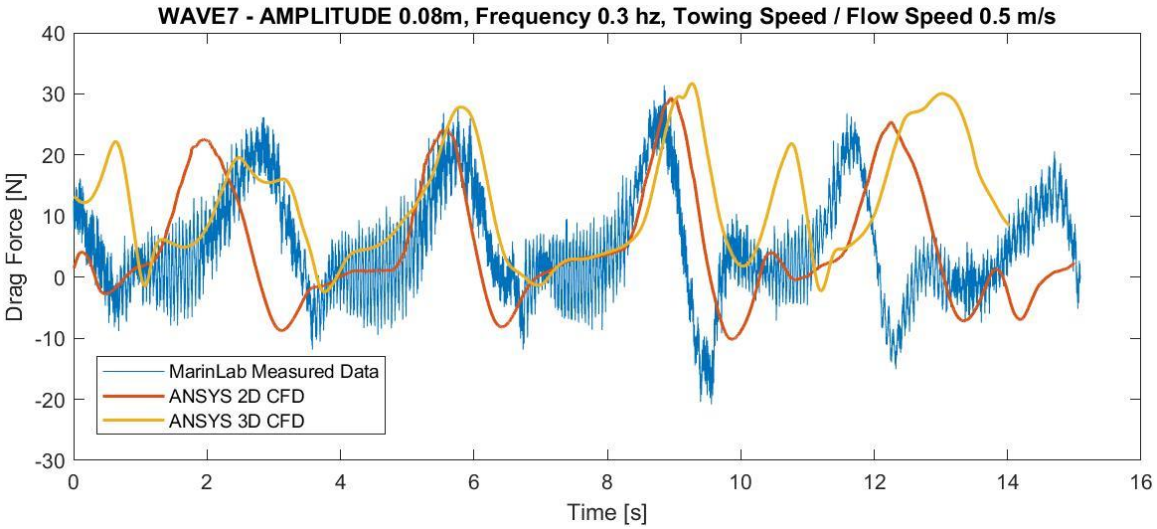

Figure 6. 20 – Wave 7, MarinLab vs 2D vs 3D

Wave 30 is an example of a case where the results from 3D simulations appear to be valid, but the 2D results are not. Figure 6.21 show the 3D simulations of wave 30 compared to MarinLab experiments. For this case, the 3D results have a decent fit compared to the experimental results. The accuracy of the average of the maximum drag force of the CFD compared with experiments is 86 %. However, the 2D results show a different story.

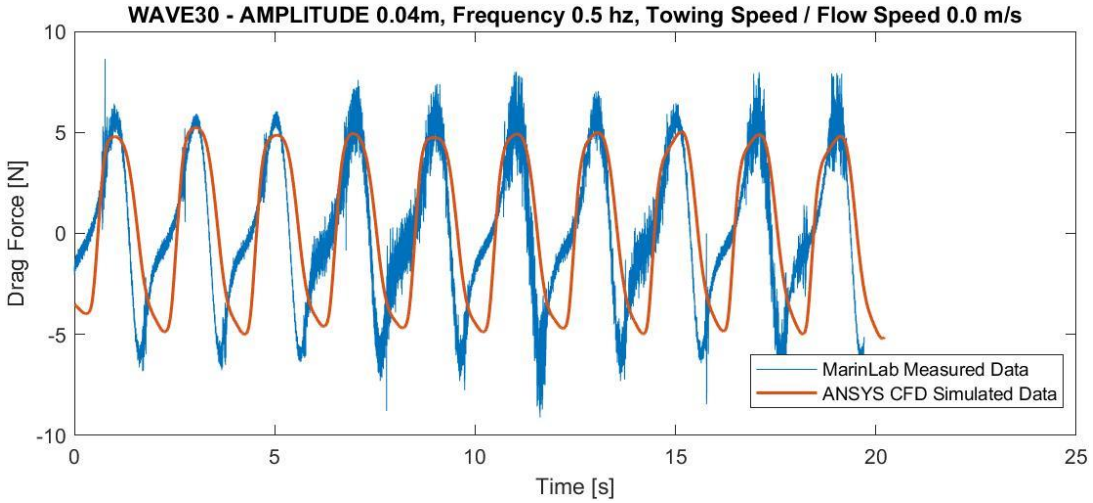

Figure 6. 21 – MarinLab experiments compared with ANSYS Fluent 3D CFD

In Figure 6.22, the results of 2D and 3D are plotted against each other. For this case, it is a noticeable deviation regarding the 2D simulation. The 3D results seem to stabilize after about 30 seconds. However, the calculated drag force from the 2D simulations keeps deviating and fluctuating through the entire 70 seconds of simulation. The 2D results also show a much larger output in the negative direction than in the positive direction. Concerning the case of wave 30, the 2D results must be regarded as useless.

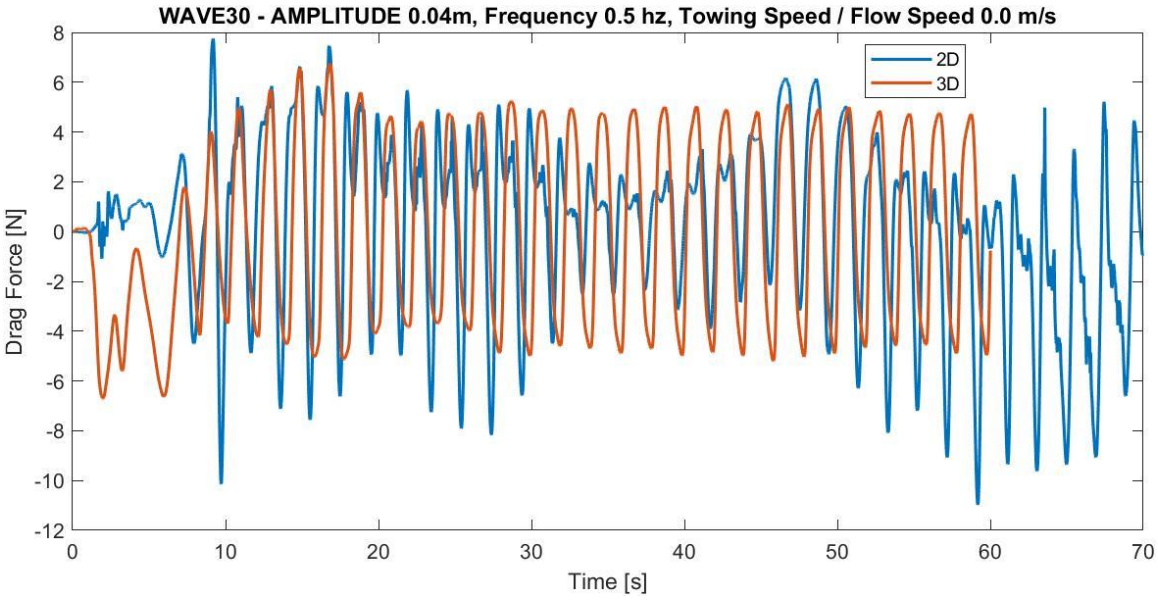

Figure 6. 22 – Comparing 2D vs 3D in the case of wave 30

6.5 Conclusion for data validation

After plotting and comparing all results from simulations and experiments, the gathered data appears to be of varying validity. However, 25 out of the 36 test cases show 80-100 % accuracy when comparing the average of the maximum drag force of CFD simulations to experiments. Looking further into the low accuracy cases, six of the 11 cases below 80 % accuracy are from the simulations at 1.0 m/s flow speed. That means that from the 30 test cases at flow speeds 0-0.5-0.75 m/s, only five of them were of accuracy below 80 %.

By looking further into the validity of the data for each parameter, some other trends become noticeable. Waves of frequencies 0.3, 0.4 and 0.5 Hz were simulated. 11 out of 12 tests at 4 Hz were within the 80-100 % accuracy range. On the other hand, only 5 of the 0.5 Hz cases showed an accuracy of over 80 %. In terms of wave amplitude, waves with amplitudes of 0.04, 0.06 and 0.08 m were simulated. 11 out of 12 cases at 0.04 m

amplitude resulted in accuracy over 80 %, in contrast to 0.08 m amplitude, where only five out of 11 cases were above 80 % accuracy.

A general trend regarding the overall curve fit is that as the speed increases, the curve fit tends to get worse. However, this might not affect the accuracy of the maximum drag force. For the 0.75 m/s cases, eight out of nine cases are within 80-100 % accuracy.

The results from 2D simulations were compared to 3D results. In general, the accuracy of the average of the maximum drag force values was higher for 3D than for 2D. However, for higher flow speed cases, the curve fit of the 2D simulations appeared to be better at modelling the negative force values than the 3D simulations.

It is concluded that results are variable in quality. However, the data are deemed to be of high enough quality to continue analysing the results. When investigating the different parameters, the emphasis should be on the data that showed the highest accuracy.

7. Discussing the results

This chapter presents an in-depth analysis of how changes in parameters affect the wave loads on the cylinder. When comparing the available data, the same procedure as described in chapter 6.3 is used to crop the valid part of the data after the simulation has stabilized. In general, this is the last 15-20 seconds of the simulation, but it may change depending on each simulation. When selecting the specific cases for analysis, the validation results from Chapter 6.3 are used. The objective is to pick out those cases that resulted in the highest graded classifications in terms of validation and base the analysis upon that data. As the 3D CFD simulations are assumed to be more accurate than the 2D simulations, this parametric study's primary focus will be on the 3D results.

7.1 Influence of amplitude change on wave loads

This chapter presents an analysis of how the changes in the amplitude of the wave will influence the force acting on the cylinder. The validation process of the CFD data gave positive results but was only executed for the drag force data, as the lift force was not measured during MarinLab experiments. Hence the analysis will mainly be concentrated on the drag force. However, it is assumed that when investigating the most valid cases of drag, the lift force is also of similar quality. Therefore, chapter 7.1.2 will contain a minor examination of the influence of changes in wave amplitude on lift force.

7.1.1 Influence of amplitude change on drag force

This chapter presents an analysis of the influence of amplitude changes on drag force. In Figure 7.1, the calculated drag force on the cylinder is plotted against time for amplitudes of 0.04 m, 0.06 m, and 0.08 m, at a constant flow speed of 0.0 m/s and a wave frequency of 0.3 Hz. Figure 7.2 shows the average of the maximum drag forces for the three mentioned cases. Figures 7.3-4 contain the equivalent plots for 0.4 Hz and Figures 7.5-6 for 0.5 Hz.

In Figure 7.1, the maximum drag force seems to vary a bit when compared with changes in amplitude. At around 9 seconds, the force seems to increase quite linearly with changes in amplitude. This is not the case at other timesteps, as between 12-15 seconds.

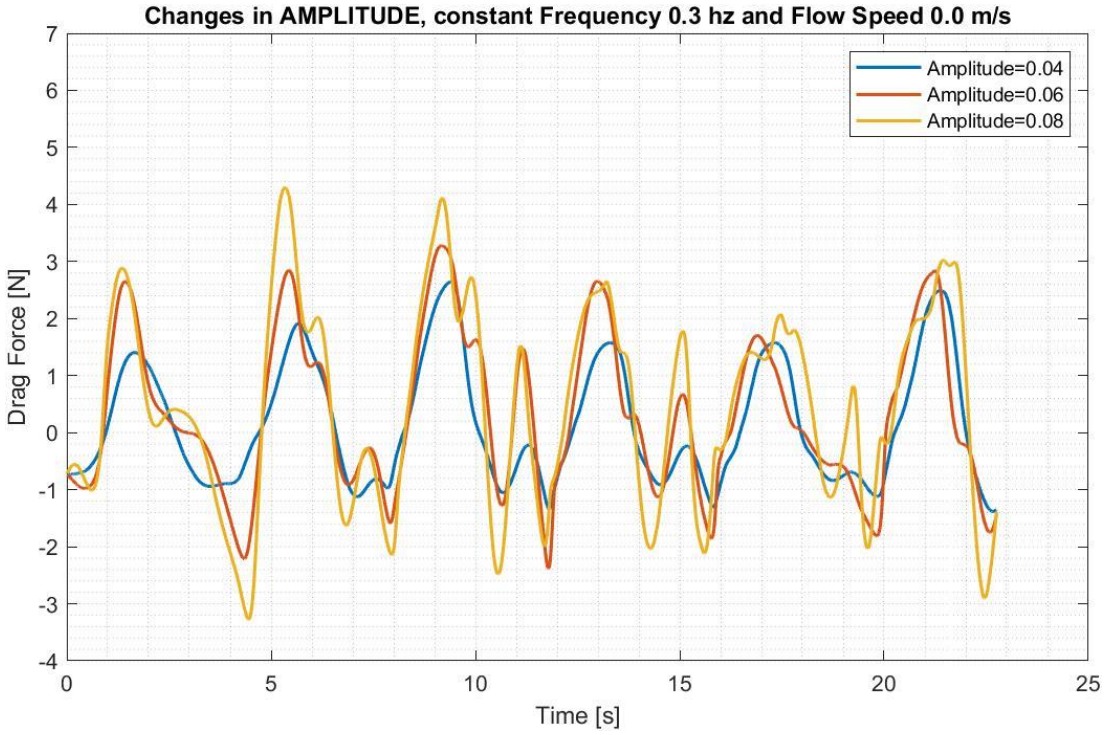

Figure 7.1 – 3D CFD: Changes in amplitude with constant frequency 0.3 Hz and flow speed 0.0 m/s

When looking at the average of the maximum drag force from the simulations presented in Figure 7.2, the increase in force seems to be quite linear. In the case of the MarinLab results, the measured drag force shows a higher increase but at a slightly decreasing rate.

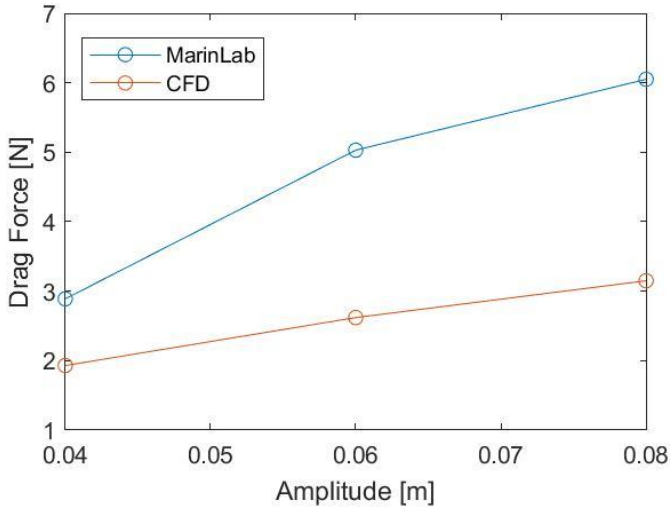

Figure 7.2 – Average maximum drag force plotted against changes in amplitude - 0.3 Hz and 0 m/s

Compared to changes in amplitude at 0.3 Hz, Figure 7.3 show a much more regular pattern of drag force in a time domain. For the cases presented in Figure 7.3, the frequency is 0.4 Hz, and these cases were all deemed as *good* (90-100 % accuracy) during the validation process in chapter 6.

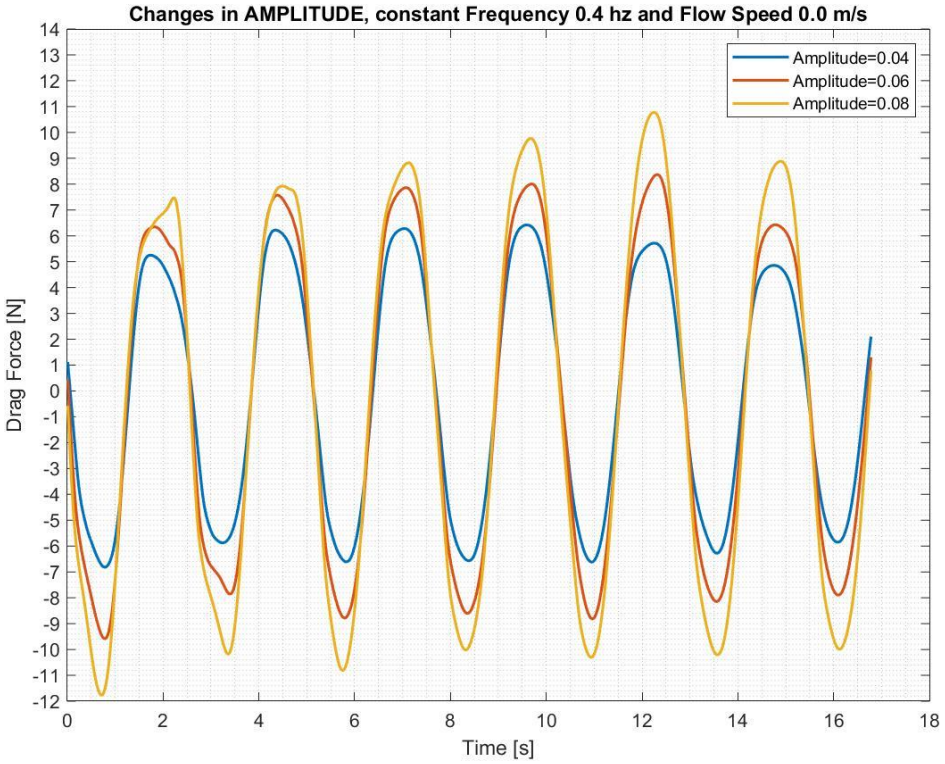

Figure 7.3 – 3D CFD: Changes in amplitude, with a constant frequency of 0.4 Hz and flow speed of 0.0 m/s

Looking at the average of the maximum values in Figure 7.4, the calculated force from CFD also appears to be much closer to the results from the experiments in MarinLab. The average max drag force for 0.4 Hz is within 90-98.3 %, whereas at 0.3 Hz, it was between 52-67%. In the case of 0.4 Hz, both the CFD and MarinLab results show an increase of drag force at a constant rate when the amplitude increases.

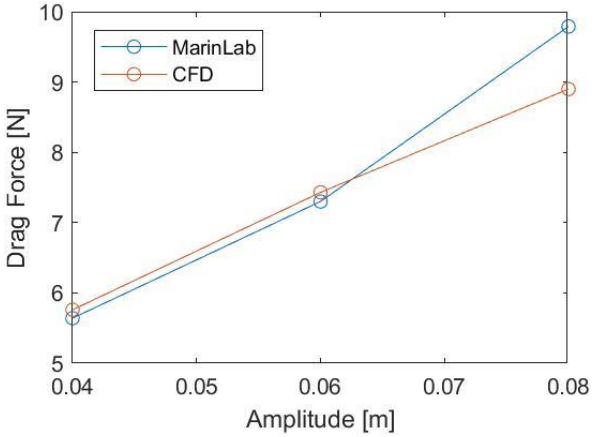

Figure 7.4 – Average maximum drag force plotted against changes in amplitude - 0.4 Hz and 0 m/s

For frequencies 0.3 and 0.4 Hz, the drag force on the cylinder seems to increase as the amplitude of the wave increases. For the 0.4 Hz cases, the drag force seems to increase close to linear. However, considering the 0.5 Hz cases, there are some apparent non-linearities in CFD results. As seen in Figure 7.5, for the amplitude of 0.08 m, there are significant fluctuations in the calculated maximum load.

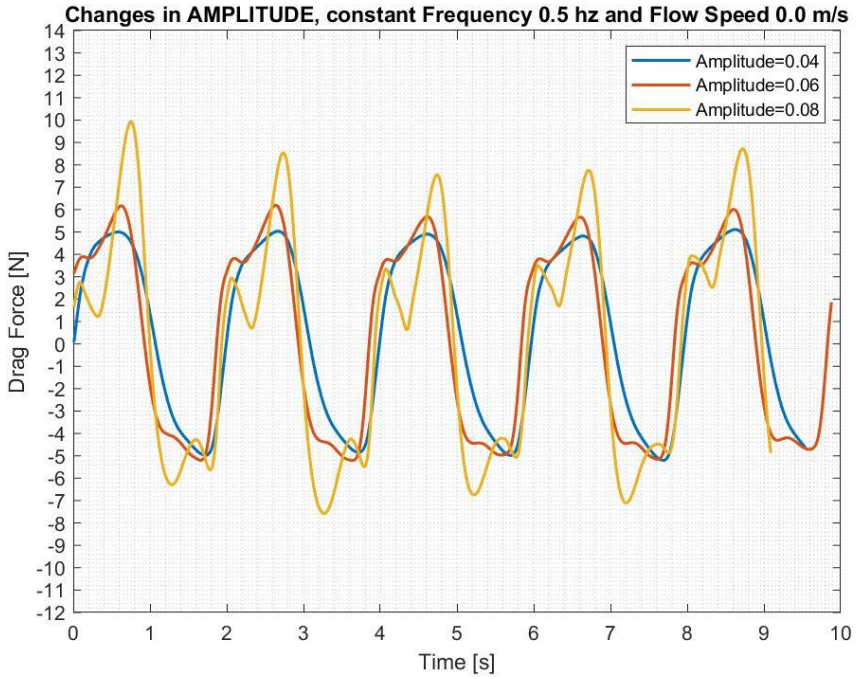

Figure 7.5 – 3D CFD: Changes in amplitude with constant frequency 0.5 Hz and 0 m/s flow speed

However, the data for the CFD and experiments at 0.0 m/s flow speed and 0.5 Hz show quite different results, as shown in Figure 7.6 of the average of the maximum drag force. The results from MarinLab show the same tendencies as for the 0.4 Hz case, but the results from CFD show a reduced increase in magnitude and a less linear increase compared with experiments.

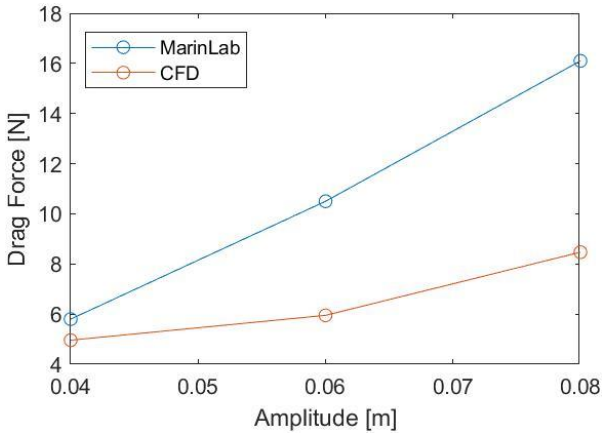

Figure 7.6 – The average of the maximum drag force plotted against changes in amplitude – at 0.5 Hz and 0 m/s

When looking at the animations of the isosurface between the air and water in Figure 7.7, for the waves of amplitude 0.08 and wave frequency of 0.5 Hz, the water starts to spoil over the cylinder at the time of impact. This differs from the smaller waves and waves of lower frequency and might influence the wave load on the cylinder.

Figure 7.7 – The water starts to spoil over the surface when the wave hits the cylinder

Inaccuracy in the loadcell may be another reason for the discrepancy. The loadcell is, as mentioned, more accurate for a bit higher loads than those that occur at 0.0 m/s flows speed. Therefore, this chapter will also include some examples from changes in 0.5 m/s and 0.75 m/s speed. Another reason for the low accuracy may be the quality of the CFD model.

Figure 7.8 shows the same waves as Figure 7.5, but in this case, it is from the data gathered during experiments in MarinLab. When comparing the results from CFD to the results from MarinLab, specifically for the case of 0.5 Hz and 0.0 m/s flow speed, the results from the experimental tests show a much more linear increase of force than for CFD. However, considering the accuracy of the loadcell for lower force values, looking at the average of the maximum drag force for changes in wave amplitude may still be useful.

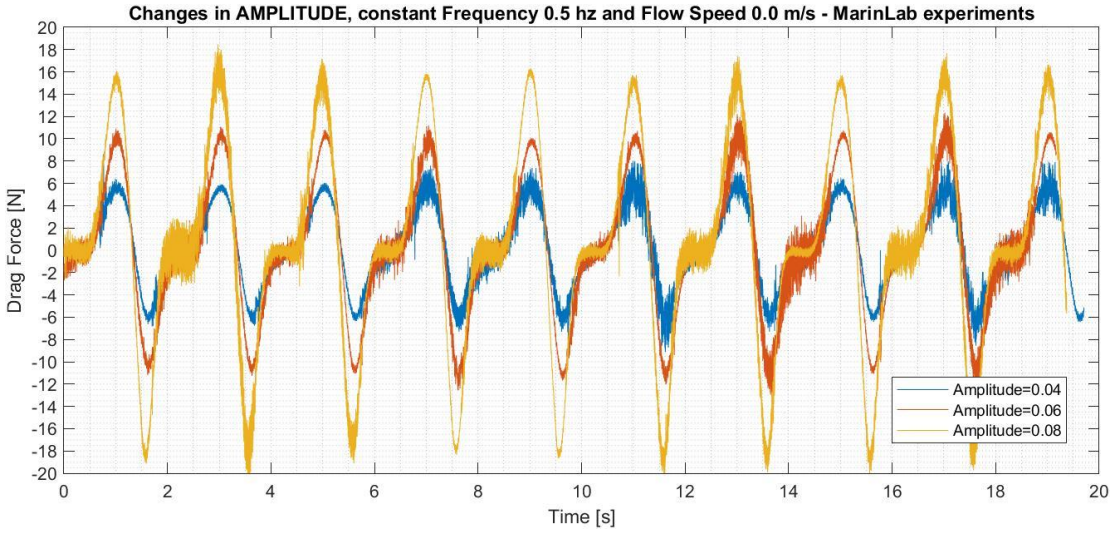

Figure 7.8 – Experimental data: Changes in amplitude at 0.5 Hz and 0.0 m/s

When assessing the validity of the data for flow speed of 0.0 m/s, the results for 0.3 Hz varies quite a bit from the tests in MarinLab. The loadcell that was used does not have satisfactory accuracy for measuring such a low force value, and because of that, the CFD results for all waves of frequency 0.3 Hz and 0.0 m/s flow speed are not that easy to validate. However, the case is quite different for waves of frequency 0.4 Hz. As seen in Figure 7.4 and Figures 6.9-6.10, the results from CFD fit very well compared to results from experiments and are therefore assumed to be reliable. In terms of waves of frequency 0.5 Hz, the results differ a bit. For amplitude 0.04 m, the results from CFD and experiments in MarinLab yield similar results. For bigger amplitudes (0.06-0.08 m), however, the results from CFD produce a significantly weaker force than the MarinLab experiments. In general, the trend is the same for all tests; an increase in amplitude means a near-linear increase in drag force.

During the validation process, the waves of frequency 0.4 Hz and flow speed 0.5 m/s appeared to fit quite well compared to the experiments performed in MarinLab, and this section presents the influence of changes in wave amplitude on drag force for waves at said parameters.

Figure 7.9 shows the average of the maximum drag force plotted against changes in amplitude. When comparing the results from CFD and MarinLab, the values are within 90-99% of each other, confirming the presumable high validity of the data. Furthermore, the drag force calculated from the CFD simulations appears to be increasing at a steady rate as the amplitude increases. The results from MarinLab show much of the same, but it appears to have a very low decreasing rate.

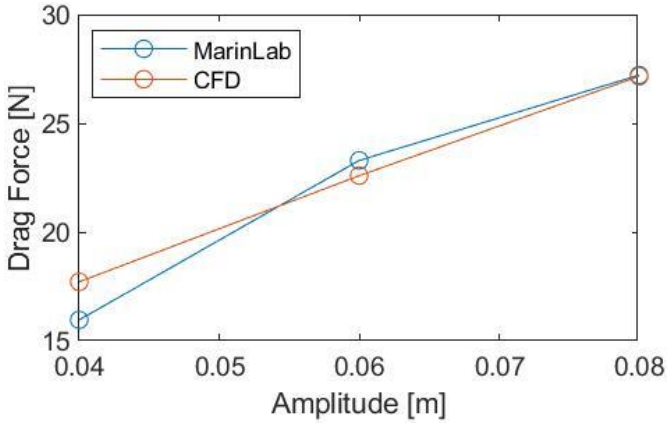

Figure 7.9 – Average max drag force plotted against changes in amplitude at 0.4 Hz and 0.5 m/s

Figure 7.10 shows the average of the maximum drag force plotted against changes in amplitude for a wave frequency of 0.4 Hz and a flow speed of 0.75 m/s. In this case, the results from CFD and MarinLab are within 92-96% of each other. Furthermore, the influence of amplitude changes on the maximum drag force shows the same tendencies for both the experimental and CFD data.

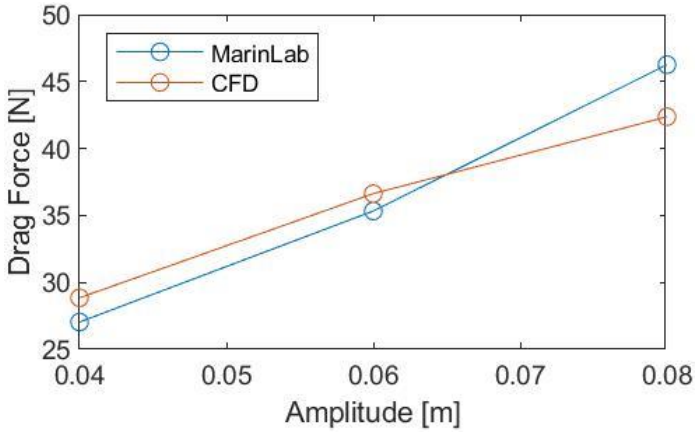

Figure 7.10 – Average max drag force plotted against changes in amplitude – 0.4 Hz and 0.75 m/s

7.1.2 Influence of amplitude change on lift force

In this chapter, it will be investigated how changes in wave amplitude influence the lift force. Unfortunately, there are no experimental data to compare directly with the 3D simulation results. However, when analysing the data that had the best fit in drag force, it is assumed that the data for lift force in the same cases should have reasonable validity.

When studying the impact of changes in amplitude on the lift force acting on the cylinder, it is assumed that the bigger the amplitude is, the higher the lift force is until the cylinder is fully submerged. This is assumed because of the formula for buoyancy (4.1) which relate the volume of the fluid displaced with the buoyancy. When the amplitude increases, the total submerged volume of the cylinder will also increase, meaning that the displacement volume increases, leading to an increase in the buoyancy force.

In Figure 7.11, the calculated drag force on the cylinder is plotted against time for three different amplitudes at a constant flow speed of 0.75 m/s and a wave frequency of 0.4 Hz. The maximum lift force is increasing with amplitude, as assumed.

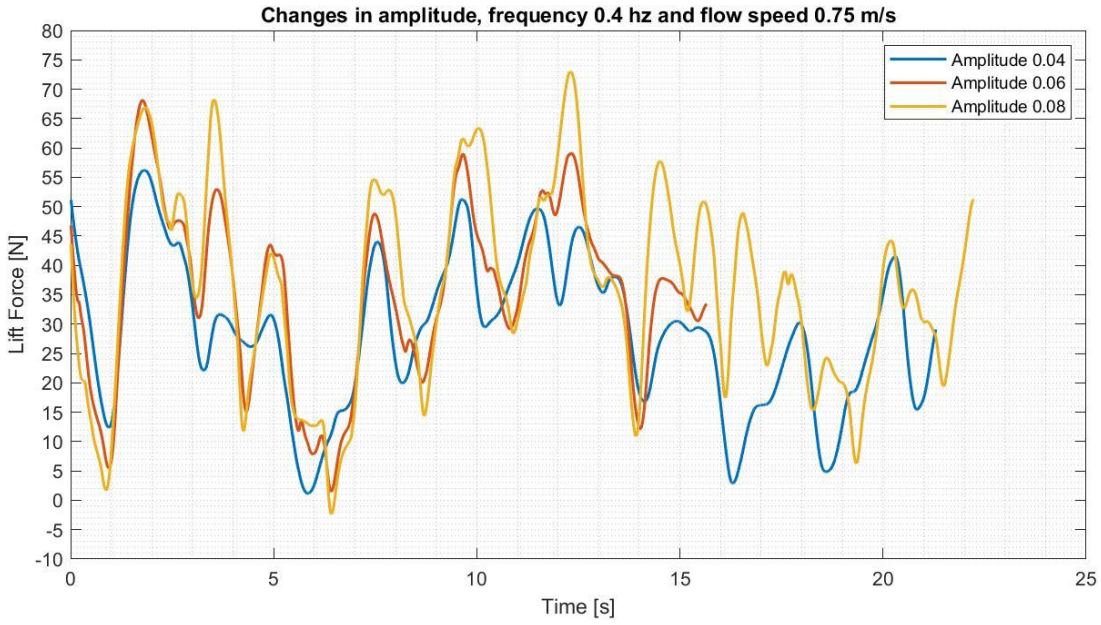

Figure 7.11 – Results from CFD: Influence of amplitude on the lift force

In Figure 7.12, the average of the maximum lift force is plotted against amplitude, and the lift force seems to increase at a decreasing rate.

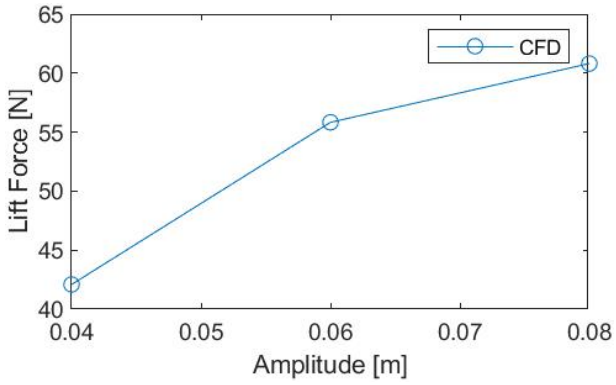

Figure 7.12 – Average of the maximum lift force plotted against increasing amplitude

7.2 Influence of wavelength change on wave loads

This chapter presents an analysis of how the influence of changes in wavelength will affect the force acting on the cylinder will be analysed. The validation process of the CFD data gave positive results but was only executed for the drag force data. Hence the analysis will mainly be concentrated on this. However, as the validity of the data from CFD appears to be of decent quality, chapter 7.2.2 will contain a minor discussion on the influence of changes in wavelength regarding lift force.

7.2.1 Influence of wavelength change on drag force

Waves 4, 5, 6, 22, 23, and 24 give good results compared to experiments in MarinLab and are therefore picked out for further investigation and analysis. Waves 4, 5 and 6 are plotted in Figures 7.13-14 and 22, 23 and 24 in Figures 7.15-16.

In Figure 7.13, waves with an amplitude of 0.06 m and a flow speed of 0.5 m/s are plotted with three different wave frequencies, 0.3 Hz, 0.4 Hz and 0.5 Hz. It is observable that as the frequency increases, the maximum drag force increases. Looking at the results from MarinLab tests in Figure 7.14, this observation is supported, with the same tendencies obvious here.

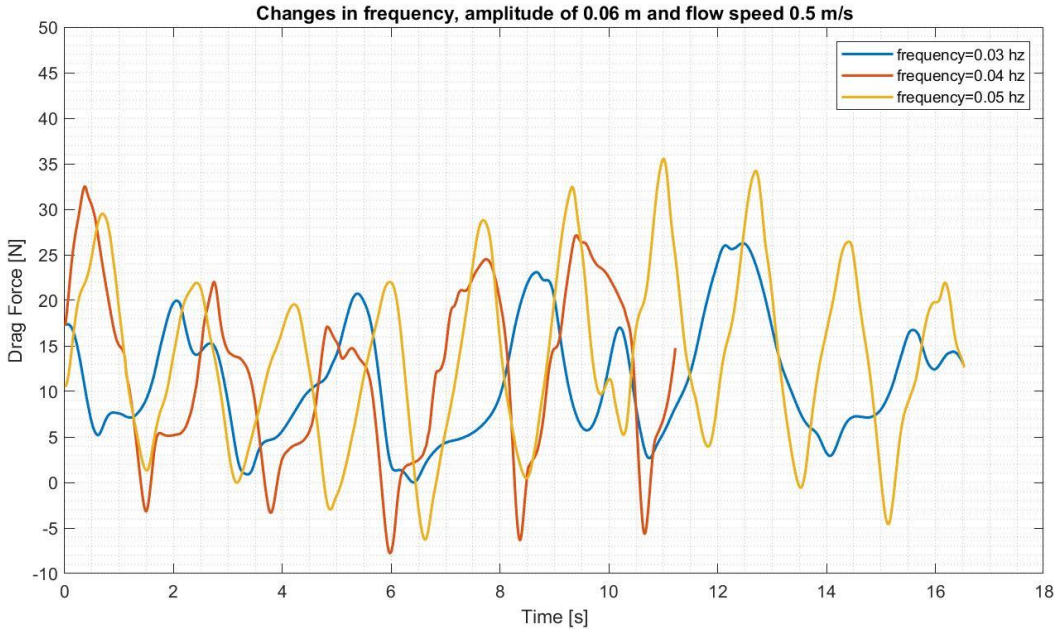

Figure 7.13 – Results from CFD: Influence of frequency on the calculated drag force

The averages of the maximum drag forces calculated from CFD and MarinLab experiments are presented in Figure 7.14. The average drag maximum seems to increase at a small decreasing rate for CFD results and MarinLab measurements as the frequency increases.

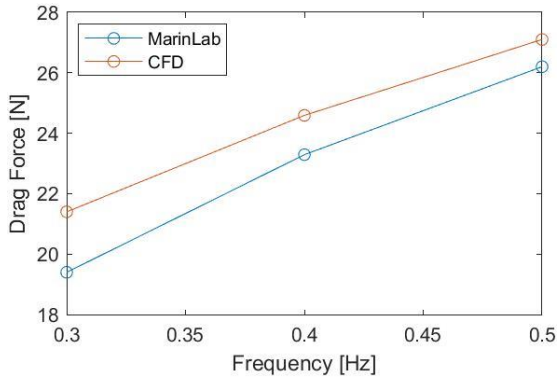

Figure 7.14 – Amplitude 0.06 m and flow speed 0.5 m/s

In Figure 7.15, waves with an amplitude of 0.06 m and a flow speed of 0.75 m/s are plotted with three different wave frequencies, 0.3 Hz, 0.4 Hz and 0.5 Hz.

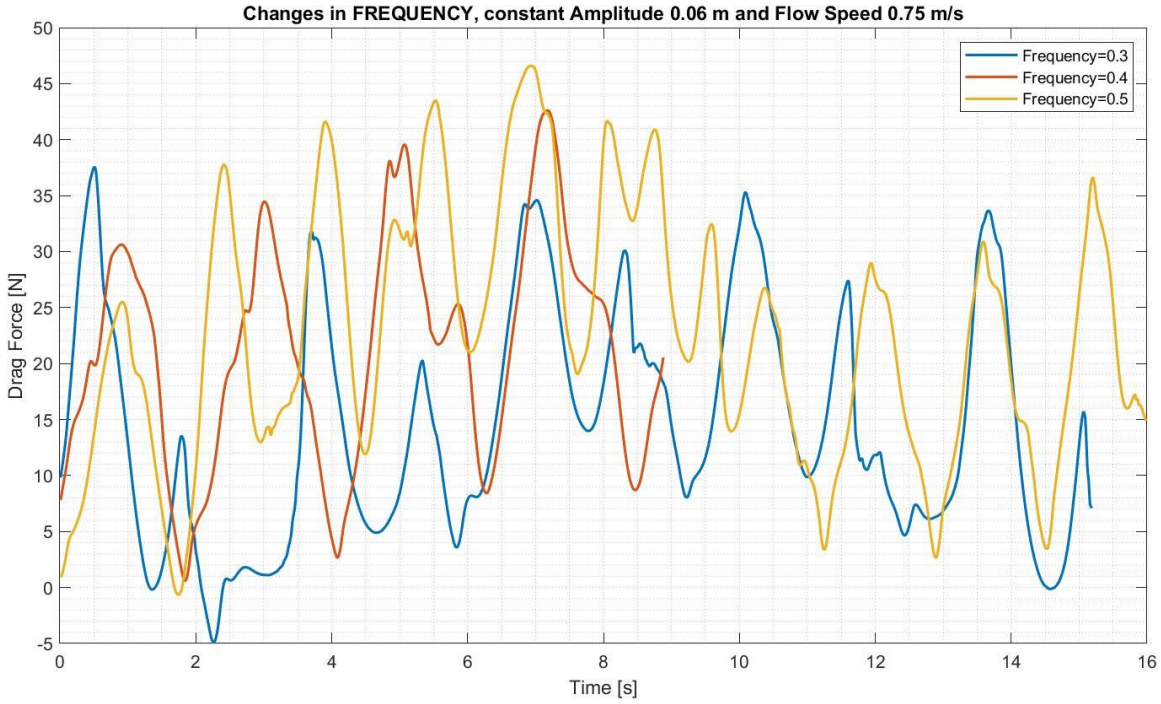

Figure 7.15 – Results from CFD: Waves 22, 23, 24

The average maximum drag forces calculated from CFD and MarinLab experiments are presented in Figure 7.16. As the frequency increases, the force increases at a linear rate.

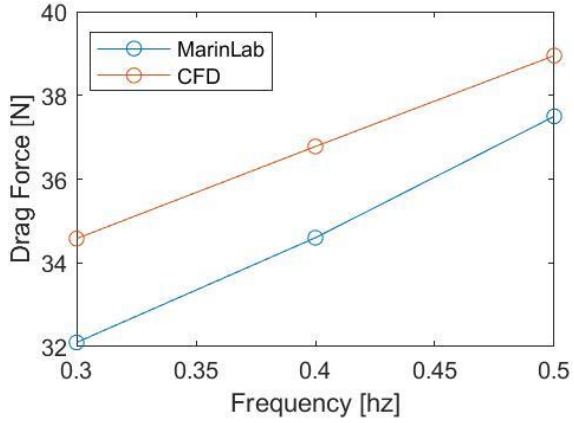

Figure 7.16 – Average max drag force plotted against frequency, constant amplitude 0.06 and flow speed 0.75 m/s

7.2.2 Influence of wavelength change on lift force

In this chapter, it will be investigated how changes in wave frequency affect the lift force. There are no experimental data to compare with directly. However, when analysing the data that had the best fit in drag force, it is assumed that the data for the lift force in the same cases should have reasonable validity.

Figure 7.17 shows the lift force from waves with an amplitude of 0.06 at three different frequencies. The flow speed is constant at 0.75 m/s, and immediately it becomes apparent that the influence of frequency has a different effect on lift force than drag force. As seen in chapter 7.2.1, an increase in frequency led to an increase in the drag force on the cylinder. However, in this case, an increase in frequency seems to result in a significant decrease in lift force.

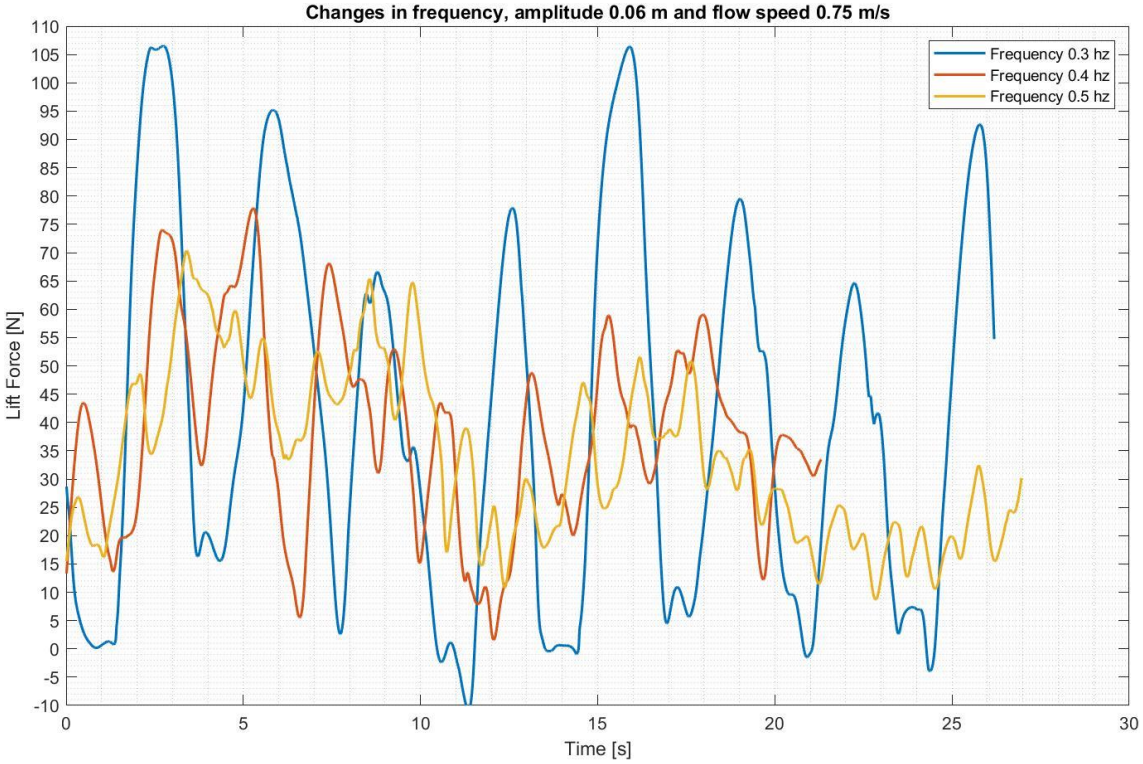

Figure 7.17 - Influence of frequency on lift force

Figure 7.18 shows the mean maximum lift force, and it confirms that as frequency increases, the lift force decreases at a decreasing rate.

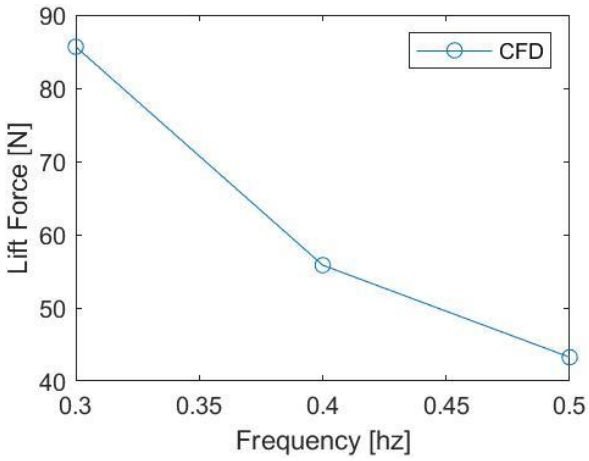

Figure 7.18 - Average max lift force plotted against frequency

7.3 Influence of flow speed change on wave force

This chapter will compare how different flow speeds affect the drag and lift force on the cylinder. Like the chapters about amplitude and frequency analysis, the drag force will be focused on because of the validated data. The analysis of how the flow speed influences the drag force is presented in chapter 7.3.1, and how the flow speed influences the lift force is presented in chapter 7.3.2.

7.3.1 Influence of flow speed on drag force

When investigating the influence of changing flow speed on drag force, waves 5, 14, 23, and 32 are chosen. These waves are all of 0.06 m amplitude and 0.4 Hz frequency and show promising results in terms of validity for all four cases. When investigating the impact of changes in flow speed on the drag force acting on the cylinder, it is expected that an increase in speed will lead to an increase in drag force. This phenomenon is observable in Figure 7.19, which shows the average of the maximum drag force for a wave with an amplitude of 0.06 m and a frequency of 0.4 Hz at four different flow speeds. As the speed increases, the drag force also increases. In the cases of 0.5 – 0.75 – 1.0 m/s, the speed is increased by 0.25 m/s for each step. The average of the maximum drag force also appears to increase at a steady rate for these cases.

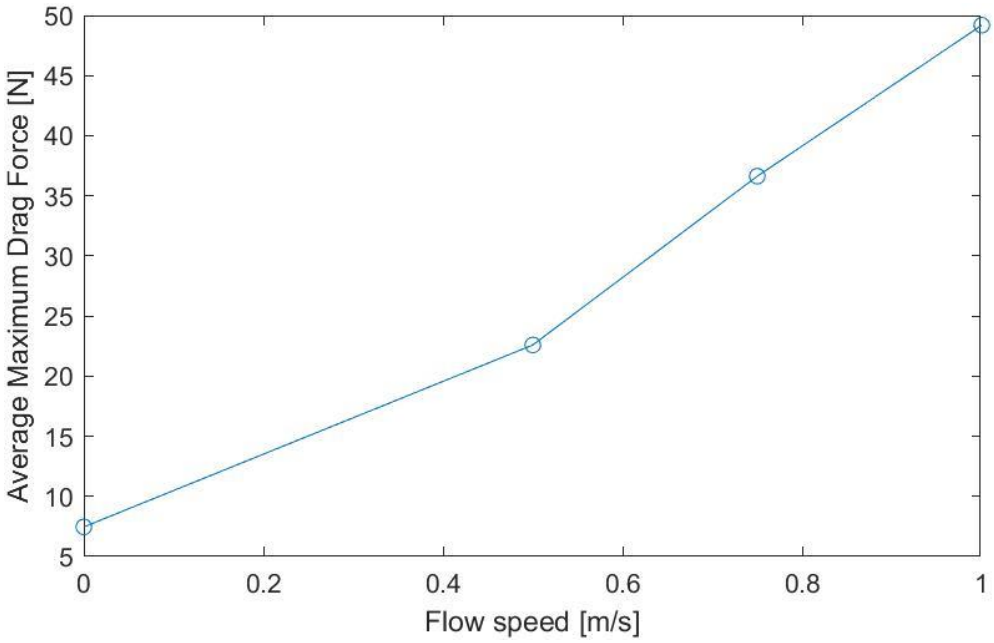

Figure 7.19 – Average of the maximum drag force plotted against changes in flow speed

7.3.2 Influence of flow speed on lift force

In the case of lift force, waves 8, 17, 26, and 35 are chosen because these four waves showed the best data validity during the validation process. These waves are all of 0.08 m amplitude and 0.4 Hz frequency. During the validation process, waves 8, 26 and 35 showed a high level of validity results for drag force (90-95% average of the maximum drag force accuracy). Wave 17 yielded worse results regarding the drag force, where the maximum drag force compared with experimental results showed an accuracy of 65 %. The maximum lift force average is plotted against the flow speed changes and presented in Figure 7.20. The speed is increased in steps of 0.0 – 0.5 – 0.75 – 1.0 m/s. It does not appear to be an obvious pattern regarding the maximum lift force as flow speed changes. This may be due to the quality of the data, or perhaps the low number of parameter changes made a pattern difficult to discover.

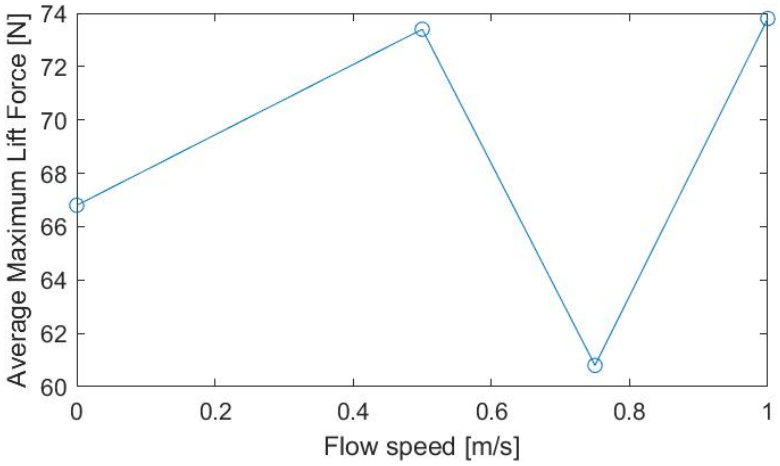

Figure 7.20 – Average of the maximum lift force plotted against changes in flow speed

7.4 Changes in submersion level

During the validation process presented in Chapter 6.3, wave 33 showed a high level of validity when comparing 3D simulations and experiments from MarinLab. For that reason, wave 33 is chosen to investigate the influence of changes in the submersion level of the cylinder. Wave 33 has an amplitude of 0.06 m, a frequency of 0.5 Hz and the flow speed is 0 m/s. After running four more simulations, only changing the submersion level of the cylinder in steps of 1 cm, as shown in Figure 7.21. The base level of the waterline indicated by 0 cm is when the cylinder is precisely halfway submerged.

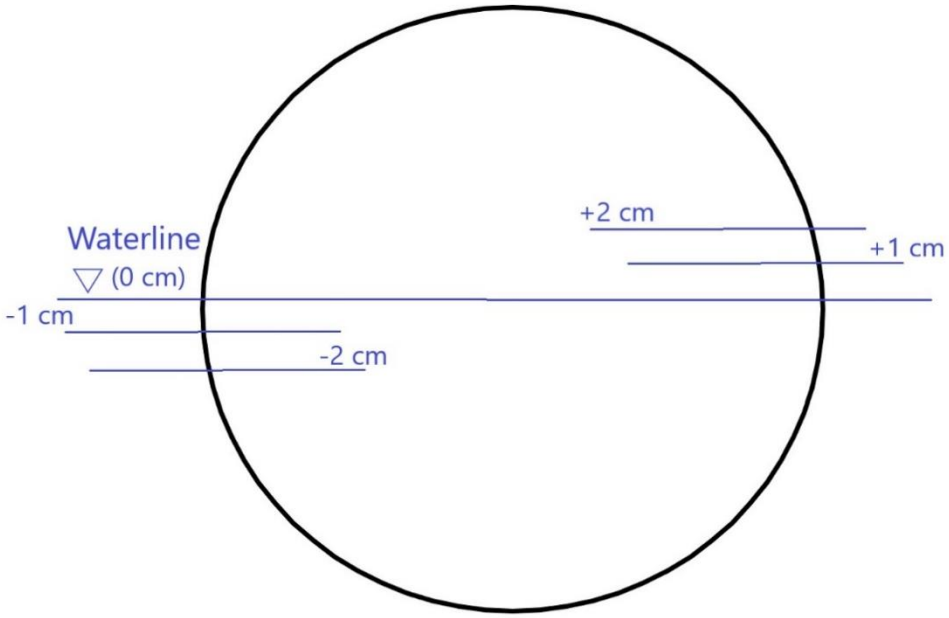

Figure 7.21 – Illustration of changes in submersion level

This chapter is divided into two subchapters, discussing the influence of submersion. Chapter 7.4.1 focuses on the impact of submersion on the drag force, and Chapter 7.4.2 is about the influence on the lift force.

7.4.1 Influence of changes in cylinder submersion level on drag force

Figure 7.22 shows the calculated drag force plotted against time for wave 33 at the five submersion levels. Immediately it is observable that the drag force increases as the cylinder is placed further down into the fluid. A higher drag force for more submersion is expected as more volume comes in contact with the fluid particles moving in the wave.

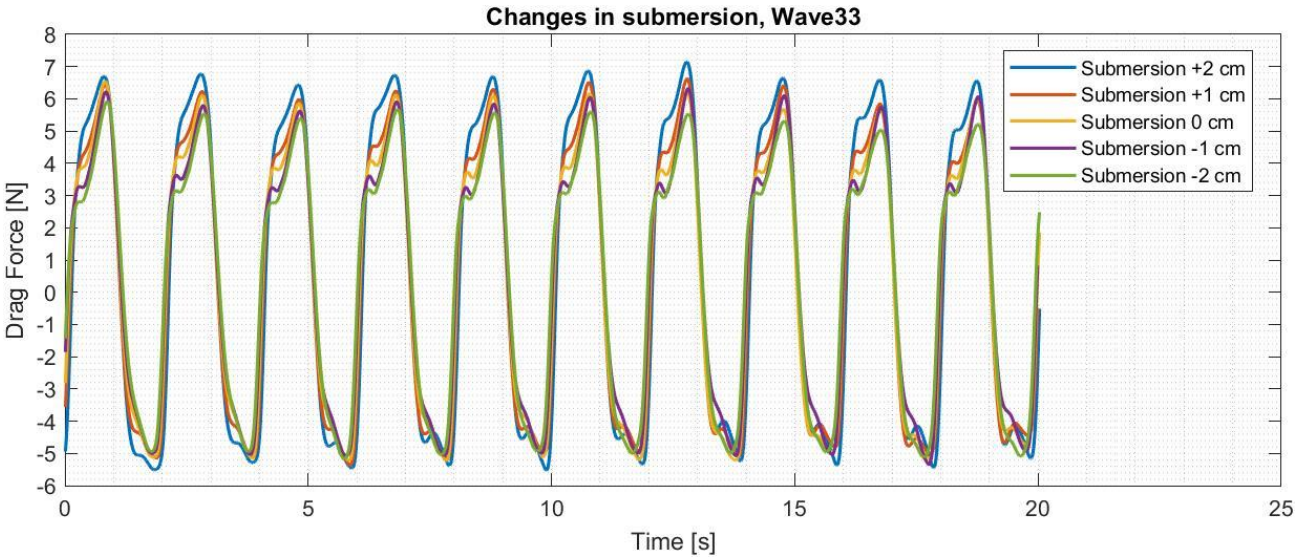

Figure 7.22 – Changes in submersion of the cylinder and the impact on drag force

Looking closer at the peak values between 14 and 15 seconds, the maximum values of the force appear to increase linearly as the cylinder is placed deeper into the fluid. A closer look at the peak values of the drag force between 14 and 15 seconds is presented in Figure 7.23.

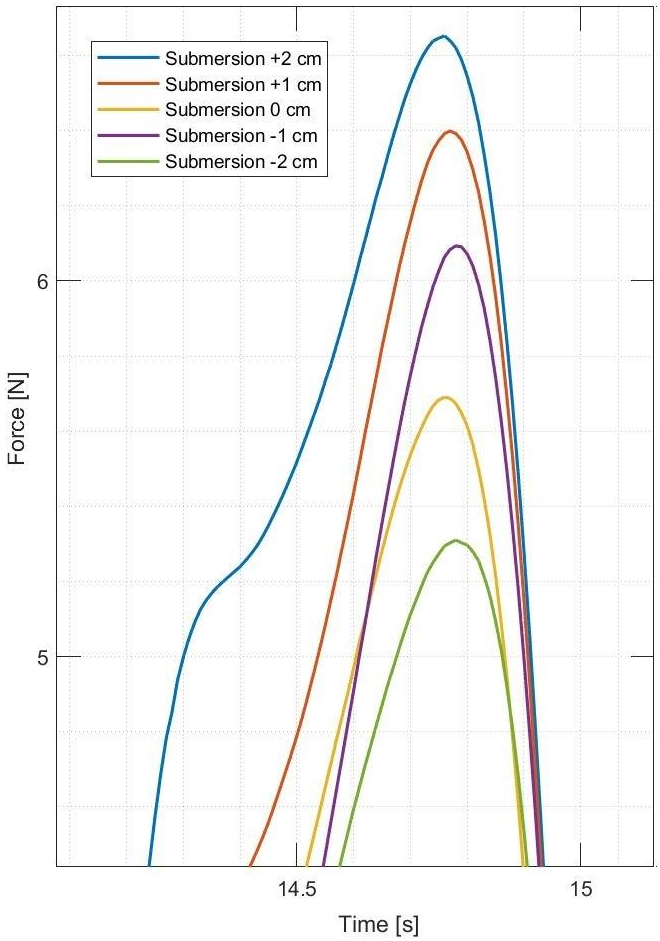

Figure 7.23 – A closer look at the calculated drag force between 14 and 15 seconds

When inspecting each peak value for the entire simulation, another pattern comes to light. In Figure 7.24, the average of the maximum drag force is plotted against changes in submersion level. The shape of the curve is reminiscent of a cubic function. Considering the profile shape of a circle, it makes sense that as the submersion level gets further away from the cylinder centre, the more drastically the drag force is changed.

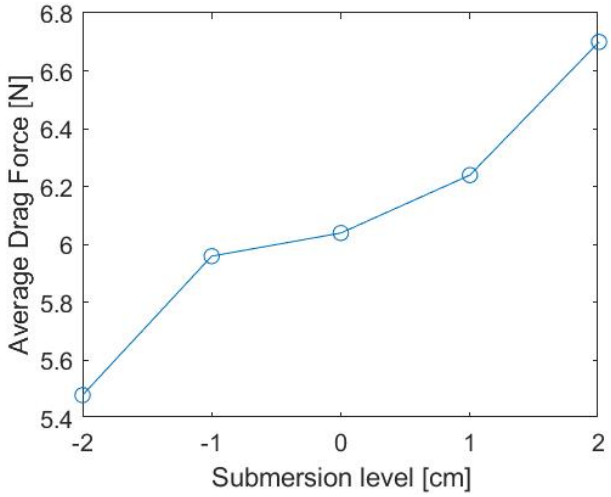

Figure 7.24 – The average of the maximum drag force plotted against the level of submersion of the cylinder

7.4.2 Influence of changes in cylinder submersion level on lift force

Figure 7.25 presents the lift force plotted against time for five submersion levels. A more straightforward pattern is apparent when comparing Figure 7.25 with the equivalent plot for drag force in Figure 7.22. The lift force increases linearly as the cylinder is placed deeper into the fluid. When considering the formula for buoyancy force (formula 4.1), it is expected that as the submersion level increases, the buoyancy force increases.

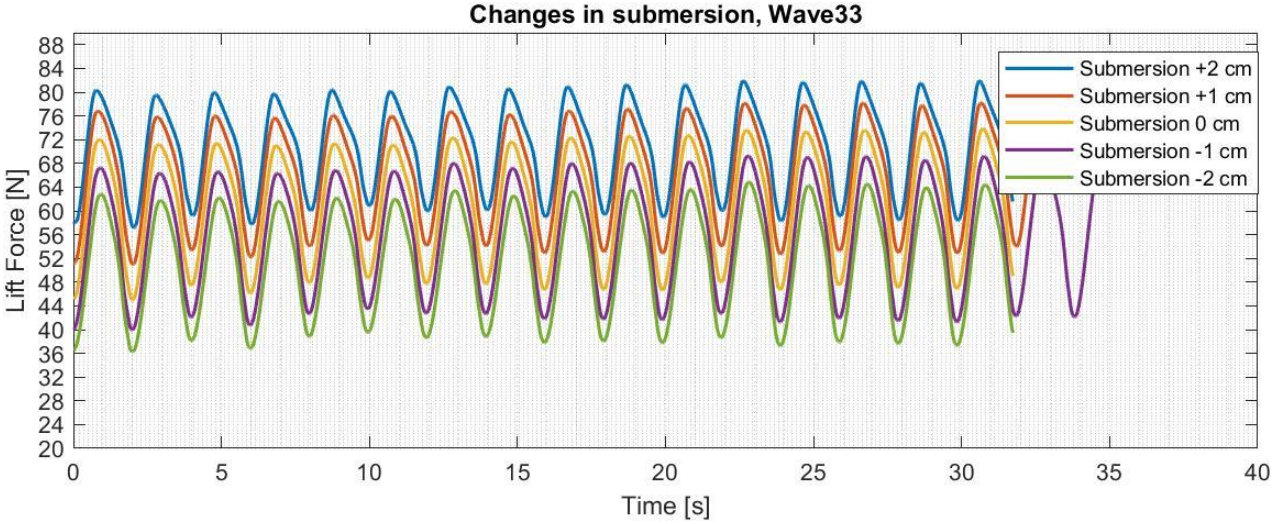

Figure 7.25 – Lift force plotted against time for five different submersion levels

This trend is confirmed when looking at the maximum average lift force, as plotted in Figure 7.26. As the submersion level increases, the average of the maximum lift force increases at a linear rate.

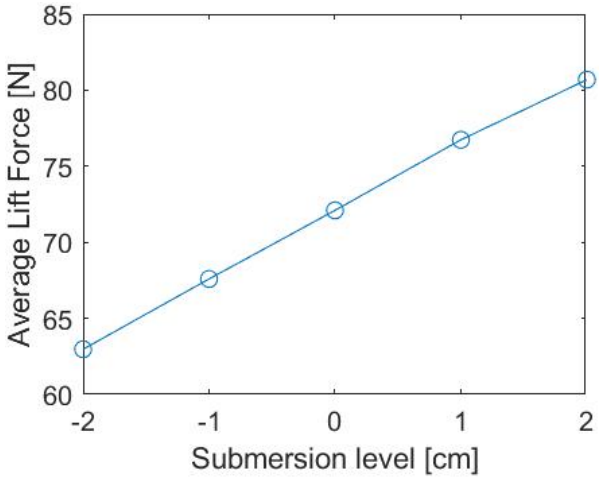

Figure 7.26 – Average of the maximum lift force plotted against changes in submersion level

8. Conclusion and further works

8.1 Conclusion

In this research, a 2D and 3D CFD model has been built and used to analyse wave load effects on a partially submerged cylinder, placed horizontally and transversely against the waves in a fixed position. In order to validate the CFD results, two different sized models have been built and tested in MarinLab, the hydrodynamical testing facility at HVL Kronstad. A total of 72 tests were completed, measuring the drag force on the cylinder at three different wave amplitudes, three different frequencies and four different flow speeds.

The validation process led to the discovery that 25 out of the 36 test cases show between 80-100 % accuracy when comparing the 3D CFD results to the experiments, regarding the average of the highest recorded values. The 3D CFD model is most accurate at flow speeds of 0.0-0.75 m/s.

A thorough analysis of all the gathered data has been performed using MATLAB, taking a deeper look into how the wave amplitude, frequency/wavelength, submersion level, and flow speed influence the drag and lift force on the cylinder.

A summary of the results from the parametric study of the wave load is presented in the list below:

- An increase in the wave amplitude results in a proportional increase of the drag force. Assuming that the data for lift force is also valid, the same phenomena also occur for the load in the vertical direction. This result is supported by the research findings of both Bijin Liu et al. (2020) and Aristodemo et al. (2017).
- An increase in the wave frequency (decrease in wavelength) leads to an increase in drag force at a low decreasing rate. However, the lift force decreases as the wave frequency increases.
- As the flow speed increases, the drag force increases at a steady rate. However, in terms of lift, the results were questionable. The speed was increased from 0.0 m/s to 0.5 m/s to 0.75 m/s to 1.0 m/s. The 0.75 m/s flow speed case showed a low accuracy during the validation process, and the calculated lift force was lower than at 0.0 m/s and 0.5 m/s.

- The influence of changing the cylinder submersion level was also investigated. Five different submersion levels were simulated in 3D CFD. As the submersion level gets further away from the cylinder centre, the more drastically the maximum drag force is changed. That means that the drag force increases at an increasing rate when the cylinder is more submerged and decreases at an increasing rate as less of the cylinder is submerged.
- The maximum lift force increases at a steady rate the more the cylinder is immersed in water.

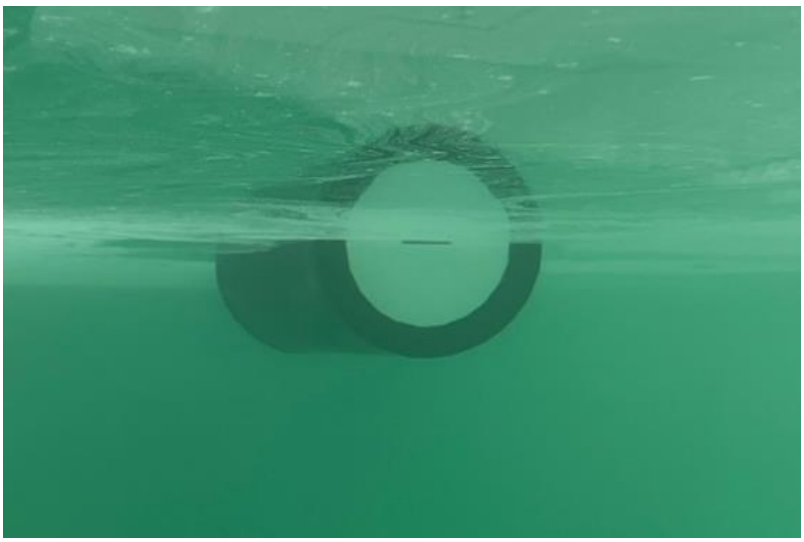

Figure 8.1 – Picture of the cylinder beneath the surface during testing in MarinLab

8.2 Further work

There are a lot of possible threads to follow and investigate at a deeper level when suggesting further work. When performing a parametrical analysis of the wave loads, the accuracy of the CFD model is vital. Designing and adapting the CFD model for each different case would lead to more valuable and trustworthy data on which to build the parametric analysis. Tailoring the mesh, especially for each simulation, could improve the accuracy of the data and, in turn, yield higher quality results. The mesh resolution required for a 0.0 m/s flow speed is not necessarily the same for one at 1.0 m/s. One model for each case might take more time to achieve but must be weighed against the value of the accuracy of the results.

Another possibility would be to increase the computational resources by acquiring access to supercomputers instead of relying on the outdated PCs that HVL has at their disposal in the Computer Lab at Kronstad. This would cut down a lot on simulation times and would open up the possibility of a higher resolution in the mesh.

In this project, the shape of a cylinder was the main geometrical feature studied. However, analysing different geometries used in Marine Engineering and comparing how the effects of wave loads differ would also be interesting and valuable from an engineering perspective. This research has looked at a circular cylinder, but another typical geometrical shape in marine engineering is the square-shaped cylinder. What happens to the wave load on a structure if it is square-shaped instead of circular? Another possibility is to evaluate the wave load when the angle of the cylinder is changed or perhaps to investigate how changing the cylinder dimensions affect the wave load.

Studying and analysing a wider range of different wave parameters could also be beneficent. Running more tests for each parameter change would lead to a more comprehensive data collection to base the analysis. Further investigating how the relations between parameter changes affect other parameters could also yield valuable results.

As described in the background theory chapter, there are other methods of calculating the wave loads on an object than CFD. Comparing the results from CFD simulations to the more standard methods based on the Morison equation and potential theory would be

another exciting project. For an engineering case, what are the pros and cons of CFD compared to other methods?

Using the collected data to build a simplified mathematical model to calculate wave load with a high enough quality so that it could potentially replace the existing models used present day would be an incredibly valuable target for further work.

9. References

Airy, G. B., 1841. *"Tides and waves",* Cambrigde: Encyclopedia Metropolitana, Mixed Sciences.

Alfonsi, G., 2009. Reynolds-Averaged Navier-Stokes Equations for Turbulence Modeling. *Applied Mechanics Reviews - APPL MECH REV. 62*, DOI: 10.1115/1.3124648, p. 3.

ANSYS, 2012. *ANSYS - Theory Guide 12.0 - Mesh Quality.* [Internet]
Available at:
https://www.afs.enea.it/project/neptunius/docs/fluent/html/ug/node167.htm
[February 2022].

ANSYS, 2014. *Introduction to ANSYS Fluent: Turbulence Modeling 15.0.* [Internet]
Available at:
https://www.researchgate.net/profile/Panayampilly_Abdul_Samad/post/y_plus_range_for_turbulent_models/attachment/59d6393c79197b8077996735/AS%3A400990483304449%401472614989133/download/Fluent-Intro_15.0_L07_Turbulence.pdf
[2022].

Aristodemo, F. &. T. G. &. M. D. &. V. P., 2017. Solitary wave-induced forces on horizontal circular cylinders: Laboratory experiments and SPH simulations. *Coastal Engineering. 129 Edition*, pp. 17-35. 10.1016/j.coastaleng.2017.08.011.

Bijin Liu, D. F. Y. Z. X. C., 2020. Experimental and numerical study on the wave force calculation of a partially immersed horizontal cylindrical float. *International Journal of Naval Architecture and Ocean Engineering*, July, pp. 733-742.

CFD Online, 2007. *www.cfd-online.com.* [Internet]
Available at: https://www.cfd-online.com/Wiki/Mesh_classification
[2021].

DNV, 2018. *Class Guideline - Wave Loads - DNVGL-CG-0130,* HØVIK: Det Norske Veritas - https://rules.dnv.com/docs/pdf/DNV/CG/2018-01/DNVGL-CG-0130.pdf .

Faltinsen, O., 1993. *Sea loads on ships and offshore structures.* Vol 1 red. Camebridge: Cambridge university press.

Fenton, J. D., 1985. A Fifth-Order Stokes Theory for Steady Waves. *Journal of Waterway, Port, Coastal, and Ocean Engineering*, March, pp. Vol 111, Issue 2.

FLOW-3D, 2021. *https://www.flow3d.com/modeling-capabilities/waves/.* [Internet]
Available at: https://www.flow3d.com/modeling-capabilities/waves/
[January 2021].

ITTC, 2017. *Recommended Procedures and Guidelines - Practical Guidelines for Ship Resistance CFD.* Zürich, International Towing Tank Conference.

Khalil, G. M., 2001. Experimental investigation of wave forces on submerged horizontal cylinders. *Indian Journal of Engineering and Materials Sciences Vol. 8*, April, pp. 59-65.

LEAP Australia, 2020. *https://www.computationalfluiddynamics.com.au/.* [Internet]
Available at: https://www.computationalfluiddynamics.com.au/turbulence-part-3-selection-of-wall-functions-and-y-to-best-capture-the-turbulent-boundary-layer/
[January 2022].

LEAP Australia, u.d. *www.computationalfluiddynamics.com.au.* [Internet]
Available at: https://https://www.computationalfluiddynamics.com.au/tips-tricks-turbulence-wall-functions-and-y-requirements/#:~:text=The%20y%2B%20value%20is%20a,are%20within%20a%20certain%20range.www.cfd-online.com/Wiki/Mesh_classification
[2021].

Marshall Bern, P. P., 2000. *Handbook of Computational Geometry.* ISBN 9780444825377 red. North-Holland: s.n.

MathWorks, 2022. *se.mathworks.com.* [Internet]
Available at: https://se.mathworks.com/products/matlab.html
[January 2022].

Menter, F., 1994. Two Equation Eddy-Viscosity Turbulence Modeling for Engineering Applications. *AIAA Journal*, p. 32.

P. K. Kundu, I. M. C. D. R. D., 2016. *Fluid Mechanics 6th Edition.* 6th Edition red. Oxford: Elsevier Inc.

Rapp, B. E., 2017. Chapter 31 - Finite Volume Method. I: I. 9781455731411, red. *In Micro and Nano Technologies, Microfluidics: Modelling, Mechanics and Mathematics.* s.l.:Elsevier, pp. 633-654.

SalMar ASA, 2022. *www.salmar.no.* [Internet]
Available at: https://www.salmar.no/en/gallery/
[May 2022].

Shuyu Sun, T. Z., 2020. Chapter two - Review of classical reservoir simulation. I: T. Z. Shuyu Sun, red. *Reservoir Simulations.* ISBN 9780128209578: Gulf Professional Publishing, pp. 23-36.

SIMSCALE, 2021. *Simscale.com.* [Internett]
Available at: https://www.simscale.com/docs/simulation-setup/global-settings/k-omega-sst/
[January 2022].

Steven H. Collicott, D. T. V. E. L. H. P. W. C., 2013. *Aerodynamics for Engineering Students (6th Edition).* ISBN 9780080966328 red. Butterworth-Heinemann: Elsevier.

Steven J. Lind, B. D. R. a. P. K. S., 2020. Review of smoothed particle hydrodynamics: towards converged Lagrangian flow modelling. *The Royal Society Publishing*, p. Proc. R. Soc. A. 476: 20190801.

Yuan, Z.-M., 2018. Side wall effects on ship model testing in a towing tank. I: Atilla: Ocean Engineering, Vol. 147.

10. Appendix A

This is the Appendix A.

10.1 2D Simulations

In Tables 9.1 – 9.3 below, the tested wave parameters are presented. All simulations were done at the dimensions and placements as described in subchapter 3.2.1.

Simulation_1					
diameter [mm]	wave heigth [mm]	no of waves	wave length [mm]	velocity [m/s]	submerge level [mm]
1500	100	1	1000	0,1	250
1500	100	1	1200	0,1	250
1500	100	1	1400	0,1	250
1500	100	1	1600	0,1	250
1500	200	1	2000	0,1	250
1500	200	1	2400	0,1	250
1500	200	1	2800	0,1	250
1500	200	1	3200	0,1	250

Simulation_2					
diameter [mm]	wave heigth [mm]	no of waves	wave length [mm]	velocity [m/s]	submerge level [mm]
1500	100	1	1000	0,5	250
1500	100	1	1200	0,5	250
1500	100	1	1400	0,5	250
1500	100	1	1600	0,5	250
1500	200	1	2000	0,5	250
1500	200	1	2400	0,5	250
1500	200	1	2800	0,5	250
1500	200	1	3200	0,5	250

Simulation_3					
diameter [mm]	wave heigth [mm]	no of waves	wave length [mm]	velocity [m/s]	submerge level [mm]
1500	100	1	1000	1	250
1500	100	1	1200	1	250
1500	100	1	1400	1	250
1500	100	1	1600	1	250
1500	200	1	2000	1	250
1500	200	1	2400	1	250
1500	200	1	2800	1	250
1500	200	1	3200	1	250

10.2 Testing Plan MarinLab Experiments

10.2.1 Big Cylinder Test Plan

Wave Number	Amplitude [m]	Frequency [Hz]	Flow / Tow Speed [m/s]	Name of data file:
1	0.04	0.3	0.5	w1a0.04f0.3h0.5
2	0.04	0.4	0.5	w2a0.04f0.4h0.5
3	0.04	0.5	0.5	w3a0.04f0.5h0.5
4	0.06	0.3	0.5	w4a0.06f0.3h0.5
5	0.06	0.4	0.5	w5a0.06f0.4h0.5
6	0.06	0.5	0.5	w6a0.06f0.5h0.5
7	0.08	0.3	0.5	w7a0.08f0.3h0.5
8	0.08	0.4	0.5	w8a0.08f0.4h0.5
9	0.08	0.5	0.5	w9a0.08f0.5h0.5
10	0.04	0.3	1	w10a0.04f0.3h1
11	0.04	0.4	1	w11a0.04f0.4h1
12	0.04	0.5	1	w12a0.04f0.5h1
13	0.06	0.3	1	w13a0.06f0.3h1
14	0.06	0.4	1	w14a0.06f0.4h1
15	0.06	0.5	1	w15a0.06f0.5h1
16	0.08	0.3	1	w16a0.08f0.3h1
17	0.08	0.4	1	w17a0.08f0.4h1
18	0.08	0.5	1	w18a0.08f0.5h1
19	0.04	0.3	0.75	w19a0.04f0.3h0.75
20	0.04	0.4	0.75	w20a0.04f0.4h0.75
21	0.04	0.5	0.75	w21a0.04f0.5h0.75
22	0.06	0.3	0.75	w22a0.06f0.3h0.75
23	0.06	0.4	0.75	w23a0.06f0.4h0.75
24	0.06	0.5	0.75	w24a0.06f0.5h0.75
25	0.08	0.3	0.75	w25a0.08f0.3h0.75
26	0.08	0.4	0.75	w26a0.08f0.4h0.75
27	0.08	0.5	0.75	w27a0.08f0.5h0.75
28	0.04	0.3	0.0	w28a0.04f0.3h0
29	0.04	0.4	0.0	w29a0.04f0.4h0
30	0.04	0.5	0.0	w30a0.04f0.5h0
31	0.06	0.3	0.0	w31a0.06f0.3h0
32	0.06	0.4	0.0	w32a0.06f0.4h0
33	0.06	0.5	0.0	w33a0.06f0.5h0
34	0.08	0.3	0.0	w34a0.08f0.3h0
35	0.08	0.4	0.0	w35a0.08f0.4h0
36	0.08	0.5	0.0	w36a0.08f0.5h0

10.2.2 Small Cylinder Test Plan

Wave Number	Amplitude [m]	Frequency [Hz]	Flow / Tow Speed [m/s]	Name of data file:
37	0.04	0.3	0.0	w37a0.04f0.3h0
38	0.04	0.4	0.0	w38a0.04f0.4h0
39	0.04	0.5	0.0	w39a0.04f0.5h0
40	0.06	0.3	0.0	w40a0.06f0.3h0
41	0.06	0.4	0.0	w41a0.06f0.4h0
42	0.06	0.5	0.0.	w42a0.06f0.5h0
43	0.08	0.3	0.0	w43a0.08f0.3h0
44	0.08	0.4	0.0	w44a0.08f0.4h0
45	0.08	0.5	0.0	w45a0.08f0.5h0
46	0.04	0.3	0.5	w46a0.04f0.3h0.5
47	0.04	0.4	0.5	w47a0.04f0.4h0.5
48	0.04	0.5	0.5	w48a0.04f0.5h0.5
49	0.06	0.3	0.5	w49a0.06f0.3h0.5
50	0.06	0.4	0.5	w50a0.06f0.4h0.5
51	0.06	0.5	0.5	w51a0.06f0.5h0.5
52	0.08	0.3	0.5	w52a0.08f0.3h0.5
53	0.08	0.4	0.5	w53a0.08f0.4h0.5
54	0.08	0.5	0.5	w54a0.08f0.5h0.5
55	0.04	0.3	0.75	w55a0.04f0.3h0.75
56	0.04	0.4	0.75	w56a0.04f0.4h0.75
57	0.04	0.5	0.75	w57a0.04f0.5h0.75
58	0.06	0.3	0.75	w58a0.06f0.3h0.75
59	0.06	0.4	0.75	w59a0.06f0.4h0.75
60	0.06	0.5	0.75	w60a0.06f0.5h0.75
61	0.08	0.3	0.75	w61a0.08f0.3h0.75
62	0.08	0.4	0.75	w62a0.08f0.4h0.75
63	0.08	0.5	0.75	w63a0.08f0.5h0.75
64	0.04	0.3	1.0	w64a0.04f0.3h1
65	0.04	0.4	1.0	w65a0.04f0.4h1
66	0.04	0.5	1.0	w66a0.04f0.5h1
67	0.06	0.3	1.0	w67a0.06f0.3h1
68	0.06	0.4	1.0	w68a0.06f0.4h1
69	0.06	0.5	1.0	w69a0.06f0.5h1
70	0.08	0.3	1.0	w70a0.08f0.3h1
71	0.08	0.4	1.0	w71a0.08f0.4h1
72	0.08	0.5	1.0	w72a0.08f0.5h1

10.3 Loadcell calibration

In appendix 9.3 the loadcell calibration sheets and plots are presented.

10.3.1 Failed Calibration

	amount of Testweights applied	weight applied [kg]	force applied [N]	mean loadcell output from Labview [mV/V]	calculated Load N	Deviation between applied force and calculated force	normaliced deviation, %	Hysteresis
weight Increasing	0	0	0	-0,111936	-0,45	0,45	0,5 %	-0,01
	1	1	9,80665	-0,183407	8,91	0,90	0,9 %	0,01
	2	2	19,6133	-0,256599	18,49	1,12	1,1 %	0,02
	3	3	29,41995	-0,329138	27,99	1,43	1,5 %	0,03
	4	4	39,2266	-0,40152	37,47	1,76	1,8 %	0,04
	5	5	49,03325	-0,475632	47,17	1,86	1,9 %	0,05
	6	6	58,8399	-0,547454	56,58	2,26	2,3 %	0,06
	7	7	68,64655	-0,6192	65,97	2,68	2,7 %	0,06
	8	8	78,4532	-0,690711	75,33	3,12	3,2 %	0,07
	9	9	88,25985	-0,761588	84,61	3,65	3,7 %	0,01
Max weight	10	10	98,0665	-0,831996	93,83	4,23	4,3 %	
weight decreasing	9	9	88,25985	-0,774922	86,36	1,90	1,9 %	
	8	8	78,4532	-0,756341	83,93	-5,47	-5,6 %	
	7	7	68,64655	-0,681604	74,14	-5,49	-5,6 %	
	6	6	58,8399	-0,603853	63,96	-5,12	-5,2 %	
	5	5	49,03325	-0,52079	53,08	-4,05	-4,1 %	
	4	4	39,2266	-0,439098	42,39	-3,16	-3,2 %	
	3	3	29,41995	-0,355813	31,48	-2,06	-2,1 %	
	2	2	19,6133	-0,273185	20,66	-1,05	-1,1 %	
	1	1	9,80665	-0,190887	9,88	-0,08	-0,1 %	
	0	0	0	-0,10689	-1,11	1,11	1,1 %	
							Linearity, %	
Maximum Values						5,49	5,6 %	

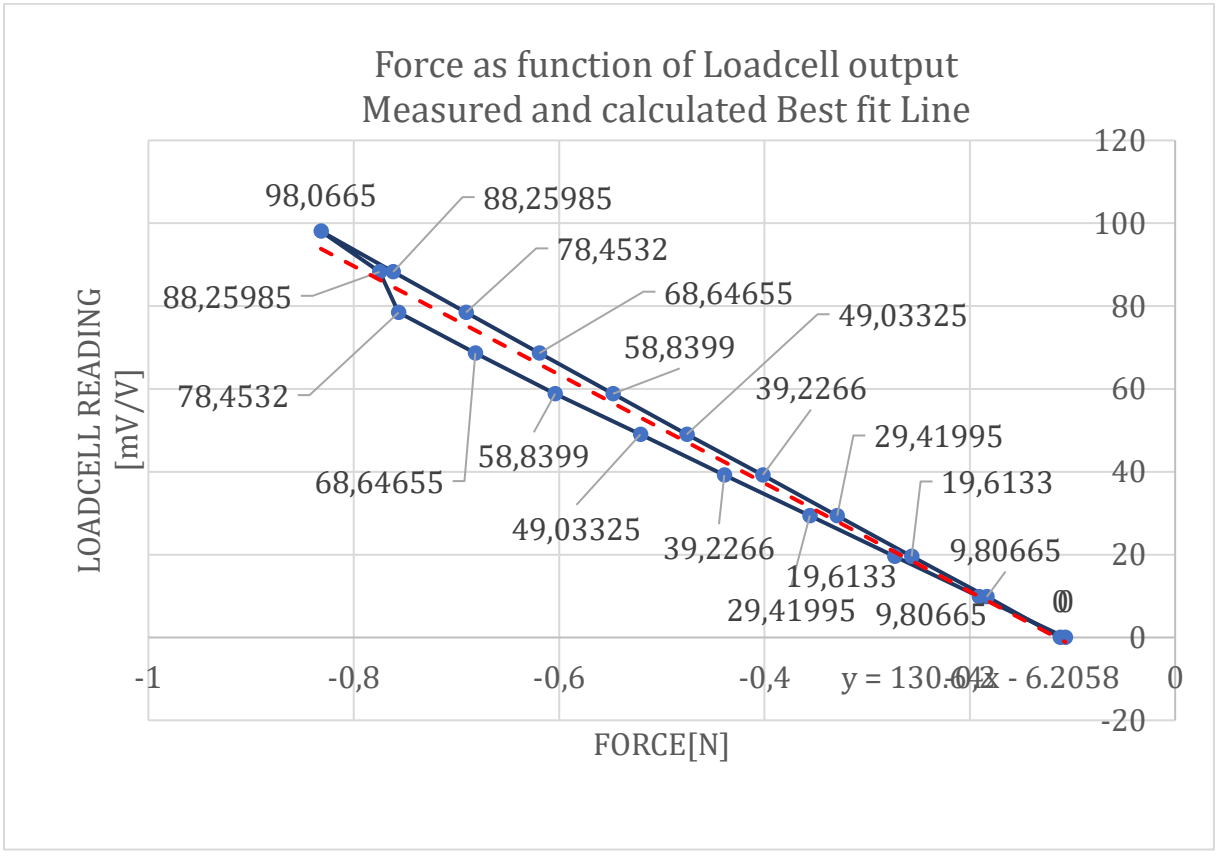

10.3.2 Calibration of Supporting Loadcell

	amount of Testweights applied	weight applied [kg]	force applied [N]	mean loadcell output from Labview [mV/V]	calculated Load N	Deviation between applied force and calculated force [N]	normalized deviation, %	Hysteresis
	0	0	0	-0,0019679	0,06	-0,06	-0,1 %	0,00
weight	1	1	9,80665	-0,0513998	9,85	-0,04	0,0 %	0,00
Increasing	2	2	19,6133	-0,100865	19,65	-0,03	0,0 %	0,00
	3	3	29,41995	-0,150308	29,44	-0,02	0,0 %	0,00
	4	4	39,2266	-0,199757	39,23	-0,01	0,0 %	0,00
	5	5	49,03325	-0,249196	49,03	0,01	0,0 %	0,00
	6	6	58,8399	-0,298704	58,83	0,00	0,0 %	0,00
	7	7	68,64655	-0,348251	68,65	0,00	0,0 %	0,00
	8	8	78,4532	-0,397866	78,48	-0,02	0,0 %	0,00
	9	9	88,25985	-0,44736	88,28	-0,02	0,0 %	0,00
Max weight	10	10	98,0665	-0,496886	98,09	-0,03	0,0 %	
	9	9	88,25985	-0,447357	88,28	-0,02	0,0 %	
weight	8	8	78,4532	-0,397751	78,45	0,00	0,0 %	
decreasing	7	7	68,64655	-0,348124	68,62	0,02	0,0 %	
	6	6	58,8399	-0,298552	58,80	0,04	0,0 %	
	5	5	49,03325	-0,249018	48,99	0,04	0,0 %	
	4	4	39,2266	-0,199493	39,18	0,04	0,0 %	
	3	3	29,41995	-0,149939	29,37	0,05	0,1 %	
	2	2	19,6133	-0,100457	19,56	0,05	0,0 %	
	1	1	9,80665	-0,0510708	9,78	0,02	0,0 %	
	0	0	0	-0,00181379	0,02	-0,02	0,0 %	
							Linearity, %	
Maximum Values						0,06	0,1 %	

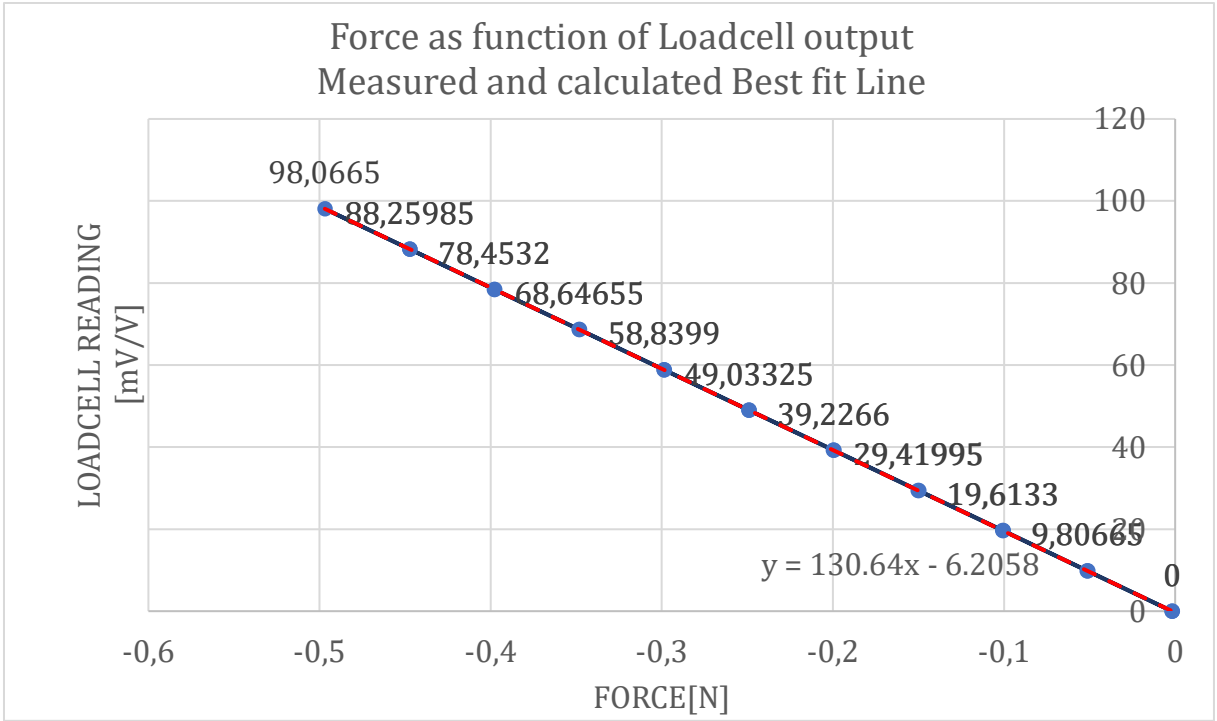

10.3.3 Final Calibration Loadcell

	amount of Testweights applied	weight applied [kg]	force applied [N]	mean loadcell output from Labview [mV/V]	calculated Load N	Deviation between applied force and calculated force [N]	normaliced deviation, %	Hysteresis
weight Increasing	0	0	0	-0,107915	-0,17	0,17	0,2 %	0,00
	1	1	9,08453	-0,179806	8,93	0,16	0,2 %	0,01
	2	2	18,1936	-0,25256	18,14	0,05	0,1 %	0,02
	3	3	27,5124	-0,326845	27,54	-0,03	0,0 %	0,03
	4	4	36,6246	-0,399598	36,75	-0,13	-0,1 %	0,04
	5	5	45,8378	-0,472693	46,01	-0,17	-0,2 %	0,05
	6	6	54,9156	-0,544251	55,06	-0,15	-0,2 %	0,06
	7	7	64,1398	-0,616825	64,25	-0,11	-0,1 %	0,07
	8	8	73,4784	-0,69002	73,52	-0,04	0,0 %	0,07
	9	9	82,6452	-0,762092	82,64	0,00	0,0 %	0,04
Max weight	10	10	92,6468	-0,839244	92,41	0,24	0,2 %	
weight decreasing	9	9	88,3796	-0,804384	88,00	0,38	0,4 %	
	8	8	82,1603	-0,757294	82,03	0,13	0,1 %	
	7	7	72,5352	-0,682216	72,53	0,00	0,0 %	
	6	6	62,2509	-0,601608	62,33	-0,08	-0,1 %	
	5	5	51,2932	-0,519362	51,91	-0,62	-0,6 %	
	4	4	41,6659	-0,438912	41,73	-0,06	-0,1 %	
	3	3	31,2988	-0,356356	31,28	0,02	0,0 %	
	2	2	20,8858	-0,273995	20,85	0,03	0,0 %	
	1	1	10,4858	-0,191386	10,39	0,09	0,1 %	
	0	0	-0,0149309	-0,108308	-0,12	0,11	0,1 %	
							Linearity, %	
Maximum Values						0,62	0,6 %	

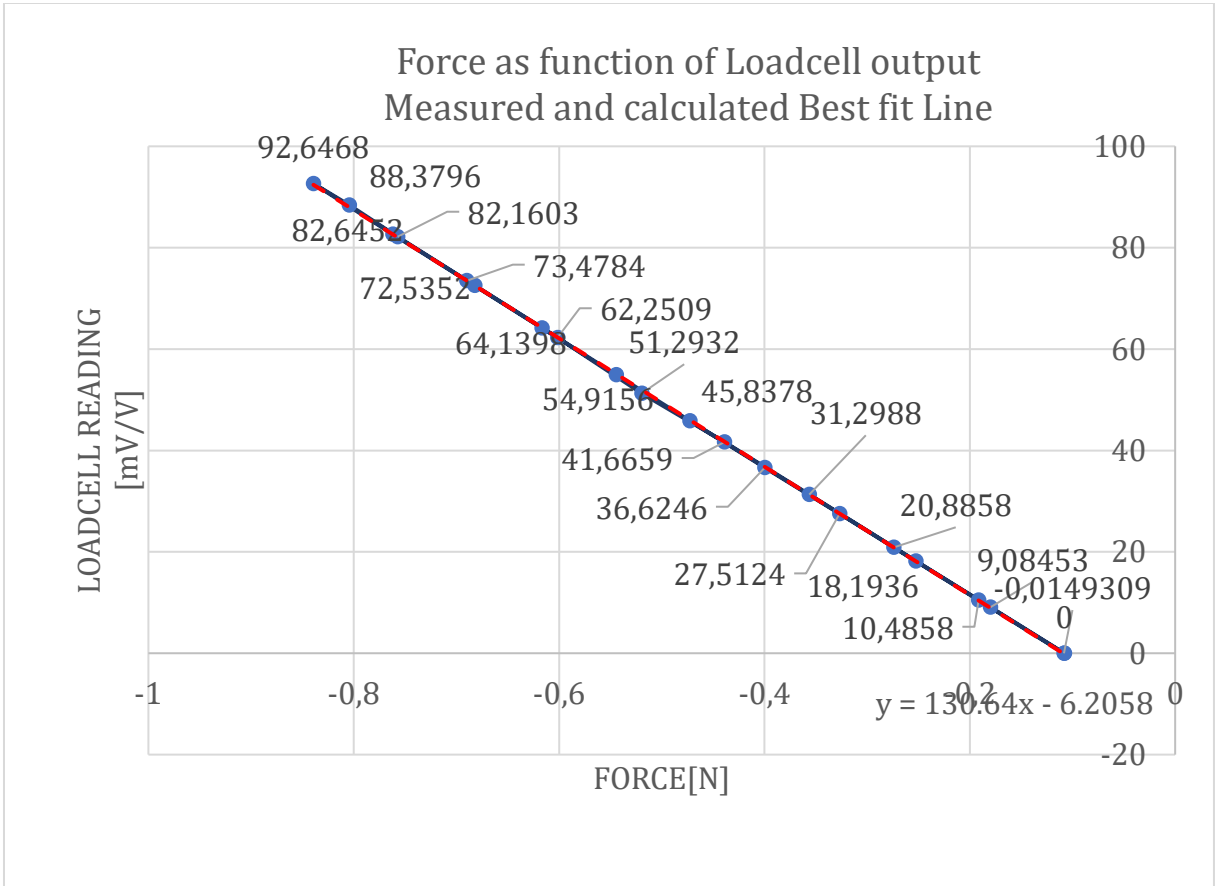

10.3.4 Calibration measurement investigation

	amount of Testweights applied	weight applied [kg]	force applied [N]	mean loadcell output from Labview [mV/V]	calculated Load N	Deviation between applied force and calculated force [N]	normaliced deviation, %	Hysteresis
weight Increasing	0	0	0	-0,102755	0,01	-0,01	0,0 %	0,00
	1	1	9,80665	-0,175555	9,75	0,06	0,1 %	0,00
	2	2	19,6133	-0,24855	19,51	0,10	0,1 %	0,00
	3	3	29,41995	-0,322116	29,36	0,06	0,1 %	0,00
	4	4	39,2266	-0,395055	39,11	0,11	0,1 %	0,00
	5	5	49,03325	-0,467871	48,85	0,18	0,2 %	0,00
	6	6	58,8399	-0,541454	58,70	0,14	0,1 %	0,00
	7	7	68,64655	-0,614345	68,45	0,20	0,2 %	0,00
	8	8	78,4532	-0,689141	78,45	0,00	0,0 %	0,00
	9	9	88,25985	-0,762073	88,21	0,05	0,0 %	0,00
Max weight	10	10	98,0665	-0,8356568	98,05	0,01	0,0 %	
weight decreasing	9	9	88,25985	-0,76555	88,68	-0,42	-0,4 %	
	8	8	78,4532	-0,689623	78,52	-0,07	-0,1 %	
	7	7	68,64655	-0,614356	68,45	0,20	0,2 %	
	6	6	58,8399	-0,542166	58,79	0,05	0,0 %	
	5	5	49,03325	-0,46887	48,99	0,05	0,0 %	
	4	4	39,2266	-0,398155	39,53	-0,30	-0,3 %	
	3	3	29,41995	-0,324116	29,62	-0,20	-0,2 %	
	2	2	19,6133	-0,25051	19,78	-0,16	-0,2 %	
	1	1	9,80665	-0,175997	9,81	0,00	0,0 %	
	0	0	0	-0,102945	0,04	-0,04	0,0 %	
							Linearity, %	
Maximum Values						0,42	0,4 %	

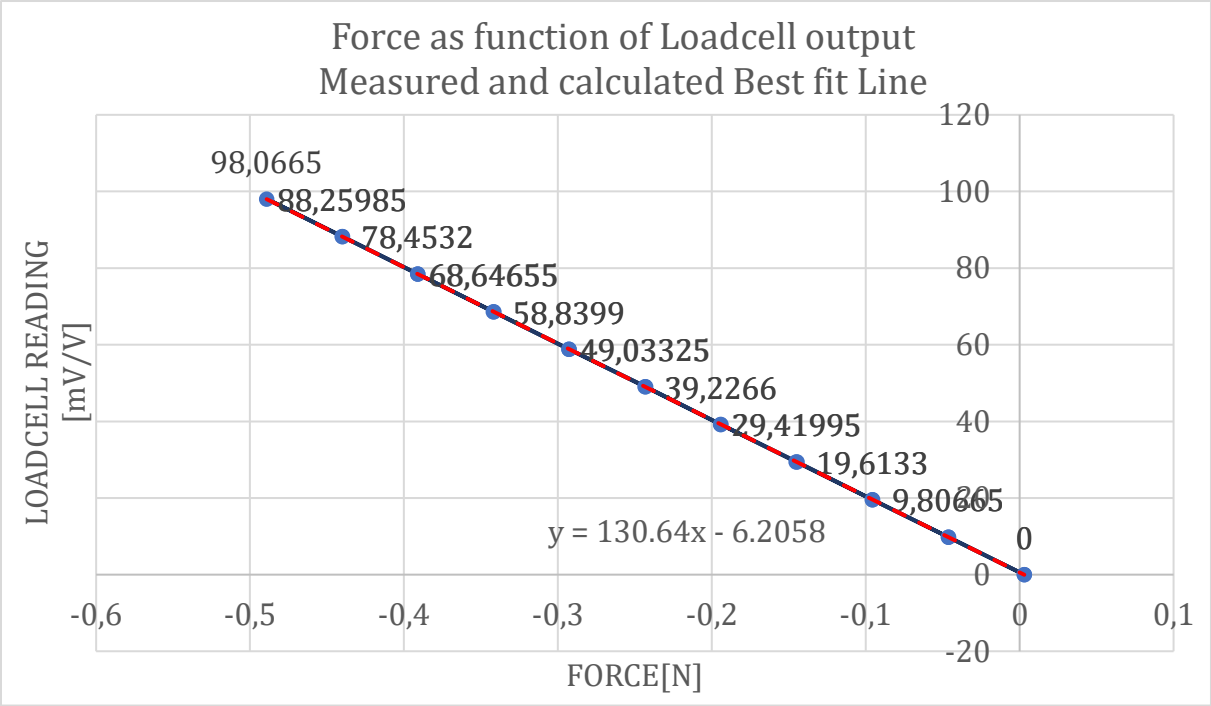

10.4 Data tables

Data tables of the Average Maximum wave loads

10.4.1 Wave frequency 0.3 Hz at 0.0 m/s flow speed - Drag

Wave frequency 0.3 hz - Flow speed 0.0 m/s			
Amplitude [m]	0.04	0.06	0.08
CFD: Average max Drag Force [N]	1.93	2.62	3.15
MarinLab: Average max Drag Force [N]	2.89	5.03	6.05

10.4.2 Wave frequency 0.4 Hz at 0.0 m/s flow speed - Drag

Wave frequency 0.4 hz - Flow speed 0.0 m/s			
Amplitude [m]	0.04	0.06	0.08
CFD: Average max Drag Force [N]	5.76	7.43	8.9
MarinLab: Average max Drag Force [N]	5.64	7.3	9.79

10.4.3 Wave frequency 0.5 Hz at 0.0 m/s flow speed - Drag

Wave frequency 0.5 hz - Flow speed 0.0 m/s			
Amplitude [m]	0.04	0.06	0.08
CFD: Average max Drag Force [N]	4.96	5.95	8.47
MarinLab: Average max Drag Force [N]	5.8	10.5	16.1

10.4.4 Wave frequency 0.4 Hz at 0.5 m/s flow speed - Drag

Wave frequency 0.4 hz - Flow speed 0.5 m/s			
Amplitude [m]	0.04	0.06	0.08
CFD: Average max Drag Force [N]	17.71	22.59	27.16
MarinLab: Average max Drag Force [N]	15.96	23.29	27.216

10.4.5 Wave frequency 0.4 Hz at 0.75 m/s flow speed - Drag

Wave frequency 0.4 hz - Flow speed 0.75 m/s			
Amplitude [m]	0.04	0.06	0.08
CFD: Average max Drag Force [N]	28.85	36.63	42.37
MarinLab: Average max Drag Force [N]	27.04	35.33	46.26

10.4.5 Wave frequency 0.4 Hz at 0.75 m/s flow speed - Lift

Frequency 0.4 Hz - Flow speed 0.75 m/s			
Amplitude [m]	0.04	0.06	0.08
Average maximum Lift Force [N]	42.09	55.83	60.81

10.4.6 Wave frequency 0.4 Hz at 0.5 m/s flow speed - Drag

Wave amplitude 0.06 m - Flow speed 0.5 m/s			
Frequency [Hz]	0.3	0.4	0.5
CFD: Average max Drag Force [N]	21.4	24.59	27.1
MarinLab: Average max Drag Force [N]	19.4	23.29	26.2

10.4.6 Wave amplitude 0.06 m at 0.75 m/s flow speed - Drag

Wave amplitude 0.06 m - Flow speed 0.75 m/s			
Frequency [hz]	0.3	0.4	0.5
CFD: Average max Drag Force [N]	34.58	36.78	38.95
MarinLab: Average max Drag Force [N]	32.1	34.6	37.5